THE INFLUENCE OF ELECTROSTATIC CHARGE ON THE FILTRATION OF HYDRAULIC FLUIDS BY FIBROUS FILTERS

By

LEONARD ERNEST BENSCH

Bachelor of Science
Oklahoma State University
Stillwater, Oklahoma
1970

Master of Science
Oklahoma State University
Stillwater, Oklahoma
1970

Submitted to the Faculty of the Graduate College
of the Oklahoma State University
in partial fulfillment of the requirements
for the Degree of
DOCTOR OF PHILOSOPHY
July, 1977

THE INFLUENCE OF ELECTROSTATIC CHARGE ON THE FILTRATION OF HYDRAULIC FLUIDS BY FIBROUS FILTERS

Thesis Approved:

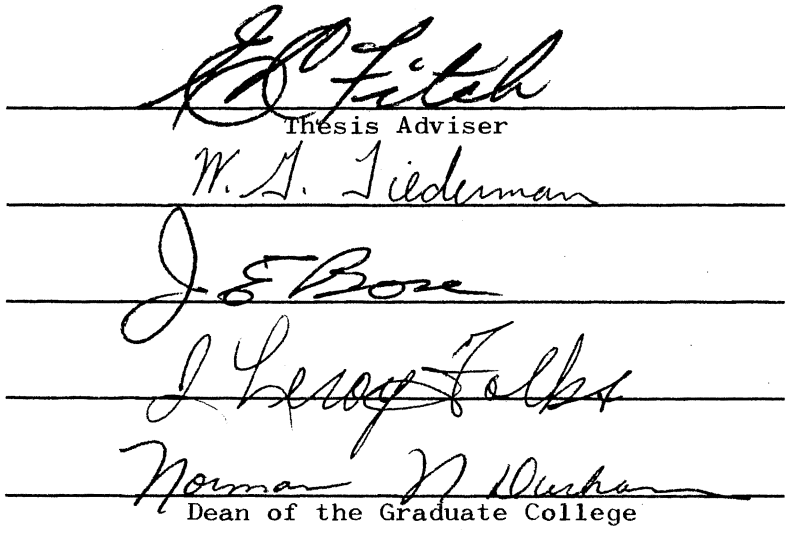

Thesis Adviser

Dean of the Graduate College

PREFACE

I would like to express my sincere appreciation and thanks to the many people and organizations who have encouraged and supported my doctoral program.

A special note of appreciation is extended to Dr. E. C. Fitch, who served as my major adviser and graduate committee chairman. His encouragement, advice, counsel, and inspiration have been of great help throughout my undergraduate and graduate program.

To the other members of my graduate committee, composed of Dr. J. E. Bose, Dr. J. L. Folks, and Dr. W. G. Tiederman, Jr., I extend my thanks for their guidance and patience during my doctoral program.

I would like to express my gratitude to the concerned filter manufacturers and users who sponsored this investigation-- Donaldson Company, Inc.; Facet Enterprizes, Inc.; John Deere Product Engineering Center; Fall Corporation; Schroeder Brothers, Inc.; and Sundstrand Aviation. In particular I would like to thank Mr. Bill Martin of Facet Enterprizes for his suggestion of this research area and for convincing me of the importance of such an investigation.

To my colleagues at the Fluid Power Research Center, Dr. G. E. Maroney, Richard Tessmann, and James Shaeffer, I extend my thanks for their suggestions during this study. I would also like to thank Lanny Grade, Larry Moore, and David Chastain for their help during the data acquisition phase, and especially Bruce Bowman for his assistance in reducing the data into a "managable" form. Thanks are also in order for

Pat Laramore, Robert Sloan, and Robert Ramsey for their professional assistance in providing the drafting and artwork for this thesis. To Velda Davis, I extend my appreciation for her helpful suggestions and for preparing the final manuscript of this thesis.

I thank my mother, father, and grandmother for providing me with the opportunity and for their faith and encouragement throughout my career.

Most of all I thank my wife, Diana, and children, Cristy and Alicia, for their sacrifices, encouragement, and understanding which have made this study possible. I would also like to thank Diana for preparation of the first draft of this dissertation.

TABLE OF CONTENTS

LIST OF TABLES

LIST OF FIGURES

NOMENCLATURE

A	Constant
A_f	Filter area, m^2
A_ℓ	Cross sectional flow area of system pipe, m^2
B	Constant
B_1	Filter fiber packing density
C	Ion concentration in fluid, $kmol/m^3$
C_o	Original total ion concentration in liquid $kmol/m^3$
C_x	Cunningham correction factor
d	Nominal pore diameter, m
D_f	Filter fiber diameter, m
$\overline{D}_g$	Geometric mean particle size
$\overline{D}_g'$	Normalized geometric mean diameter
$\overline{D}_{go}$	Geometric mean diameter with no charge
F_p	Filter parameter constant
$F(ta)$	Dimensionless function of t_a
$F(z)$	Normal probability integral
h	Filter medium thickness, m
I_i	Steady current generated at liquid/wall interface, amp
I_o	Current carried in liquid at time = 0, amp
I_s	Streaming current, amp
I_t	Current carried in liquid at time t, amp
K	Fluid electrical conductivity, $1/\Omega$ m

K_e Equilibrium conductivity $1/\Omega m$

K_o Proportionality constant, $m^{3n-1}/\Omega C^n$

ℓ_d Length of pipe downstream of filter between filter and reservoir, m

ℓ_o Equivalent electrode separation, m

ℓ_u Length of pipe upstream of filter after reservoir outlet, m

ℓ_x Length of line from reservoir to upstream sample point, m

n constant in exponent

$\bar{N}$ cumulative particle count, particles/ml

N_d Particle concentration downstream of filter, particles/ml

$\bar{N}_d$ Downstream cumulative particle count, particles/ml

N_i Particle concentration in injection fluid, particles/ml

$\bar{N}_i$ Injection fluid cumulative particle count, particles/ml

N_o Particle concentration originally in system at t=o, particle/ml

N_u Particle concentration upstream of filter, particles/ml

$\bar{N}_u$ Upstream cumulative particle count, particles/ml

P Filter porosity

q_c charge on collector per unit area C/m^2

q_p Charge on particle C/m

Q Volume flow rate through filter, ℓ/min

Q_i Volume flow rate of injection, ℓ/min

r Multiple correlation coefficient

r^2 Coefficient of determination

R Charge transfer ratio

R_o Total electrical resistance of fluid between electrodes, Ω

s Electrostatic charge density, C/m^3

s_d Charge density downstream of filter, C/m^3

$\hat{s}_d$ Steady state downstream charge density, C/m^3

s_f Charge density generated by filter, C/m^3

s_i Charge density at reservoir inlet, C/m^3

s_o Initial charge density, C/m^3

s_r Reservoir charge density, C/m^3

$\hat{s}_r$ Steady state reservoir charge density, C/m^3

s_u Charge density upstream of filter, C/m^3

$\hat{s}_x$ Steady state charge density at upstream sample point, C/m^3

t Time, sec or min

t_a Transport number of that ion species in fluid which has charge of polarity opposite to that of the fixed charge associated with the filter

T Tortuosity of filter pores

u Mobility of ions, $m^2/volt\ sec$

v Superficial flow velocity through filter, m/sec

V System fluid volume, ℓ

y_o Ordinate of the limiting particle trajectory in the undisturbed flow in front of fiber, m

z Variable in probability integral

Z_f Sign of filters fixed charge ($\pm$ 1)

α Constant

α_1 Constant

α_2 Constant

β Filtration ratio

β_{avg} Average filtration ratio

ϵ Dielectric constant of the liquid

ϵ_o Absolute dielectric constant of a vacuum
$= 8.85 \times 10$ sec/Ωm
$= 8.85 \times 10$ C/dyne cm^2

ϵ_p Dielectric constant of particle

γ_1 Constant

γ_2 Constant

γ_3 Constant

γ_4 Constant

μ Fluid viscosity

η_{avg} Average separation efficiency

η_s Single fiber efficiency

η_{s1} Single fiber efficiency due to charged collector and charged particle

η_{s3} Single fiber efficiency due to charged collector and uncharged particle

$\eta_{s/q}$ Single fiber efficiency due to charge only

Φ Particle retention ratio

Φ_o Retention ratio with no charge

σ_g Geometric standard deviation

σ'_g Normalized geometric standard deviation

σ_{go} Geometric standard deviation with no charge

τ Relaxation time, sec

τ_e Time constant = $\epsilon\epsilon_o/K_e$, sec

θ_1 Constant

θ_2 Constant

CHAPTER I

INTRODUCTION

The degree of filtration required to protect current hydraulic systems is becoming more and more critical. Higher system pressure and greater complexity both demand more protection from abrasive contaminants. Excluding catastrophic failure due to fatigue, overpressurizations, etc., the service life of most hydraulic components can be related directly to the amount of contamination entrained in the circulating fluid.

From a hydraulic system designers viewpoint the filter requirement can be simply stated as a filter which will provide adequate protection from particulate contaminants for a designated length of time with minimum pressure differential or flow restriction. From the filter manufacturers viewpoint this means that continual improvements must be made in the filter's particle separation characteristics as well as the contaminant capacity and pressure drop versus flow performance. It, therefore, becomes increasingly important to study the effects of all operating and design parameters on the performance of hydraulic filters for current as well as future applications.

It is well known that electrostatic forces play a significant role in the filtration of aerosols. In fact, the electrostatic precipitator relies entirely upon this phenomenonon. Only recently, however, has it been realized that under certain conditions, electrostatic forces can significantly alter the separation performance of a hydraulic fluid filter.

The passage of hydrocarbons through microporous media (filters) can result in the generation of static electricity. This is attributed to the presence of ions in the fluid which separate into positive and negative charges. Since hydrocarbon liquids are generally poor conductors of electricity, such charges tend to accumulate as long as fluid movement continues. The flow of electricity produced by the capture (or loss) of electrons is commonly called streaming current. This streaming current and resulting charge has been recognized in fuel filtration systems as the cause of many accidental explosions due to electrical discharges in the atmosphere (1, 2).

The electrostatic charge which may build up in a filtered hydraulic system may have a definite effect upon the ability of the filter to separate and retain particulate contaminant. Conditions encountered in many fibrous filters are such that electrostatic forces may be a dominant factor in the removal of particles especially for particle sizes in the range at and below the effective filter pore size. The charge generation rate for fuels has been shown to be a function of the fluid properties, filter properties and flow rate.

Static electricity generation in hydraulic systems has been visually recognized by the author either by sparks from or within a filter housing or a drop of oil which falls in an arc toward the filter housing. This phenomenon has generally occurred when testing fine filter elements with housing bodies made of plastic or electrical insultating materials. However, recent tests witnessed at various laboratories indicated that charging may occur under a number of conditions espcially with low relative humidity in the surrounding environment. The results from these tests certainly implied that this static charge has a definite influence

upon the separation characteristics of a filter.

Because of these discoveries, this research effort was undertaken to investigate the static charge phenomenon and its influence upon the filtration of hydraulic fluids. In specific, the areas investigated included static charge generation and charge accumulation in a hydraulic system environment. A generalized mathematical model for predicting electrostatic charge accumulation and relaxation in a hydraulic system was developed and verified. In addition, models for the particle separation performance characteristics of hydraulic filters including the influence of static charge were also developed and empirically verified.

The remainder of this dissertation presents and discusses the results of the total research program. The following chapters reviews previous related investigations in the areas of static charge generation, charge relaxation, and filtration performance modeling. Chapter III presents the development of models for predicting static charge accumulation and filtration performance as a function of charge level and other parameters. Chapters IV and V delineate the results of experimental programs to verify the charge accumulation and filter performance models, respectively. Finally, the remaining Chapters VI and VII discuss applications of the research to current problems and present a summary and conclusions for the research effort. The Appendices contain detailed descriptions of the test facilities and procedures as well as a selected experimental data.

CHAPTER II

RELATED INVESTIGATIONS

An extensive literature survey has revealed that a number of investigations have been conducted relative to static charge generation in fuel systems. These studies have generally been concerned with charge accumulation from a safety standpoint. Only a few technical works have been published relative to the charge resulting from the flow of a hydrocarbon fluid through a microporous filter. None of the investigations found, however, have been concerned with hydraulic fluids. The literature is almost completely void of investigations relating to static charge effects on particle capture and retention in hydrocarbon fluids.

Electrostatic Charge Generation

The charging process in a hydrocarbon fluid system actually begins before the fluid is in motion. At the interface between the liquid and the solid boundary, an uneven distribution of ions is observed. The solid phase (in this case, the pipe wall or filter pore surface) will carry a net charge of one polarity and the liquid phase will contain an equal but opposite charge. This is the concept of the electric double layer (1). A strictly non-ionic liquid would have the properties of an insulator. Ultra-pure hydrocarbons approach this category, however, even minute traces of contaminants can significantly alter this property.

The streaming current is generated as the fluid flows past the solid

boundary picking up electrical charge from the double layer area. Since filters present a tremendous amount of surface area in which this charge separation can occur, they constitute a major source of electrostatic charge generation. Klinkenberg (1) utilized the classic work of Helmholz to evaluate the streaming current in an insulating tube. This development assumes that the double layer is thin relative to the pipe diameter and thus is not particularly suited for prediction of streaming current generated in microcapillaries. Other investigators (3, 4) have studied flow in microcapillaries and have removed the restriction concerning the relatively small double layer thickness. These authors, however, have not considered the problem of low fluid conductivity or tortuous passage hydrodynamics.

The conductivity, K, of the fluid (the inverse of resistivity) is a measure of the discharge time of a capacitor which uses the fluid as a dielectric. The units of conductivity are $\frac{1}{\text{Ohm m}}$ or $\frac{\text{mho}}{\text{m}}$. A very pure hydrocarbon may have a conductivity of $10^{-3} > K > 10^{-13}$ mho/m; superpure $10^{-15} > K$; however, a fluid with ionic additives would be expected to yield a much larger value. An often used quantity which depends most heavily upon fluid conductivity is relaxation time, τ, which is defined as:

$$\tau = \frac{\mathbf{c}\, \mathbf{c}_o}{K} \qquad (2\text{-}1)$$

where:

$\mathbf{c}$ = dielectric constant of the liquid

$\mathbf{c}_o$ = absolute dielectric constant of a vacuum

One of the first reported studies dealing with charge generation during hydrocarbon flow through a microporous filter was reported by

Gavis and Wagner (5) in 1968. They conducted a number of experiments then developed expressions empirically, based upon ideas drawn from theory. They utilized n-heptane fluid doped with various amounts of an ionizing additive to control the conductivity. The test filters were various types of Millipore membrane disks. Their test results indicated the polarity of the charge generated was a function of the mechanical properties. The describing relationship they developed can be expressed as:

$$I_s = 2 \times 10^{-4} \, d \, A_f \, PF \, C_o \left(\frac{v\tau}{d}\right)^{1.75} \qquad (2\text{-}2)$$

where:

I_s = streaming current, amp

d = nominsl pore diameter, m

A_f = filter area, m^2

P = filter porosity (void volume/total volume)

F = Faraday constant

C_o = original total ion concentration in liquid, mol/m^3

v = superficial flow velocity, or volume flow rate per total cross-sectional area, m/sec

for $\frac{v\tau}{d} < 5 \times 10^{-3}$.

The term, $v\tau/d$, rewritten as $v/(d/\tau)$ is the ratio of the convective velocity to conductive velocity of ionic movement. They determined C_o experimentally from the conductivity, K, and an empirical estimate of ion mobility. They concluded that current generated was independent of the ratio of pore length to diameter and that the charging rate should be independent of the structure of the microporous medium.

Another pertinent study was conducted by Leonard and Carhart (6)

on the effect of conductivity on charge generation in hydrocarbon fuels flowing through fiber glass filters. They utilized JP-4 and JP-5 jet fuel with various amounts of conductivity improver additives. Their results showed that the magnitude of the streaming currents developed increased to a maximum then decreased as conductivity was increased. Experimentally, they determined that for a given filter and fluid, the current developed increased with increasing flow rate. This is in agreement with the work previously conducted by Gavis and Wagner.

Lauer and Antal (7) conducted an investigation of charge generation of several hydrocarbons flowing through low conductivity filter media. They found for zylene flowing through teflon media that streaming current was found to be linearily proportional to flow velocity and increased with decreasing pore size. Among other things, they confirmed some of the previous conclusions of Gavis and Wagner (5).

Probably the most pertinent study to date was conducted by Huber and Sonin (8) in which they considered the flow of n-heptane doped with anti-static additive through microporous disk filters. Their experiments were conducted in a similar manner to those by Gavis and Wagner (5); however, their theory was derived in a generalized nature. They concluded (9) that the equations developed by Gavis and Wagner should not be interpreted as having general validity and that the correlation established between streaming current, filter pore radius and fluid conductivity is in error. Huber and Sonin's theory considered a fixed charge which is adsorbed on the interior surfaces of the porous filter. Previous investigators had omitted this phenomena. Huber and Sonin's governing equation for high fixed charge density (8) is the following:

$$I_s = - \frac{Z_f A_f}{\ell_o} \left[\frac{T^2}{P} \frac{v h K}{u} + F(t_a) \frac{\varepsilon \varepsilon_o v^2}{u} \right] \qquad (2\text{-}3)$$

where:

Z_f = sign of filter's fixed charge (± 1)

ℓ_o = equivalent electrode separation, $\ell_o \equiv K A_f R_o$, m

T = tortuosity of filter pores

h = filter medium thickness, m

u = mobility of ion (with sign opposite to that of filters fixed charge) m^2/volt sec.

$F(t_a)$ = dimensionless function of t_a given by Equation (17) of Reference (8).

t_a = transport number of that ion species in fluid which has charge of polarity opposite to that of the fixed charge associated with the filter.

R_o = total electrical resistance of fluid between electrodes.

Huber and Sonin's experiments (10) as well as those conducted by Gavis and Wagner correlate extremely well with the theory of Huber and Sonin. An important result of Huber and Sonin's studies is that the streaming current is not dependent upon filter pore size nor on fluid conductivity K alone; but I_s depends upon the equivalent electrode spacing which includes the resistance of the fluid between the measuring electrodes.

Charge Relaxation

Because of the recirculating nature of hydraulic systems, it is necessary to consider the relaxation or dissipation characteristics of electrostatic charge in hydraulic fluids. In general, the charge that has been entrained in a liquid will dissipate when the source of the

charge is removed. The relaxation of charge for a stationary fluid was reviewed by such investigators as Klinkenberg (1), Winter (11), and Agnew (12) who concluded that the relaxation is governed by an exponential law that is dependent upon the initial fluid charge and the fluid relaxation time constant. Vallenga and Klinkenberg (13) and Carruthers and Marsh (14) continued the analysis for a fluid flowing through pipes.

For a fluid at rest, all investigators mentioned above conclude that the charge decay can be described by the following equation:

$$\frac{ds}{dt} = - \frac{s}{\tau} \qquad (2\text{-}4)$$

where:

s = electrical charge density per unit fluid volume, C/m^3

τ = fluid relaxation time, sec. = $\mathbf{C}\ \mathbf{C}_o/K$

Equation (2-4) is based upon the assumption that transport of charge by diffusion or convection can be ignored. The equation is derived from Ohm's Law which requires the above assumption. Diffusion and convection should be included for an accurate description; however, diffusion effects only become important in small laboratory apparatus or very near an interface where large concentration gradients occur so that in full scale equipment the contribution of diffusion can be ignored (15). For a fluid in motion, convection effects can be eliminated by letting the elemental volume of charge "ds" move along with the liquid (13). This corresponds to the Lagrangian description of motion in hydrodynamics. Equation (2-4) then becomes the governing relationship for the discharge or relaxation of electrically charged hydrocarbon liquids.

Winter (11) and later Vallenga and Klinkenberg (13) discuss two different types of fluid conductivity--equilibrium and effective. The

equilibrium conductivity is the conductivity measured in a fluid at rest or under steady-state conditions (e.g., one moving in a long straight path) when it is under no significant electrical unbalance. The effective or "in situ" conductivity corresponds to the rate of relaxation of charge in a fluid at any charged condition to which it is subjected.

Exponential Law of Charge Relaxation

For a hydrocarbon liquid with relatively high equilibrium conductivity (magnitude much higher than a pure hydrocarbon), it is normal and generally permissible to ignore the difference between effective and equilibrium conductivity. Essentially, then, the conductivity can be treated as a constant for a high conductivity liquid. Thus, integration of Equation (2-4) yields:

$$s = s_o \, e^{-t/\tau}$$

for τ = constant and s_o the initial charge density. Equation (2-5) is generally used to describe the relaxation of a charged hydrocarbon liquid with constant electrical conductivity.

If the liquid is in motion such as flow in a pipe, Carruthers and Marsh (14) conclude that a total description of the relaxation must include the charge which is generated at the liquid/wall interface during passage through the pipe. They developed, from the concepts in Reference (1), an equation for the current carried by the liquid as

$$I_t = I_o \, e^{-t/\tau} + I_i(1 - e^{-t/\tau}) \qquad (2\text{-}6)$$

where:

I_t = current carried in the liquid at time t, amp

I_i = Steady current generated at the liquid/wall interface, amp

I_o = Current carried in the liquid at time = o, amp

The first term in Equation (2-6) represents the exponential law of relaxation while the second term is the current generated by the flow of the liquid. Equation (2-6) was developed for pipe with a high electrical conductivity such as is generally the case in hydraulic test systems. The value of I_i can be calculated by methods presented by Klinkenberg (1).

Hyperbolic Law of Charge Relaxation

Vallenga and Klinkenberg (13) present a different theory for charge relaxation that does not assume constant conductivity. The effective conductivity they conclude is a linear function of the charge density or:

$$K = CFu \neq \text{constant}$$

where:

C = ion concentration, mol/m^3

u = ion mobility, $m^2/volt\ sec.$

Since the charge density $s = CF$ and $\tau = \epsilon\ \epsilon_o/K$, the equivalent of Equation (2-4) for non-constant K is:

$$\frac{ds}{dt} = -\frac{u\ s^2}{\epsilon\ \epsilon_o} \qquad (2\text{-}7)$$

which can be integrated to give:

$$\frac{1}{s} = \frac{u\ t}{\epsilon\ \epsilon_o} + \frac{1}{s_o} = \frac{t/\tau_o + 1}{s_o} \qquad (2\text{-}8)$$

where τ_o is the relaxation time and s_o is the initial charge density both at time = o.

Equation (2-8) is the hyperbolic law of charge relaxation as derived by Vallenga and Klinkenberg and describes the rate of discharge of an electrically charged liquid if the conductivity is directly proportional to the charge density.

Charge Effects on Particle Capture

The important mechanisms for particle separation in a fibrous filter other than sieving or mechanical blockage are generally classified as:

1. Direct interception
2. Inertial impaction
3. Browman diffusion
4. Gravity settling
5. Electrostatic precipitation

Figure 1 illustrates these mechanisms for flow past a typical filter fiber. Electrostatic attraction can occur as a result of electrostatic forces drawing a particle from the fluid to the fiber surface. As shown in Figure 1, it is possible to collect particles by electrostatic means when the particle is so far from the fiber that other mechanisms such as direct or inertial interception would be ineffective. If the electrostatic forces are large enough to draw a particle from the flow stream, then this capture mechanism may become quite significant.

A thorough survey of the literature revealed no previous investigations of the effects of electrostatic charge on filtration by fibrous hydraulic filters. A number of investigators (16-21), however, have studied the effect of electric forces on the filtration of aerosols by fibrous filters. The primary differences between aerosol and liquid

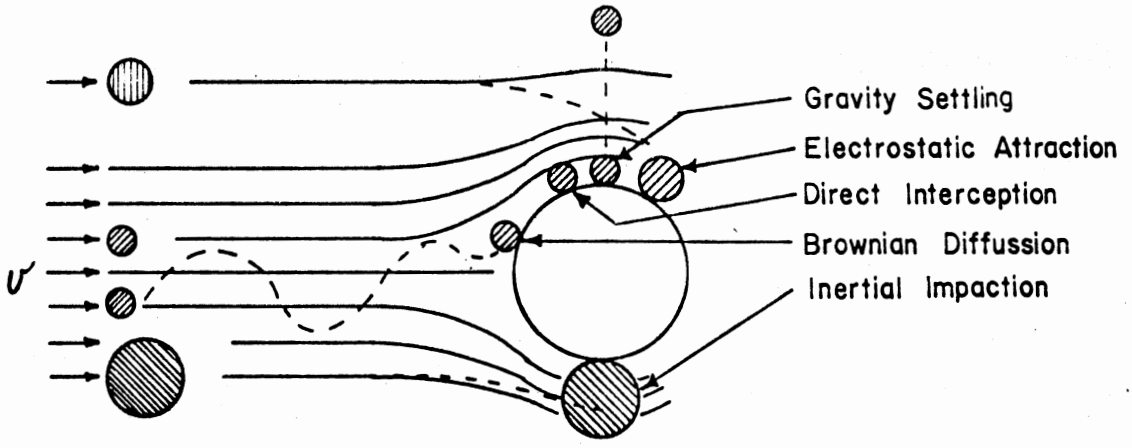

Figure 1. Typical Particle Capture Mechanisms for Fibrous Filters

filtration are the fluid viscosity and chemical properties; therefore, the theory developed for aerosol filtration should have applicability to liquid filtration with slight modification to account for these variables. The following is a review of those works.

Electrostatic charges may affect the particle separation performance of a filter in two ways: (1) particles may be attracted to the fibers from a distance, and (2) the electrostatic forces may increase the ability of a fiber to retain a particle once they have come in contact. The experiments of Loffler (22), however, have shown for aerosols that these forces are not dominant adhesive forces once a particle has been captured. His data indicated that Van der Wals forces were the important adhesive forces. This should be even more true for liquid filters where the higher viscosities would tend to detach the particles from a fiber with even greater drag force. Thus, this study is only concerned with the effects of the electrostatic capture mechanism.

Kraemer and Johnstone (16) investigated the electrostatic collection of particles by a spherical collector. In doing so they classified the electrical forces into five categories as follows:

1. Coulombic forces between a charged particle and a charged collector.
2. Force between a charged particle and its image on an uncharged collector.
3. Force between a charged collector and its image on an uncharged aerosol particle.
4. Force of repulsion on particle being collected by like charge on surrounding particles.

5. Force between a charged particle and the total charge induced in the collector by surrounding charged aerosol.

For the case of hydraulic filtration where the fluid carries a charge due to "election stripping" in the filter it is reasonable to assume that the filter fibers will be charged. It is possible that the contaminant particles may or may not be charged depending upon whether or not the particles take on a charge from the fluid. If the electrostatic charge accumulates in the recirculating system, then it is possible for the particles to be charged with the same polarity as the fluid (opposite of the filter fibers); however, if the charge in the fluid is relaxed before it circulates around the system, the particles would most likely not be charged. Because of this situation, it would be possible that either cases 1 or 3 above (charged or uncharged particles) might be applicable to hydraulic filters.

Kraemer and Johnstone (16) developed equations for cases 1 and 3 above for both spherical and cylindrical collectors. Their expression for single fiber efficienty of a cylindrical collector for case 1 with both collector and particle charged was:

$$\eta_{s1} = \frac{C_x q_c q_p}{3\mu \epsilon_o D_p v} \qquad (2\text{-}9)$$

where:

η_{s1} = single fiber efficiency for case 1 above

C_x = Cunningham correction factor

q_c = charge on collector per unit area, C/m^2

q_p = charge on particle, C

μ = fluid viscosity, cp = .01 dyne sec/cm^2

D_p = particle diameter, m

v = fluid velocity, m/sec

For case 3 above with charged collector and uncharged particles, their equation was:

$$\eta_{s3} = \left[\frac{\pi(\epsilon_p - 1)\, C_x\, q_c^2\, D_p^2}{2(\epsilon_p + 2)\, \mu\, D_f\, v_o\, \epsilon_o}\right]^{0.33} \qquad (2\text{-}10)$$

where:

η_{s3} = single fiber efficiency for case 3 above

ϵ_p = dielectric constant of particle

D_p = fiber diameter, m

Single fiber efficiency is generally defined as the ratio of the flow stream area from which all particles are removed to the projected fiber area, both areas taken perpendicular to the direction of free stream flow. Figure 2 illustrates the relationship for single fiber efficiency with the limiting trajectory exaggerated for electrostatic influences. The single fiber efficiency, η_s, is then defined by the following equation:

$$\eta_s = \frac{2\, y_o}{D_f} \qquad (2\text{-}11)$$

where y_o is the ordinate of the limiting particle trajectory in the undisturbed flow in front of the filter fiber and D_f is the fiber projected diameter. The single fiber efficiency, thus, is basically an indication of the ability of a filter fiber to capture particles from the flow stream around it. As illustrated in Figure 2, when electrostatic forces are involved, single fiber efficiency may easily be greater than unity.

If we let the constants θ_1 and θ_2 be defined as follows:

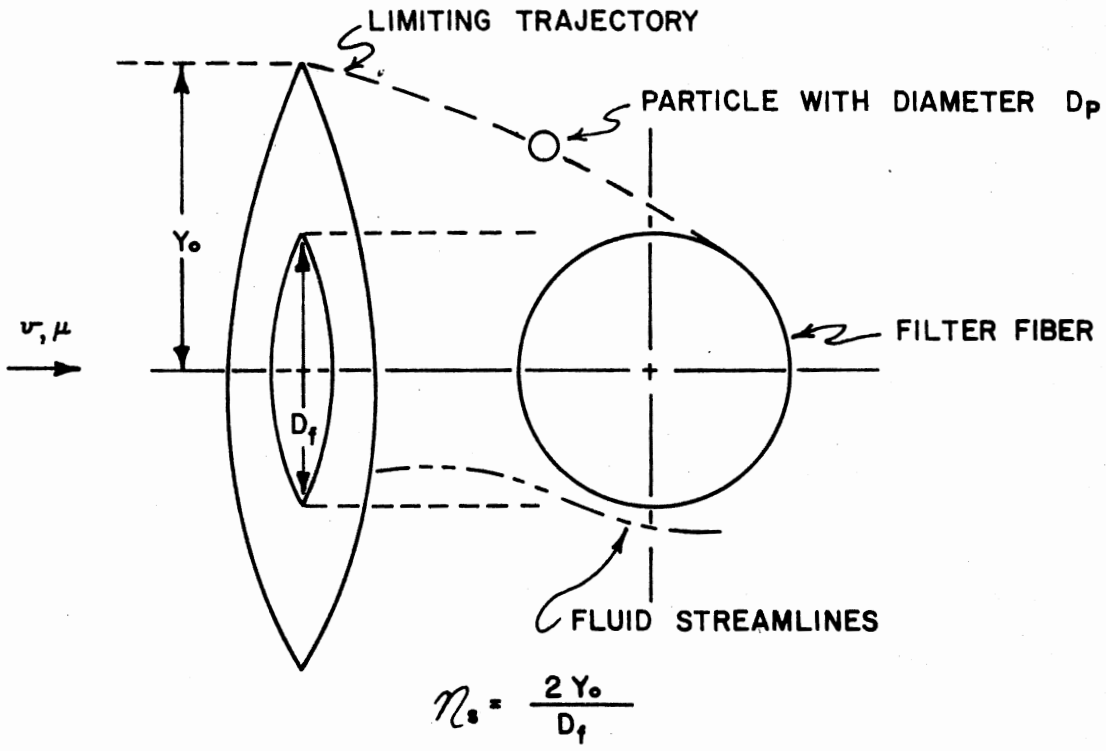

Figure 2. Model of Particle Trajectory Near Single Fiber With Electrostatic Influence

$$\theta_1 \equiv \frac{C_x}{3\mu\, \epsilon_o\, v} \tag{2-12}$$

$$\theta_2 \equiv \left[\frac{\pi\,(\epsilon_p - 1)\, C_x}{2(\epsilon_p + 2)\mu\, D_f\, v_o\, \epsilon_o}\right]^{0.33} \tag{2-13}$$

then Equations (2-9) and (2-10) can be rewritten as

$$\eta_{s1} = \frac{\theta_1\, q_c\, q_p}{D_p} \tag{2-14}$$

$$\eta_{s3} = \theta_2\, q_c^{.66}\, D_p^{.66} \tag{2-15}$$

Both Equations (2-14) and (2-15) predict that the single fiber efficiency should increase as charge levels increase. However, a primary difference between the two equations is that Equation (2-14) predicts decreasing efficiency with increasing particle size; whereas, Equation (2-15) predicts the opposite effect. It will later be shown that the form of Equation (2-15) for uncharged particles is generally more applicable to hydraulic system filtration because of the increasing efficiency with increasing particle size.

For a higher degree of accuracy, Loffler and Muhr (21) suggest the addition of an adhesion probability to the single fiber efficiency expressions. The adhesion probability they define as the ratio of the number of particles adhering to a fiber to the number of colliding particles. Earlier experiments by Loeffler were mentioned where adhesion probabilities less than unit were determined for solid particles with fluid velocities greater than 25 cm/sec. Loffler and Muhr found that the collision efficiency (product of single fiber efficiency and adhesion probability) depends upon the particle and fluid physical

properties, the flow velocity, and fiber size.

Direct measurement of single fiber efficiency or of collision efficiency as defined by Reference (21) as a function of each of the significant variables, is an ideal fundamental approach. However, this is not practical for measurements on complete filters. If a viscous liquid is the surrounding fluid medium, this measurement task becomes increasing difficult. The approach taken by many investigators is to measure experimentally the overall separation efficiency then develop empirical equations to describe the phenomena.

Measurement of Filter Efficiency

A number of studies have been conducted at Oklahoma State University during the past several years relative to the measurement and description of hydraulic filter separation efficiency (23-26). Tucker (23) in his Ph.D. dissertation considered hydraulic fluid flow through wire cloth filter media and developed expressions for filter efficiency based upon the filter pore size distribution. The equations developed by Tucker are not directly applicable to fibrous or depth type filters because of the randomness and complicated nature of the pore structure.

A standardized and realistic test has been developed for hydraulic filters as a result of investigations reported in References (24) (25). This test, called the multi-pass test, has since become a national and international standard method (27) and is being utilized worldwide to determine the performance of hydraulic filters. The multi-pass test basically involves injecting a specified contaminant, AC Fine Test Dust, into the circulating filter test system and extracting samples of the influent and effluent fluids to determine the separation performance.

Figure 3 is a simplified representation of the multi-pass test circuit.

Equations can be developed (24) to describe the contamination level and effective filtration characteristics as a function of time and the operating variables. The basic governing equation can be written in integral form as:

No. Particles in Reservoir of Size D_p	=	No. Particles Originally of Size D_p	+	No. Particles Injected of Size D_p	-	No. Particles Removed of Size D_p

$$N_u V = N_o V + \int N_i Q_i \, dt - \int (N_u - N_d) Q \, dt \qquad (2\text{-}16)$$

where:

N_u = particle concentration of size D_p per unit volume of fluid at point upstream of filter, particles/ml

N_d = particle concentration of size D_p per unit at point downstream of filter, particles/ml

N_o = initial particle concentration of size D_p, particles/ml

N_i = particle concentration of size D_p in injection fluid, particles/ml

Q = volume flow rate through filter, ℓ/min

Q_i = volume flow rate of injection, ℓ/min

V = circulating volume of fluid in system, ℓ

Equation (2-16) describes the particle concentration of a given size particle D_p in the upstream fluid.

If the filter separation efficiency, N, is defined as:

$$\eta = 1 - \frac{N_d}{N_u},$$

then Equation (2-16) can be rewritten as:

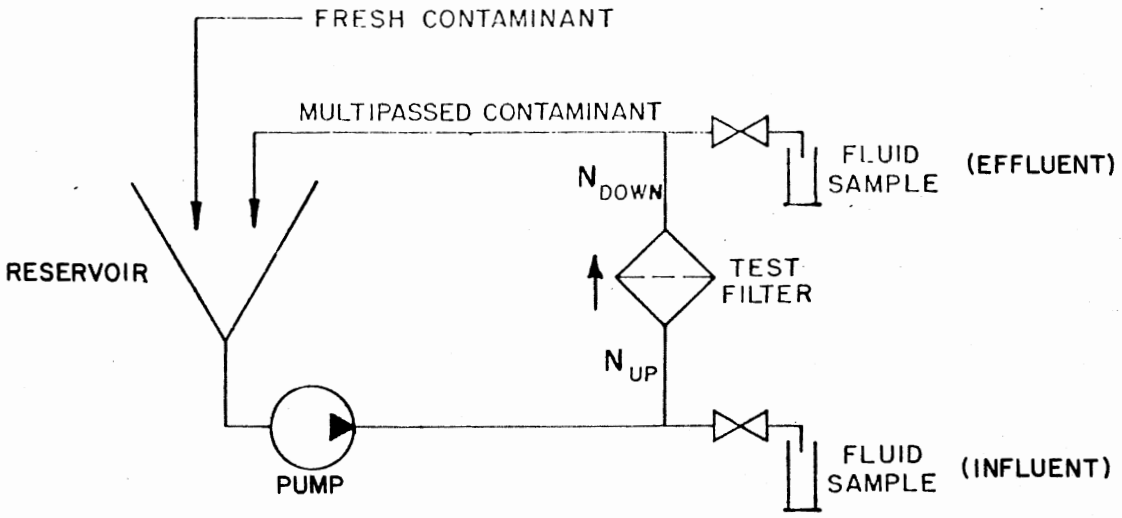

Figure 3. Simplified Schematic of Multi-Pass Filter Test Circuit

$$N_u V = N_o V + \int N_i Q \, dt - \int \eta N_u Q \, dt \qquad (2\text{-}17)$$

Equation (2-17) can then be differentiated to give:

$$\frac{d N_u}{dt} + \frac{\eta Q}{V} N_u = \frac{N_i Q_i}{V} \qquad (2\text{-}18)$$

Equation (2-18) represents the controlling differential equation which describes the concentration of a given particle size upstream of the filter at any time, regardless of the injection rate. Integration of Equation (2-18) results in

$$N_u(t) = \frac{N_i Q_i}{\eta Q} \left(1 - e^{-\frac{\eta Q}{V} t}\right) \qquad (2\text{-}19)$$

if it is assumed that η is constant and N_o is negligible. Figure 4 illustrates the solution to Equation (2-19). It can be seen that the contamination level will stabilize at some level equal to $N_i Q_i/\eta Q$. The time constant for the stabilization period is given by $V/\eta Q$. The standard multi-pass test method (27) requires a ratio of $V/Q = 0.25$ min.; thus, the time constant becomes simply $0.25/\eta$ minutes. Because a filter generally exhibits higher separation efficiencies at higher particle sizes, the time required for stabilization of particle concentration is usually higher for smaller particle sizes.

It is generally more common in the Fluid Power Industry to report contamination levels on a cumulative basis, or in other words, particles per unit volume greater than a given size. Thus, a common term used to describe the filter separation characteristics is the filtration ratio or beta ratio (β) which is defined as the ratio of the cumulative particle concentration greater than some size D_p upstream of the filter to the respective concentration in the downstream fluid or:

$$\beta = \frac{\overline{N}_u}{\overline{N}_d} \tag{2-20}$$

where:

$\overline{N}_u$ = upstream cumulative particle concentration greater than size D_p, particles/ml

$\overline{N}_d$ = downstream cumulative particle concentration greater than size D_p, particle/ml

Equation (2-18) can be rewritten in cumulative terms as the following:

$$\frac{d\,\overline{N}_u}{dt} + \frac{(\beta - 1)Q}{\beta V}\,\overline{N}_u = \frac{\overline{N}_i\, Q_i}{V} \tag{2-21}$$

where $\overline{N}_i$ is the cumulative particle concentration of the injection fluid. Because of the similarities of Equations (2-18) and (2-21) it is expected that the cumulative particle concentration would behave in a manner as illustrated in Figure 4.

Fitch and Tessmann (26) extended the concepts of Tucker (23) to graphically model the separation characteristics of a hydraulic filter based upon cumulative particle size distributions resulting from the multi-pass test. They considered the percent of contaminant which permeates through a filter to result in penetration and retention curves as a function of particle size. Figure 5 illustrates these characteristics for a typical filter.

This study will utilize the multi-pass filter test method and modeling concepts similar to those presented by Tucker (23) and Fitch and Tessmann (26) to produce accurate filtration performance models for hydraulic filters. The theory for the electrostatic capture mechanism will then be utilized for illustrating the change in the performance

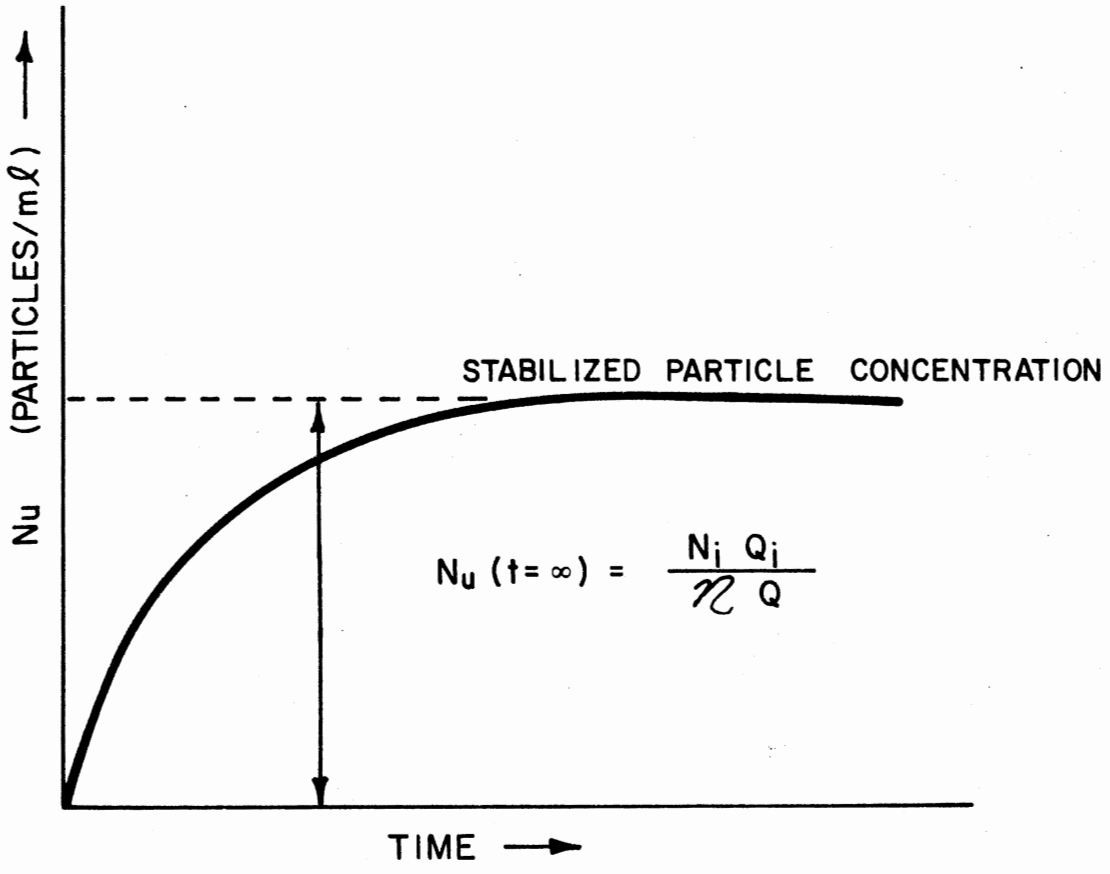

Figure 4. Graphical Representation of Multi-Pass Filtration Equation

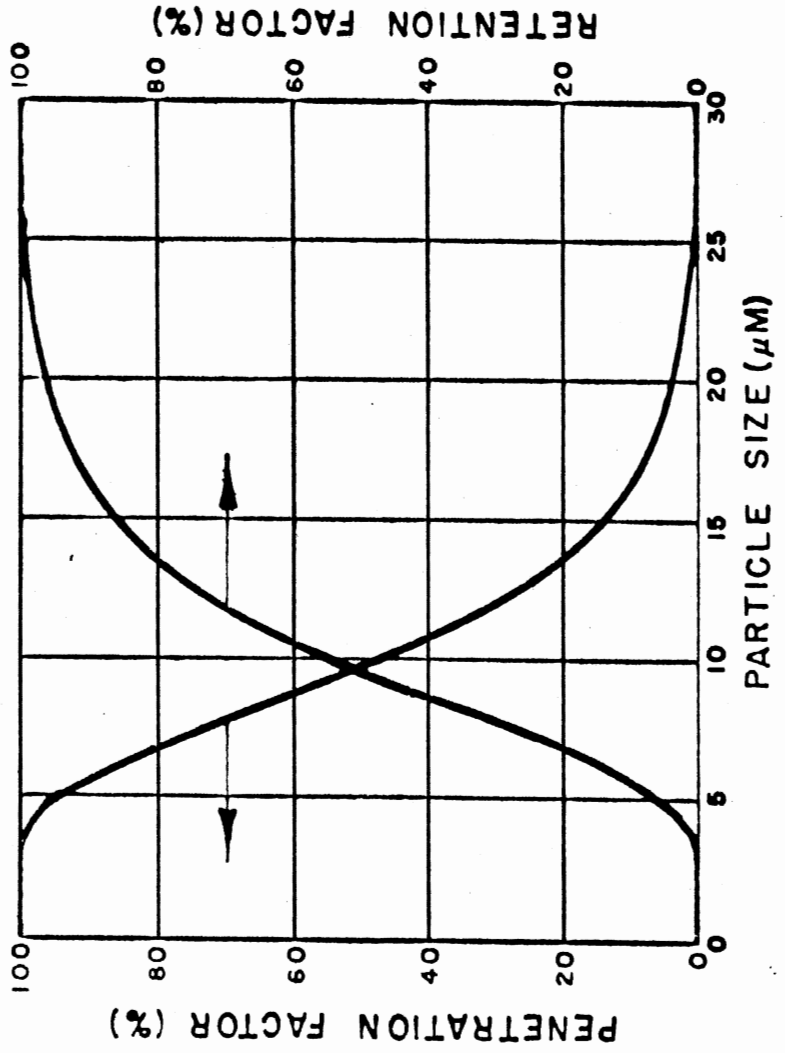

Figure 5. Filter Element Performance Characteristics Expressed on a Cumulative Basis

characteristics with electrostatic influences. The following chapter presents the development of the relationships for hydraulic fluid filters.

CHAPTER III

DEVELOPMENT OF THEORETICAL MODELS

Chapter II presented a review of previous investigations which were related to the present study. Relationships were shown for charge generation, charge relaxation, charge effects on aerosol filter performance, and filtration models. This chapter shows the development of models to describe such parameters in terms of hydraulic system filtration.

Electrostatic Charge Accumulation Models

The flow of hydraulic fluid in a typical fluid power system is not representative of the fueling process from the standpoint that the hydraulic fluid is continuously being recirculated while fuel generally passes through a system one time into a receiving vessel such as storage tank or vehicle reservoir. All previous investigations reported in the literature have dealt with charge generation and relaxation in a fuel type system. The theory developed is therefore not directly applicable to a hydraulic system because charge generated by a liquid passing through a hydraulic filter may not be fully discharged before it again enters the filter during recirculation. Based upon the theories presented by Vallenga and Klinkenberg (13), descriptive equations for the charge accumulation in a hydraulic system will be developed. Theories for both exponential and hyperbolic decay are included.

Exponential Charge Accumulation Model

According to most investigators cited in Chapter II, the discharge or relaxation of electrostatic charge can be modeled by an exponential law. In order to relate this law in terms of a multi-pass hydraulic system, consider the schematic illustrated in Figure 6. For the purposes of this derivation it will be assumed that the pipe wall and reservoir are electrically conductive (metal) and that the system is grounded. In addition, the flow rate Q and the charge generated by the filter s_f are assumed to be constant.

Since the system is grounded, the charge in each incremental fluid volume can be expressed in accordance with the exponential law given by Equation (2-4). A differential equation can be written for the charge density in the fluid at the outlet of the reservoir (assuming instantaneous and uniform mixing) as follows:

Rate of change in charge density at outlet of reservoir	= −	Exponential decay in reservoir	−	Rate leaving outlet of reservoir	+	Charge rate added to reservoir inlet

$$\frac{d s_r}{dt} = - \frac{s_r}{\tau} - s_r \frac{Q}{V} + s_i \frac{Q}{V} \qquad (3\text{-}1)$$

where:

s_r = charge density of fluid at reservoir outlet, C/m^3

s_i = charge density of fluid at reservoir inlet, C/m^3

From Equation (2-5) the charge density at the reservoir inlet can be written in terms of the downstream charge density as the following:

$$s_i = s_d e^{-\left(\frac{A_\ell \ell_d}{Q \tau}\right)} \qquad (3\text{-}2)$$

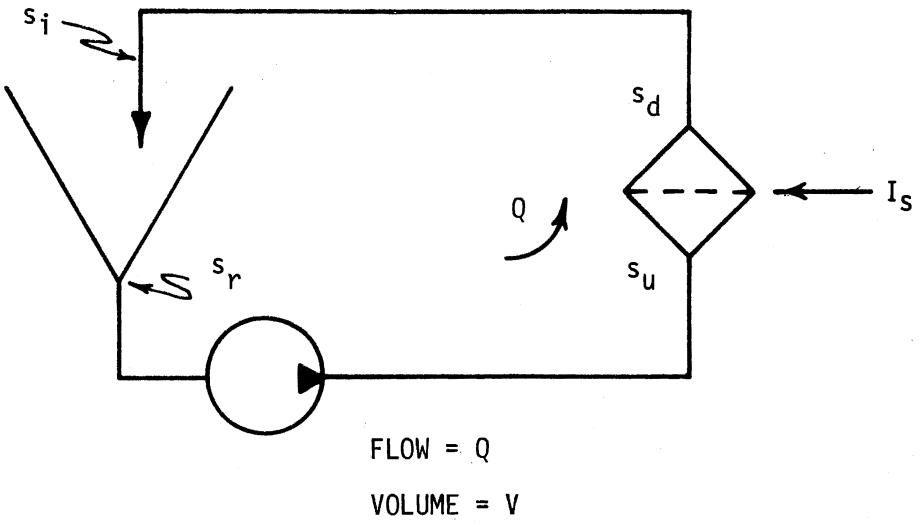

Figure 6. Charge Accumulation Schematic of Multi-Pass Hydraulic System

where:

s_d = charge density downstream of filter, C/m^3

A_ℓ = cross sectional flow area of system pipe, m^2

ℓ_d = length of pipe downstream of filter between filter and reservoir, m

Note that the quantity $A_\ell \ell_d/Q$ is the equivalent time required for a differential volume of fluid to pass from the system filter to the reservoir. This can be referred to as the residence time in the downstream line.

An equation similar to Equation (3-2) can be written for the upstream charge density as follows:

$$s_u = s_r e^{\frac{-A_\ell \ell_u}{Q\tau}} \tag{3-3}$$

where:

s_u = charge density upstream of filter, C/m^3

ℓ_u = length of pipe upstream of filter after reservoir outlet, m

The term $A_\ell \ell_u/Q$ is the residence time in the upstream piping.

If the current generated by the filter is the constant value, I_s, then the charge density added to the system per unit time can be expressed as:

$$s_f = \frac{I_s}{Q} \tag{3-4}$$

where s_f is the charge density added to the fluid by the filter expressed in units of C/m^3.

Let the two constants γ_1 and γ_2 be defined as follows:

$$\gamma_1 \equiv e^{-A_\ell \ell_d/Q\tau} \tag{3-5}$$

$$\gamma_2 \equiv e^{-A_\ell \ell_u/Q\tau} \tag{3-6}$$

then combining Equations (3-2), (3-3), and (3-4) gives the following equation for the charge density at the inlet of the reservoir, s_i, in terms of the charge at the outlet, s_r, and the filter generation rate, s_f:

$$s_i = \gamma_1 s_d = \gamma_1(s_u + s_i) = \gamma_1 s_f + \gamma_1 \gamma_2 s_r \tag{3-7}$$

Substitution of Equation (3-7) into Equation (3-1) results in the controlling differential equation for the charge accumulation:

$$\frac{ds_r}{dt} + \left(\frac{1}{\tau} + \frac{Q}{v} - \gamma_1 \gamma_2 \frac{Q}{V}\right)s_r = \frac{\gamma_1 Q}{V} s_f \tag{3-8}$$

Integration of Equation (3-8) for time invariant parameters gives the following:

$$s_r = \frac{\gamma_1 s_f}{\frac{V}{Q\tau} + 1 - \gamma_1 \gamma_2}\left[1 - e^{-\left(\frac{1}{\tau} + \frac{Q}{V} - \gamma_1 \gamma_2 \frac{Q}{V}\right)t}\right] \tag{3-9}$$

where s_o is the initial charge density in the fluid at $t = o$ and is generally negligible with respect to s_r at $t > 0$.

When t becomes large with respect to $\frac{1}{\tau} + \frac{Q}{V}(1 - \gamma_1 \gamma_2)$, then Equation (3-9) can be expressed as follows:

$$\hat{s}_r(t = \infty) = \frac{\gamma_1 s_f}{\frac{V}{Q\tau} + 1 - \gamma_1 \gamma_2} \tag{3-10}$$

where $\hat{s}_r$ is the limiting value of s_r as $t \to \infty$. For high flow rates and

low fluid electrical conductivities, the values γ_1 and γ_2 are approximately equal to unity. This implies that little charge relaxation is occurring during the flow of the fluid through the pipes. In this case Equation (3-10) is reduced to

$$\hat{s}_r = \frac{s_f}{V/Q\tau} \tag{3-11}$$

The term $V/Q\tau$ or $(V/Q)/\tau$ is the ratio of residence time of the fluid in the reservoir to the fluid charge relaxation time. For large values of residence time the steady-state charge level, $\hat{s}_r$, becomes small because the fluid has a chance to discharge in the reservoir. If V/Q is small, however, the reservoir charge level can build to extreme amounts.

As an example of the relationship of Equation (3-11), consider a hydraulic fluid with dielectric constant equal to 2.0 and conductivity equal to 1×10^{-12} mho/m; thus, the relaxation time is equal to

$$\tau = \frac{\epsilon \epsilon_o}{K} = \frac{(2)(8.85 \times 10^{-12} \text{ sec}/\Omega\text{m})}{1 \times 10^{-12}/\Omega\text{m}} = 17.7 \text{ sec} = 0.3 \text{ min}$$

Figure 7 illustrates the relationship between $\hat{s}_r$ and s_f for various ratios of V/Q. For the standard multi-pass filtration performance test (27) the ratio V/Q = 0.25 minutes, thus the charge accumulating in the reservoir is approximately 1.2 times greater than the charge generated by the filter.

In summary the exponential equation for describing the charge build-up in a recirculating system is based upon the following assumptions:

1. Fluid conductivity is constant.
2. Mean velocity of charge carriers and mean velocity of liquid are equal.

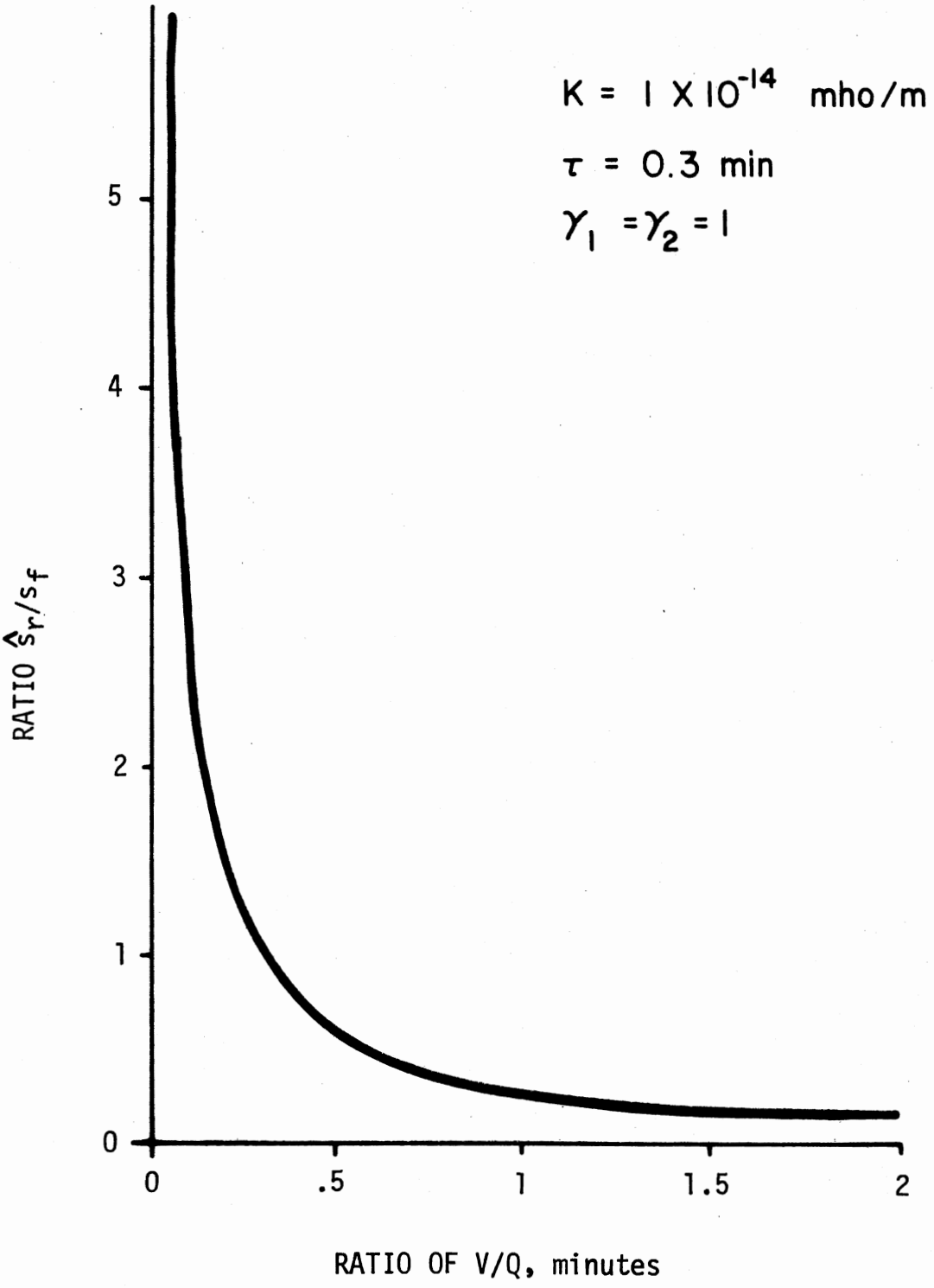

Figure 7. Relationship Between Charge Accumulation and Reservoir Residence Time

3. Electric field is constant over cross-section of liquid and piping.
4. Uniform instantaneous fluid and charge mixing in reservoir.
5. Pipe and reservoir walls are metal (electrically conductive) and grounded.
6. No significant charge is generated outside of the filter.

For greater accuracy, the charge generated at the liquid/wall interface in the piping can be added to the equation for charge accumulation. Tests conducted as part of this investigation without a filter in the circuit showed that this charge generation was generally low for most situations encountered. Thus, Equations (3-9) and (3-10) can be utilized to predict static charge accumulation under the exponential charge relaxation rule.

Generalized Charge Accumulation Model

The hyperbolic law of charge relaxation as presented by Vallenga and Klinkenberg (13) could also be used to predict charge accumulation. This rule applies when the electrical conductivity of the fluid is directly proportional to the charge density. This would occur, in an extreme case, when all ions of one polarity, depending upon the affinity that the particular filter has for absorbing a certain polarity ion, are removed from the liquid. Such a condition could generally exist only for fluids with an extremely low equilibrium conductivity and the effective conductivity would, thus, be entirely due to ions of the sign that constitute the net charge density.

The hyperbolic model requires that the equilibrium conductivity be equal to zero when there is no unbalance of charge in the fluid. Because

common hydraulic fluids definitely have a measurable conductivity in an equilibrium state, it is reasonable to assume that the charge relaxation could not follow the hyperbolic model precisely. A more generalized and realistic model for the conductivity of hydraulic fluids can be written as a combination of an equilibrium conductivity term and an additional term that is a function of the charge density. Thus, the conductivity can be expressed as:

$$K = K_e + K_o \, s^n \tag{3-12}$$

where:

K = effective conductivity, $1/\Omega m$

K_e = equilibrium conductivity, $1/\Omega m$

K_o = proportionality constant, $m^{3n-1}/\Omega C^n$

s = charge density, C/m^3

n = constant in exponent

Such a conductivity generalized model has characteristics of both the exponential law where conductivity is constant and the hyperbolic law where effective conductivity increases as charge increases. Figure 8 illustrates the relationship between conductivity and charge density for the various models.

In order to utilize Equation (3-12), the actual fluid charge density is normalized by a theoretical value which the fluid would possess at equilibrium conditions. By using the relationships from Reference (13) this reference value would be K_e/u where u is the ion mobility. Thus, the constant K_o in Equation (3-12) can be expressed as:

$$K_o = \frac{u^n}{K_e^{n-1}} \tag{3-13}$$

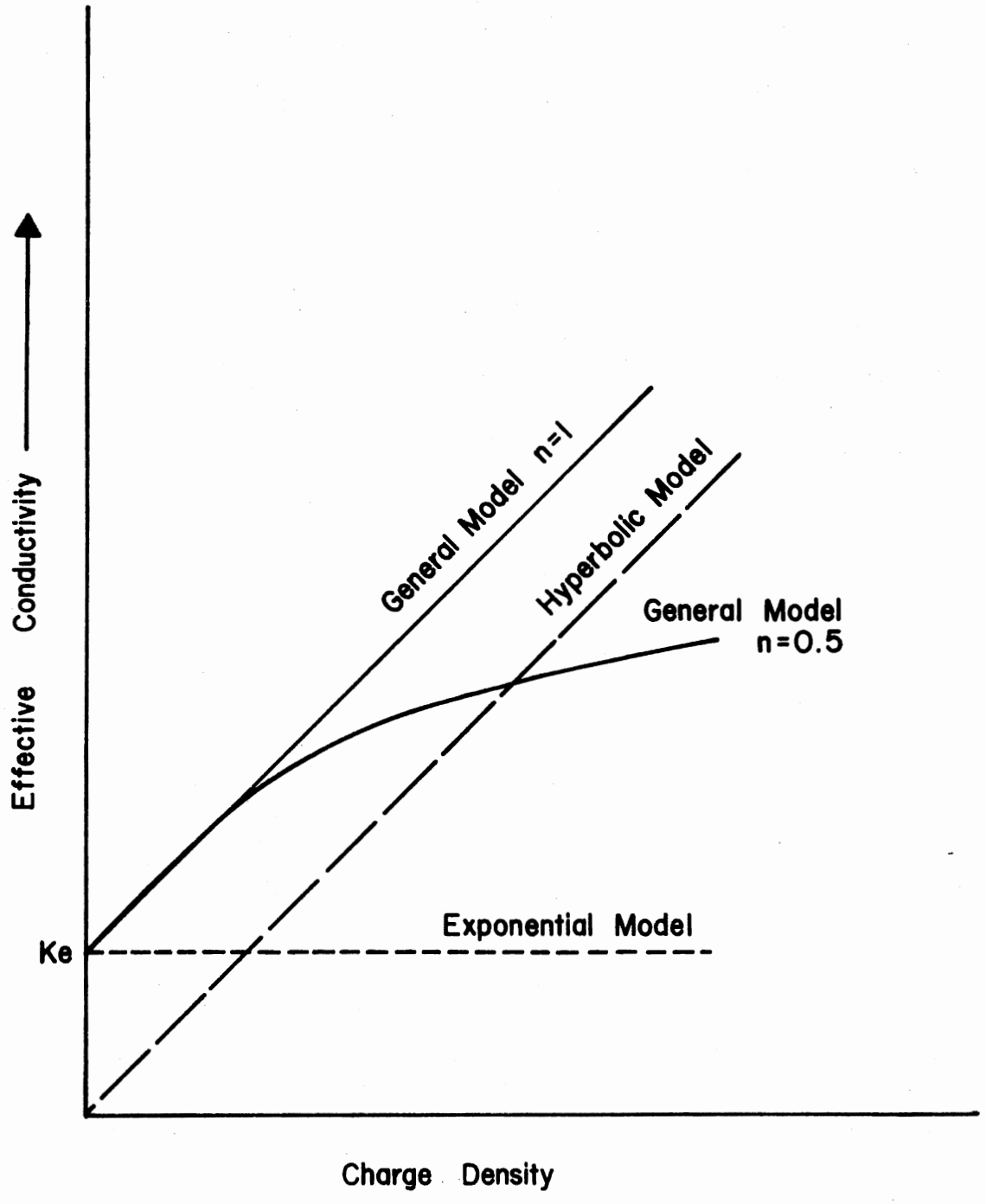

Figure 8. Various Fluid Conductivity Models

The generalized charge relaxation law can then be derived by using Equation (3-12) in Equation (2-4) to obtain the following:

$$\frac{ds}{dt} = -\frac{s}{\tau} = -\frac{s(K_e + K_o s^n)}{\varepsilon \varepsilon_o} = -\frac{s K_e}{\varepsilon \varepsilon_o} - \frac{K_o s^{n+1}}{\varepsilon \varepsilon_o} \qquad (3\text{-}14)$$

The first term of Equation (3-14) represents the term found in the exponential model and the second term is the relationship due to charge effects. Integration of Equation (3-14) results in the following:

$$s = \left[-\frac{K_o}{K_e} + (s_o^{-n} + \frac{K_o}{K_e}) e^{\frac{n K_e t}{\varepsilon \varepsilon_o}} \right]^{-\frac{1}{n}} \qquad (3\text{-}15)$$

where s_o is the initial charge density at time = o.

Equation (3-15) represents a generalized model for the relaxation of charged hydraulic fluid when the fluid is undergoing no movement. Substituting Equations (3-14) into Equation (3-1) for a multi-pass hydraulic system configuration gives the following:

$$\frac{d s_r}{dt} = -\frac{s_r K_e}{\varepsilon \varepsilon_o} - \frac{K_o s_r^{n+1}}{\varepsilon \varepsilon_o} - s_r \frac{Q}{V} + s_i \frac{Q}{V} \qquad (3\text{-}16)$$

From Equation (3-15), s_i can be expressed in terms of charge density immediately downstream of the filter as:

$$s_i = \left[-\frac{K_o}{K_e} + (s_d^{-n} + \frac{K_o}{K_e}) e^{\frac{n K_e A_\ell \ell_d}{Q \varepsilon \varepsilon_o}} \right]^{-\frac{1}{n}} \qquad (3\text{-}17)$$

and the charge immediately upstream of the filter can be expressed as:

$$s_u = \left[-\frac{K_o}{K_e} + (s_r^{-n} + \frac{K_o}{K_e}) e^{\frac{n K_e A_\ell \ell_u}{Q \varepsilon \varepsilon_o}} \right]^{-\frac{1}{n}} \qquad (3\text{-}18)$$

Let the constants τ_e, γ_3 and γ_4 be defined as:

$$\tau_e \equiv \frac{\mathfrak{C}\,\mathfrak{E}_o}{K_e}$$

$$\gamma_3 \equiv \exp\left(\frac{n\,A_\ell\,\ell_d}{Q\,\tau_e}\right)$$

$$\gamma_4 \equiv \exp\left(\frac{n\,A_\ell\,\ell_u}{Q\,\tau_e}\right)$$

then substitution of Equations (3-17) and (3-18) into Equation (3-16) give the following:

$$\frac{d\,s_r}{dt} = -\frac{s_r}{\tau_e} - \frac{K_o\,s_r^{n+1}}{\mathfrak{C}\,\mathfrak{E}_o} - \frac{s_r\,Q}{V} + \frac{Q}{V}\left\{\gamma_3\left[s_f + \gamma_4 s_r^{-n} + \frac{K_o}{K_e}(\gamma_4 - 1)\right]^{-\frac{1}{n}} + \frac{K_o}{K_e}(\gamma_3 - 1)\right\}^{-\frac{1}{n}} \tag{3-19}$$

Equation (3-19) is the governing differential equation for charge relaxation under the generalized law. Under steady-state conditions (for $t \to \infty$) the right hand side of Equation (3-19) can be set equal to zero then solved for $\hat{s}_r$ in terms of s_f as was done with the exponential model previously. Equation (3-19) is rather complex equation for such a simple system as assumed for the multi-pass system; however, a solution can readily be accomplished on a computer or the equation can be solved in parts. The next chapter presents graphical illustrations of charge relaxation under the generalized model for a particular test facility and hydraulic fluid.

Hydraulic Filter Performance Models

Because of the complicated structure of a fibrous hydraulic filter, it is not generally practical to derive equations for overall separation

efficiency based upon the fundamental properties of the filter fibers themselves. A generally accepted technique is to consider the filter on a macroscopic basis and develop empirical equations describing the separation characteristics. The following is a development of a proposed model for the separation performance of a hydraulic filter as a function of particle size.

If a hydraulic filter is considered as a "black box", one can describe the particle separation characteristics by merely examining the influent and effluent particle size distributions. As shown in the previous chapter the filtration ratio (β) characteristics can be determined by dividing the upstream contamination level by the downstream. Likewise the efficiency is simply $1 - 1/\beta$. If the particle size distribution in the upstream and downstream fluids can be mathematically described, the efficiency or "effective pore size distribution" can also be determined.

It is well documented (28-31) that most particle size distributions occurring in nature exhibit a log-normal frequency distribution of size. Herdan (28), states that pulverized silica, granite, calcite, limestone, quartz, ... all give size distributions which can be satisfactorily fitted by the logarithmic form of the normal law. The probability density function for a log-normal distribution is given by

$$f(D_p) = \frac{1}{\sqrt{2\pi}\,\ln \sigma_g} \exp\left[-\frac{(\ln D_p - \ln \overline{D}_g)^2}{2 \ln^2 \sigma_g}\right] \quad D_p > 0,\ \sigma_g > 1 \qquad (3\text{-}20)$$

$$= 0 \qquad \text{elsewhere}$$

where:

D_p = particle size

$\overline{D}_g$ = geometric mean particle size

σ_g = geometric standard deviation

The particle size distribution for AC Fine Test Dust which is utilized in the standard multi-pass filter test has a log-normal distribution. For simplicity, Cole (31) made the assumption that $\ell n\, \overline{D}_g$ is small compared to $\ell n\, D_p$ (actually $\overline{D}_g$ was assumed equal to unity, thus, $\ell n\, \overline{D}_g = 0$) and arrived at the log-log squared distribution commonly used in the Fluid Power Industry for plotting the cumulative size distribution of system contaminants. Thus, Equation (3-20) can be reduced to:

$$\ell n\, \overline{N} = \ell n\, A - B\, \ell n^2\, D_p \qquad (3\text{-}21)$$

where A and B are constants. Figure 9 illustrates the size distribution of AC Fine Test Dust plotted on log-log^2 coordinates.

The log-normal distribution has a special characteristic, unlike the normal or Gaussian distribution, in that all moments (multiplication of the distribution by the variable itself) of the log-normal distribution have similar distribution forms. An efficiency calculated from two log-normal particle size distributions should, thus, also be distributed log-normally. Corte (32), in describing the pore size distribution of a fibrous paper from a geometric consideration of the random nature of the fiber network also concluded that the size distribution followed a log-normal law.

From an experimental standpoint, it is convenient to plot particle separation characteristics on log probability coordinates in order to determine the parameters of the log-normal equation describing the phenomenon. As an example, consider a filter with efficiency characteristics described by the graph of Figure 10. The "geometric mean" particle size is read directly from the graph at the 50% separation

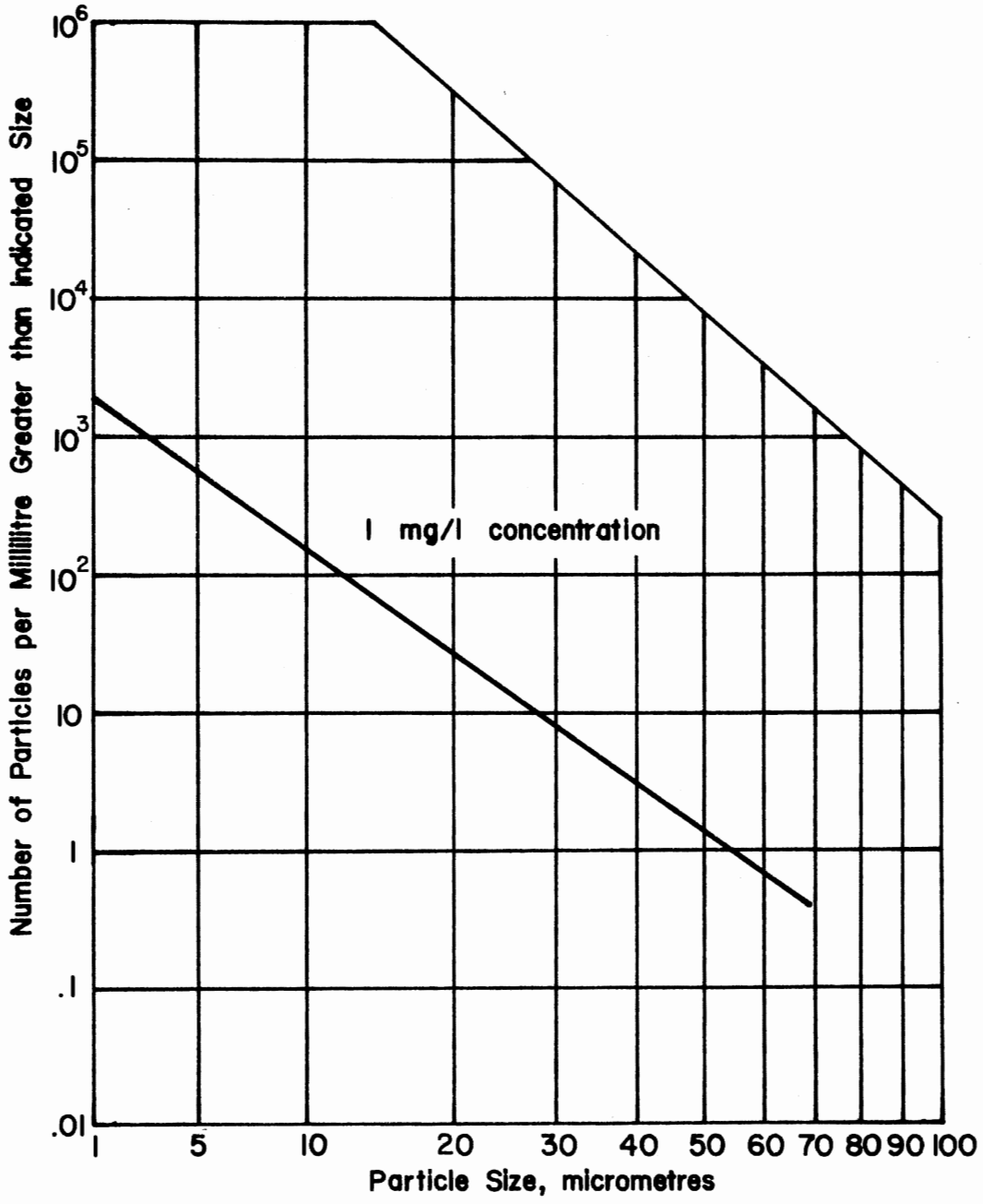

Figure 9. Particle Size Distribution of AC Fine Test Dust

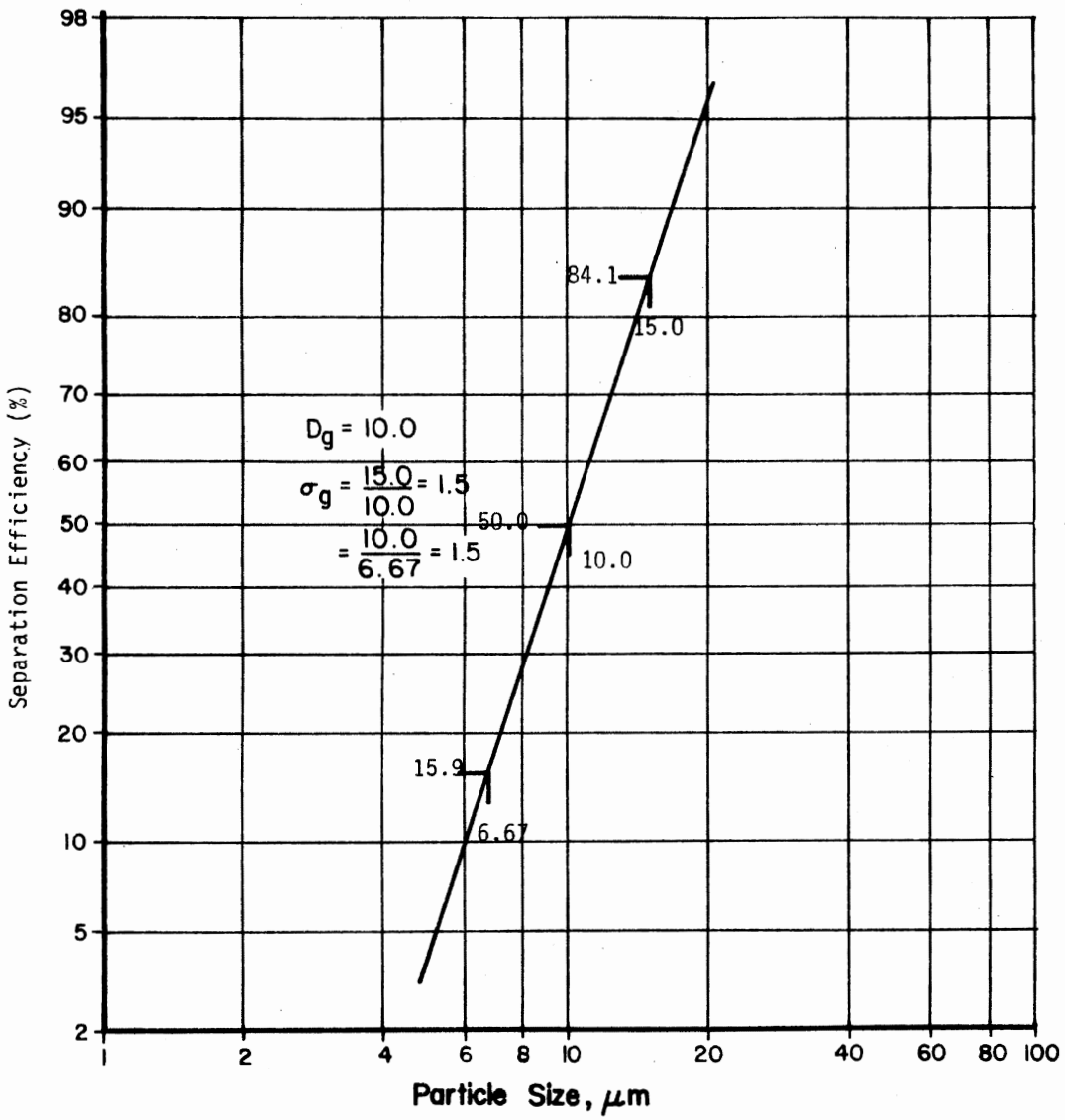

Figure 10. Example Filter Efficiency Characteristics

efficiency point as 10 μm. The geometric standard deviation for a log-normal distribution can be found by using the following relationship (30):

$$\sigma_g = \frac{84.13\% \text{ size}}{50\% \text{ size}} = \frac{50\% \text{ size}}{15.87\% \text{ size}} \qquad (3\text{-}22)$$

$$\sigma_g = 1.5 \text{ for example filter}$$

The efficiency at any given particle size is described by the following equation:

$$\eta(D_p) = \int_0^{\ln D_p} \frac{1}{\sqrt{2\pi}\ \ln \sigma_g} \exp\left[-\frac{(\ln D_p - \ln \overline{D}_g)^2}{2 \ln^2 \sigma_g}\right] d \ln D_p \qquad (3\text{-}23)$$

where the values of $\overline{D}_g$ and σ_g are determined from the log-probability graph. Since such probability integrals cannot be evaluated by exact methods, series approximations or tables are generally used. In order to use standard tables, it is more convenient to change the log-normal probability integral to one having a standard normal form with zero mean and a variance of unity. It can be shown using techniques from Reference (33) that the log-normal probability integral of Equation (3-23) can be determined as:

$$\eta(D_p) = F\left(\frac{\ln D_p - \ln \overline{D}_g}{\ln \sigma_g}\right) \qquad (3\text{-}24)$$

where F(z) is the probability that a random variable having a standard normal distribution assumes a value less than or equal to z. The values for F(z) can be found in standard tables in most statistical reference books.

For the example filter given in Figure 10, the total efficiency

curve is described by the two parameters $\overline{D}_g$ and σ_g (10.0 and 1.5, respectively). In order to calculate the efficiency at some other particle size, e.g., 12.5 μ M, Equation (3-24) can be applied as follows:

$$\eta(12.5) = F\left(\frac{\ell n\ 12.5 - \ell n\ 10.0}{\ell n\ 1.5}\right) = F(.55) = .709 = 70.9\%$$

which is agreement with the curve of Figure 10.

Fitch and Tessmann (34) presented a set of models for hydraulic filter separation performance based upon several hundred filter test conducted at Oklahoma State University. Figure 11 illustrates these models plotted on a special "beta" scale ordinate (34) versus $\log^2$ particle sized on the abscissa. The β_{10} identifiers on each model corresponds to the filtration ratio or β value at ten micrometers.

The filtration ratios for the filter models of Figure 11 can be converted to efficiency by $1 - 1/\beta$. When these curves are transposed on log-probability coordinates, their approximate straight-line relationships are obvious as illustrated in Figure 12. This implies that they definitely do follow the log-normal law and, thus, the efficiency can be described by the probability integral of Equation (3-23) or solved for by using Equation (3-24). It should be noted that most of the lines on Figure 12 are approximately parallel which indicates that the geometric standard deviation term in the probability model is approximately constant. The only line which deviated significantly from the parallel lines was the curve for the $\beta_{10} = 1000$ model. There were very few filters in this performance range which were evaluated to establish the beta ten models; thus, errors in the estimated curve are possible and, in fact, if more data were available, the efficiency model for the

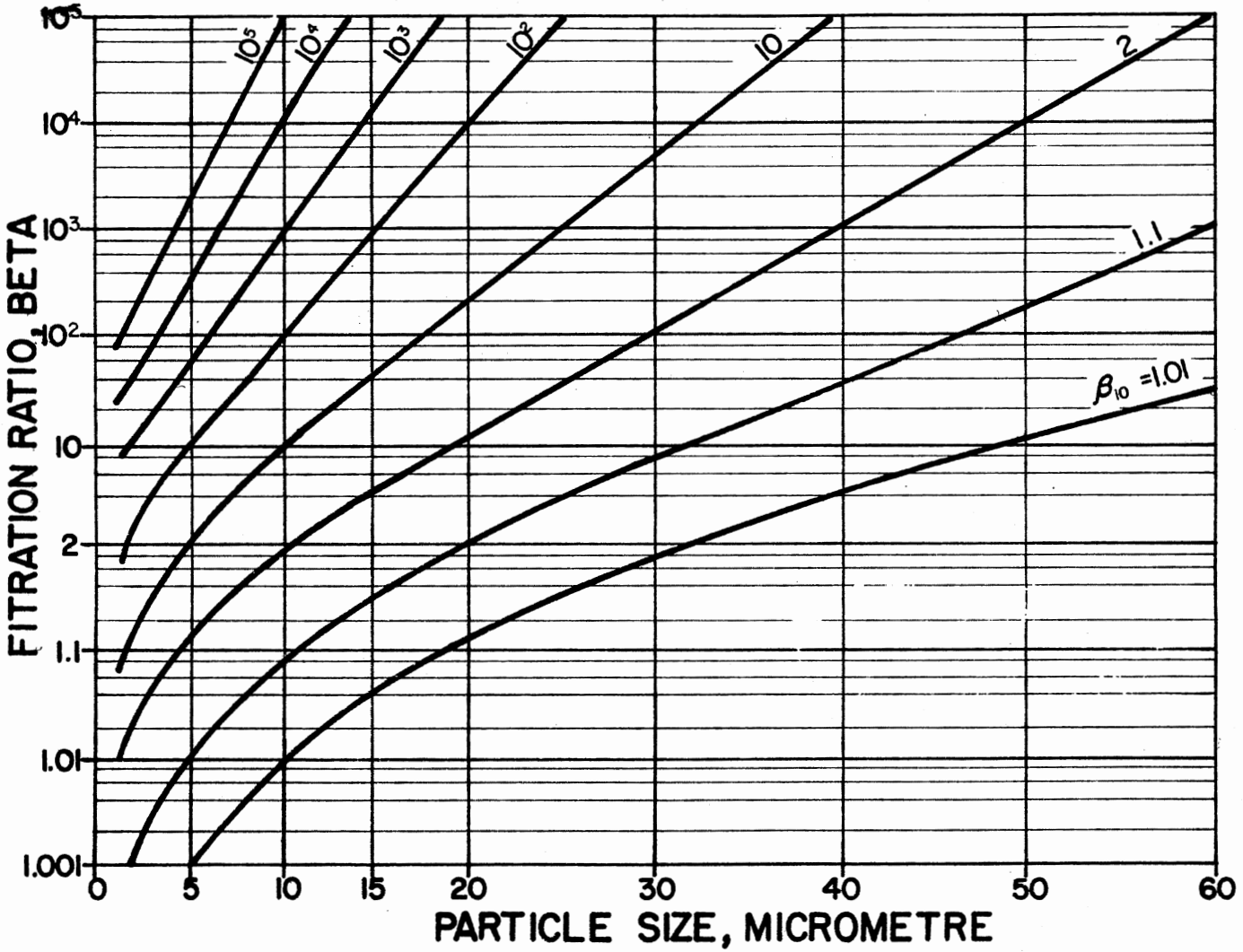

Figure 11. Beta Ten Filter Models

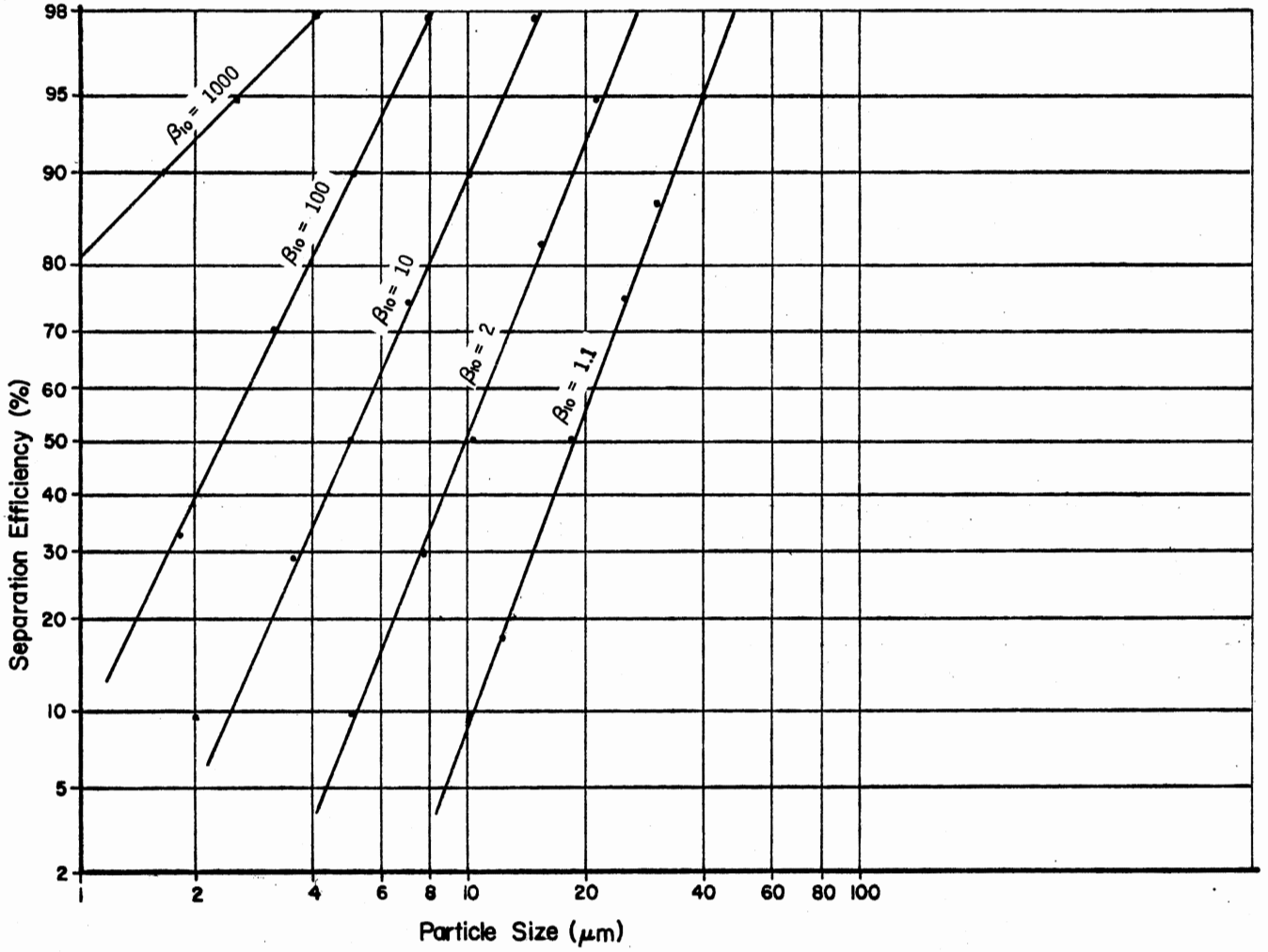

Figure 12. Beta Ten Filter Models on Log-Probability Coordinates

β_{10} = 1000 filter might be parallel to the others.

With a log-normal model for the performance characteristics of hydraulic filters such as given by Equation (3-23), the efficiency at each particle size can be found. If electrostatic charge influences the performance of a filter, it should be recognizable in the values for $\overline{D}_g$ and σ_g and also on plots on log probability coordinates. Chapter V illustrates this effect of electrostatic charge, and presents empirical developments of relationships between charge and filtration efficiency.

CHAPTER IV

CHARGE ACCUMULATION TEST RESULTS

In order to determine levels of electrostatic charge which can accumulate in a recirculating hydraulic system and also to verify the relationships developed in the previous chapter, a number of experimental tests were conducted. Because the fluid conductivity appeared to be an important controlling parameter, several tests were performed to determine the relationship between conductivity, relative humidity, particulate contamination, and additives. In addition, experiments were conducted to determine the effects of conductivity and flow rate upon charge accumulation.

Fluid Conductivity Experiments

Personal experiences and discussions with other laboratories have led the author to believe that the electrostatic charge accumulation in a hydraulic test stand is a function of the relative humidity of the surrounding atmosphere. The most obvious method by which relative humidity may affect charge generation is by an apparent change in the effective fluid conductivity. A series of tests were conducted to determine this effect of relative humidity.

The multi-pass filter test stand described in Appendix A was utilized in these experiments. Before starting, the stand was drained and thoroughly flushed, then new fluid was added directly from an

unopened drum. MIL-H-5606 hydraulic fluid was utilized in all experiments because it is commonly used in aircraft hydraulic systems and is specified in the standard multi-pass filter test procedure (27). The fluid was allowed to circulate while the relative humidity of the surrounding environment was maintained constant for up to 48 hours. Measurements of fluid conductivity were then made using the DC method described in Appendix C. Table I and Figure 13 delineate the results from this experimental phase.

TABLE I

EFFECT OF RELATIVE HUMIDITY ON CONDUCTIVITY*

RH%	Conductivity, pmho/m
23	2.4
35	3.4
45	4.3
55	4.9
70	6.2
80	7.6

*MIL-H-5606, 38°C.

In addition to relative humidity, it was expected that particulate contamination added to the test fluid would also affect the conductivity.

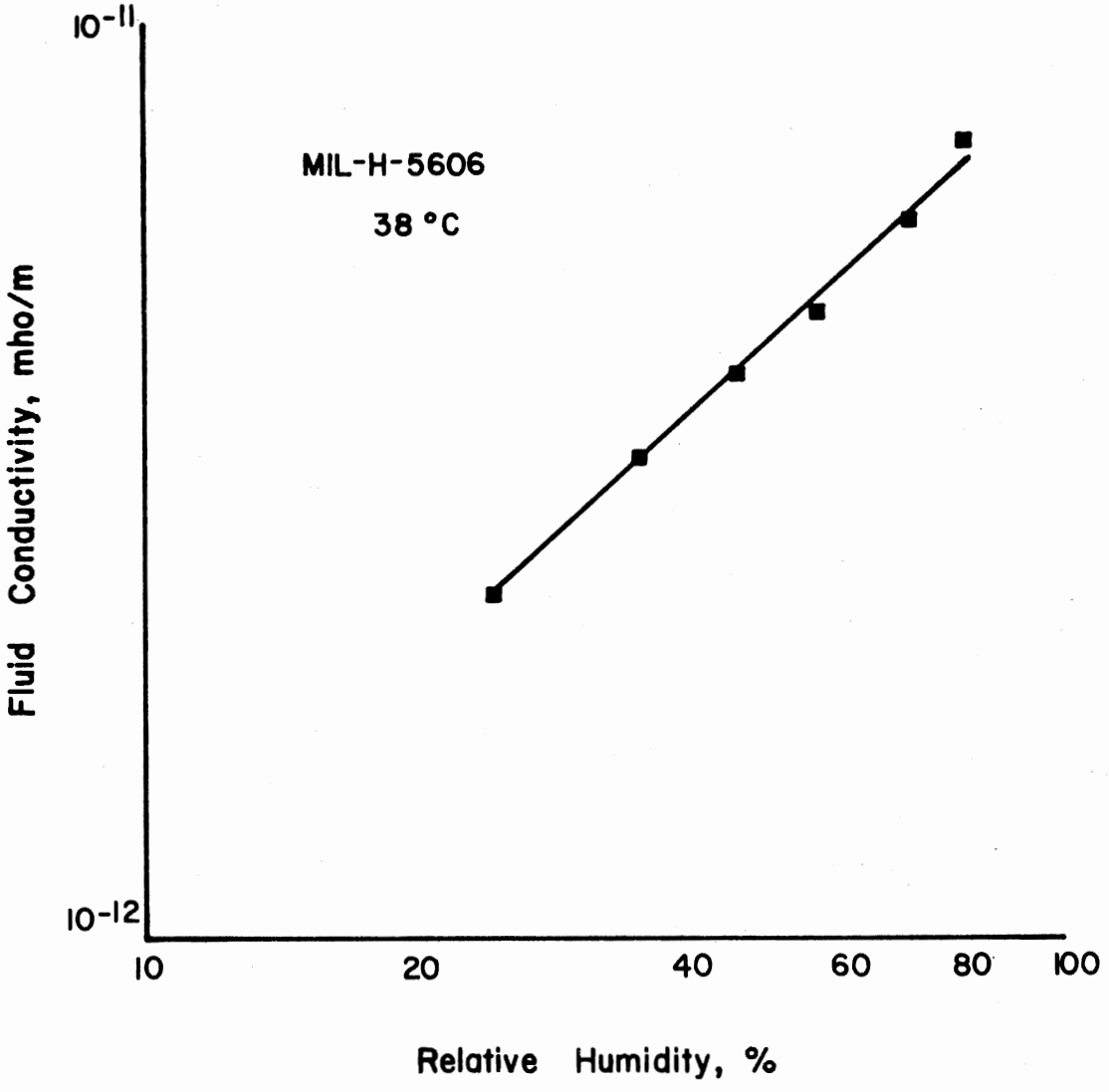

Figure 13. Effect of Relative Humidity on Conductivity

Experiments were conducted by adding a controlled quantity of both AC Fine Test Dust and classified 0-5 μm dust to the MIL-H-5606 hydraulic fluid. AC Fine Test Dust (ACFTD) has a particle size distribution spanning 0-80 μm while the classified dust utilized was segregated into a 0-5 μm size interval. Table II and Figure 14 present the results of these experimental tests.

TABLE II

EFFECT OF PARTICULATE CONTAMINATION ON FLUID CONDUCTIVITY*

Type of Dust Added	Amount (mg/l)	Conductivity (pmho/m)
ACFTD	0	2.4
ACFTD	10	2.5
ACFTD	25	2.7
ACFTD	50	3.0
ACFTD	100	3.0
ACFTD	200	3.3
0-5 μm	0	2.4
0-5 μm	50	4.0
0-5 μm	100	5.1

*MIL-H-5606, 23% R.H., 38° C.

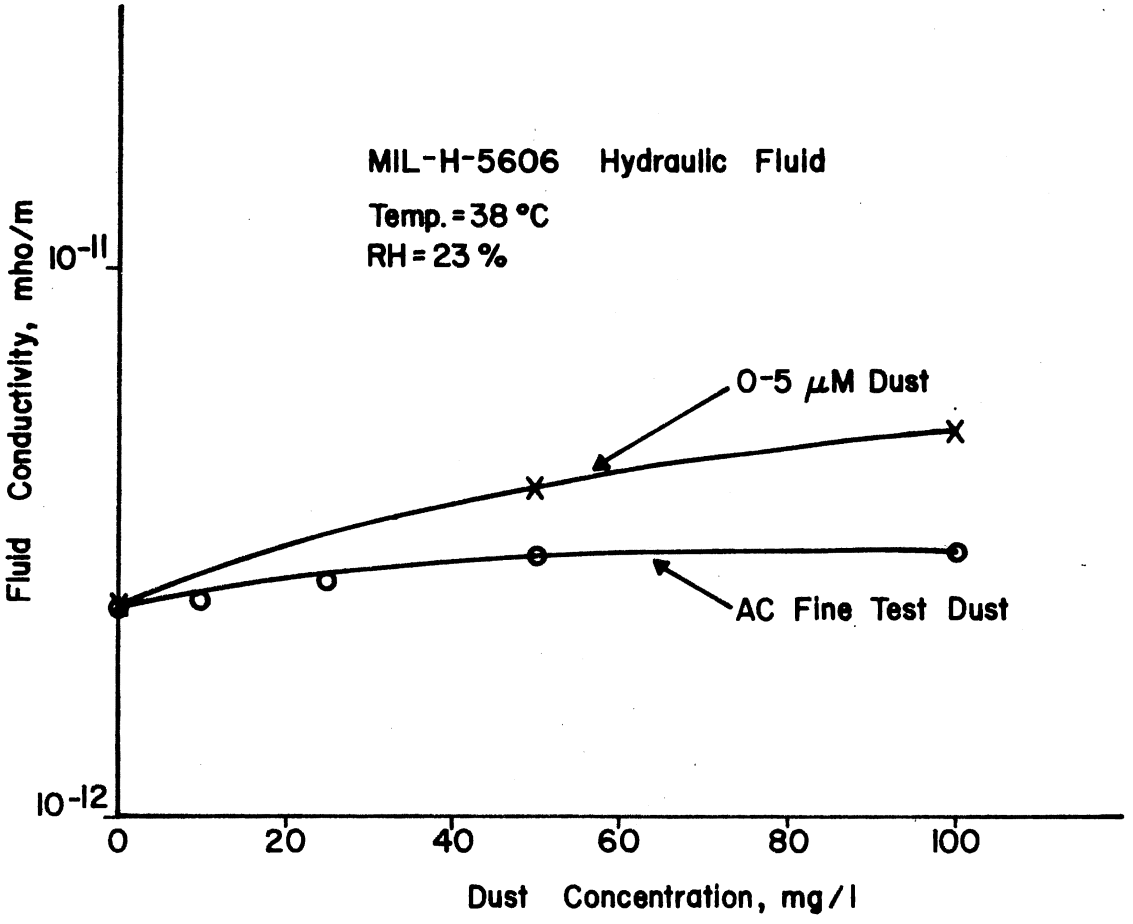

Figure 14. Effect of Particulate Contamination on Conductivity

It can be seen from Table II and Figure 14 that dust added to the base test fluid does indeed increase the measured conductivity. The 0-5 μm dust increased the conductivity a greater amount than the AC Fine Test Dust of the same concentration by weight. This is probably due to the much larger total surface area presented by an equal weight of smaller particles. Neither the addition of the full distribution AC Fine Dust nor the classified 0-5 μm fraction increased the conductivity as much as the relative humidity. In fact, neither the dust nor relative humidity can provide the order of magnitude changes in conductivity necessary to significantly affect the electrostatic charge generation and accumulation.

One final series of experiments were conducted on the fluid conductivity involving the addition of antistatic additives. Two types of additives — Shell ASA-3 and Ethyl DCA 48 — both commercially available, were added in various quantities to the test fluid. These additives were specifically formulated to increase the conductivity of hydrocarbons and thus reduce charge accumulation. They have been successfully used to prevent potential explosions in fueling systems due to static discharge.

Table III and Figure 15 illustrate the effects of the additives on the equilibrium conductivities of the hydraulic fluid. Both additives have similar effects which are much more dramatic than either relative humidity or particulate contamination. By adding a small quantity of either of the additives, the conductivity can be increased by orders of magnitude. On a relative basis, humidity changes or particulate impurities can only provide a small conductivity improvement.

TABLE III

EFFECT OF FLUID ADDITIVES ON CONDUCTIVITY*

Additive	PPM Additive	Temperature	Conductivity, pmho/m
ASA-3	2	38°C	16.9
ASA-3	5	38°C	39.9
ASA-3	10	38°C	65.4
ASA-3	40	38°C	247
DCA-48	0.05	21°C	4.8
DCA-48	0.1	21°C	5.3
DCA-48	0.5	21°C	5.8
DCA-48	1.0	21°C	7.0
DCA-48	5	21°C	22.6
DCA-48	10	21°C	33.5
DCA-48	50	21°C	89.3
DCA-48	100	21°C	136
DCA-48	500	21°C	372

*MIL-H-5606, 35% R.H.

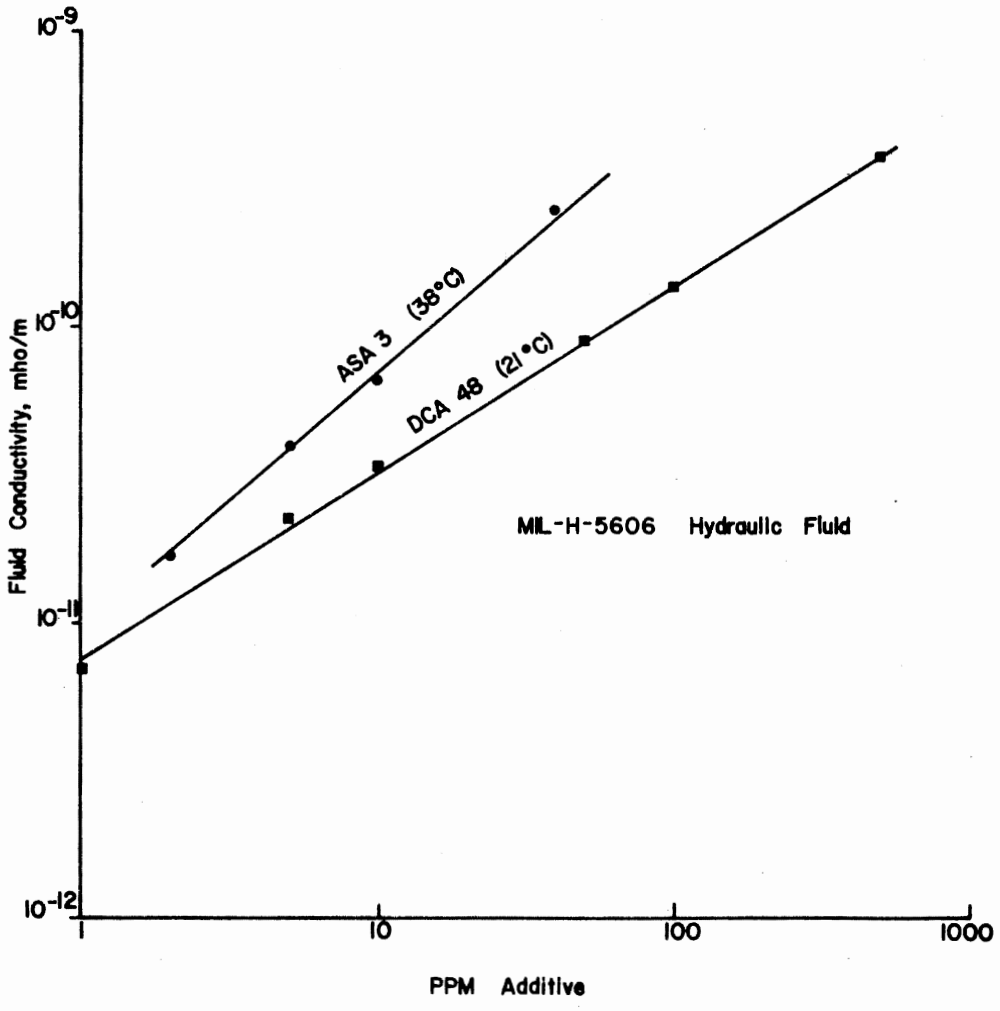

Figure 15. Effect of Additive Concentration on Fluid Conductivity

Charge Accumulation Characteristics

Before the experimental program was initiated, it was felt that electrostatic charge generated by flow through a test filter would accumulate a recirculating test facility. Because filter characteristics, flow rate, and conductivity were believed to be the most influential parameters controlling charge accumulation, and experimental program was devised to evaluate such interactions and to verify the charge accumulation models developed in the previous chapter.

A total of six different filter models were selected for this program as well as the particle separation tests discussed in the next chapter. The filters were donated by the filter manufacturers sponsoring this research effort as noted in the Preface. The filters span a range of efficiencies at 10 μm from 6% to greater than 98% and are representative of hydraulic filters utilized in current hydraulic systems throughout the industry. The manufacturer's rated flow for the filters was approximately 76 l/min with the exception of one filter which was rated at 114 l/min. The filter dimensional characteristics and rated flows are given in Table IV. In order to maintain confidentiality with the filter manufacturers who submitted the filters, they are identified simply as A, B, C, D, E, and F. Each letter identifier represents an entirely different filter type.

Streaming Current Measurements

Concurrent with the tests of conductivity versus relative humidity, measurements of streaming current were taken for the six test filters at different flow rates covering a range from 19 l/min up to 170 l/min.

TABLE IV

TEST FILTER DESCRIPTIONS

Filter Identification	Element Length, cm	Element Width, cm	Approximate Medium Surface Area, m^2	Rated Flow, l/min
A	22.8	11.2	0.768	114
B	20.2	11.0	0.728	76
C	20.2	11.0	0.628	76
D	20.2	11.0	0.465	76
E	22.9	9.8	0.850	76
F	11.0	7.8	0.243	76

Streaming current was measured with a Keithley model 610 C electrometer by placing electrode grids upstream and downstream of the test filter housing as described in Appendix C. Appendix C also contains typical data collected.

Because the complete test system utilized was grounded — metal piping, metal fittings, metal housing, etc. — it is recognized that the streaming current values measured are probably not equal to the exact values generated by the filters. Some of the charge generated would be transferred back upstream of the filter through the piping thus the current measurements would not be correct. The values measured, therefore, can not be taken as precise numbers but can be utilized to illustrate trends. It can be concluded from the measurements that the streaming current does increase with increasing flow rates. Tests conducted at various fluid conductivities produced similar effects; however, the current generated was much lower at higher conductivities.

Charge Accumulation Model Verification

To provide a technique for measuring the electrostatic charge accumulating in a recirculating hydraulic system, a method for measuring charge density in the fluid was developed. The procedure utilized is described in Appendix C and involves the use of a Faraday cage constructed with two concentric stainless steel cylindrical vessels. The fluid was introduced into the inner container and the potential between the two containers was measured with the Keithley electrometer. The electrostatic charge density could then be calculated from the measured voltage, the cell capacitance and the fluid quantity.

In order to verify the charge accumulation models developed in

Chapter III it would be ideal to measure the charge density in the reservoir for a given filter charge generation rate. However, in the actual case, the charge generated by the filter is unknown in advance and the charge density directly within the reservoir is difficult to measure. It is convenient to sample the system fluid upstream and immediately downstream of the test filter as illustrated in Figure 16.

The charge accumulation models presented in Chapter III for the exponential and generalized relaxation laws can be rewritten in terms of the steady state charge densities at other points in the system. If the value, $\hat{s}_x$, represents the steady state charge density at the upstream sample point then it can be described in terms of the value, $\hat{s}_d$, measured at the downstream sample point. For convenience we will introduce the value, R, as the charge transfer ratio such that R is expressed as follows:

$$R = \frac{\hat{s}_d}{\hat{s}_x}$$

The charge transfer ratio is thus the ratio of the charge density at the downstream sample point to the charge density at the upstream sample point under steady state conditions.

In order to calculate values of R for the test facility utilized, the following constants were measured:

ℓ_d = length of line downstream sample point to reservoir = 4.06 m

ℓ_x = length of line from reservoir to upstream sample point = 1.91 m

A_ℓ = cross-sectional flow area of lines = 3.84×10^{-4} m^2

ϵ = fluid dielectric constant = 1.79

V = system volume 40 ℓ

u = ion mobility = 5×10^{-9} m^2/volt sec (typical)

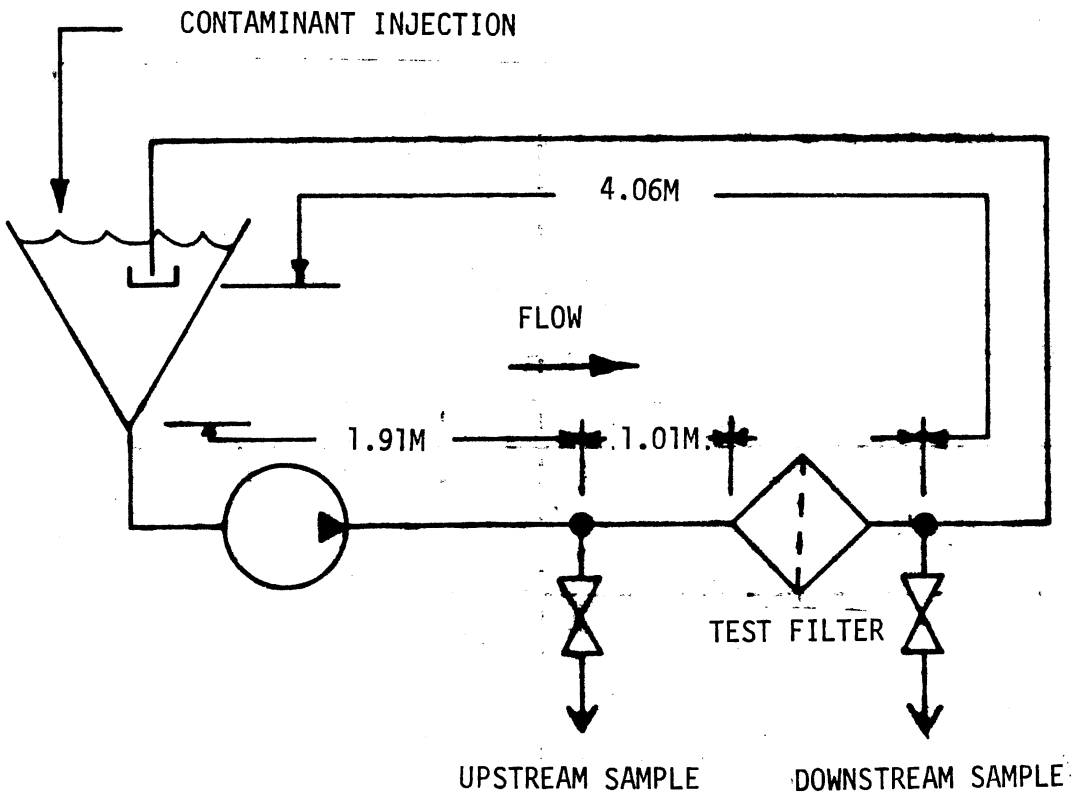

Figure 16. Test Schematic for Charge Accumulation Model

The value for ion mobility was not measured but taken as a typical value reported by References (5, 10). Figure 17 presents theoretical curves for the charge transfer ratio under the stated conditions at various conductivities and flow rates in accordance with the exponential relaxation law. Figure 18 illustrates similar curves for the generalized relaxation law; however, the conductivity was held constant at a value of 3.4×10^{-12} mho/m and the downstream charge density was allowed to vary since this level influences the charge relaxation under the generalized model. It can be noted that the curves in Figure 18 approach a curve in Figure 17 (for $K \approx 3/4 \times 10^{-12}$ mho/m) when the downstream charge density is low. At this point, the effects of the charge level upon the effective fluid conductivity in the generalized model become insignificant and the two models are equivalent.

Measurements of upstream and downstream charge density were made at various relative humidities and with various concentrations of anti-static additives. The data obtained for the tests at various humidities and no additive are presented in Appendix D. When the anti-static additive, ASA-3, was introduced into the fluid the upstream charge densities were so low that accurate measurements were impossible, thus no data were available at the extremely high conductivities.

Figure 19 illustrates the results from the charge values measured at a conductivity of 3.4 pmho/m for the various filters. The flow rate was varied from 19 to 170 l/min during these tests. It can be seen from Figure 19 that the measured charge transfer ratio was always higher than the theoretical values based upon the exponential model from Chapter III. The exponential law assumes that the effective conductivity is constant and equal to the equilibrium conductivity. The exponential law appears

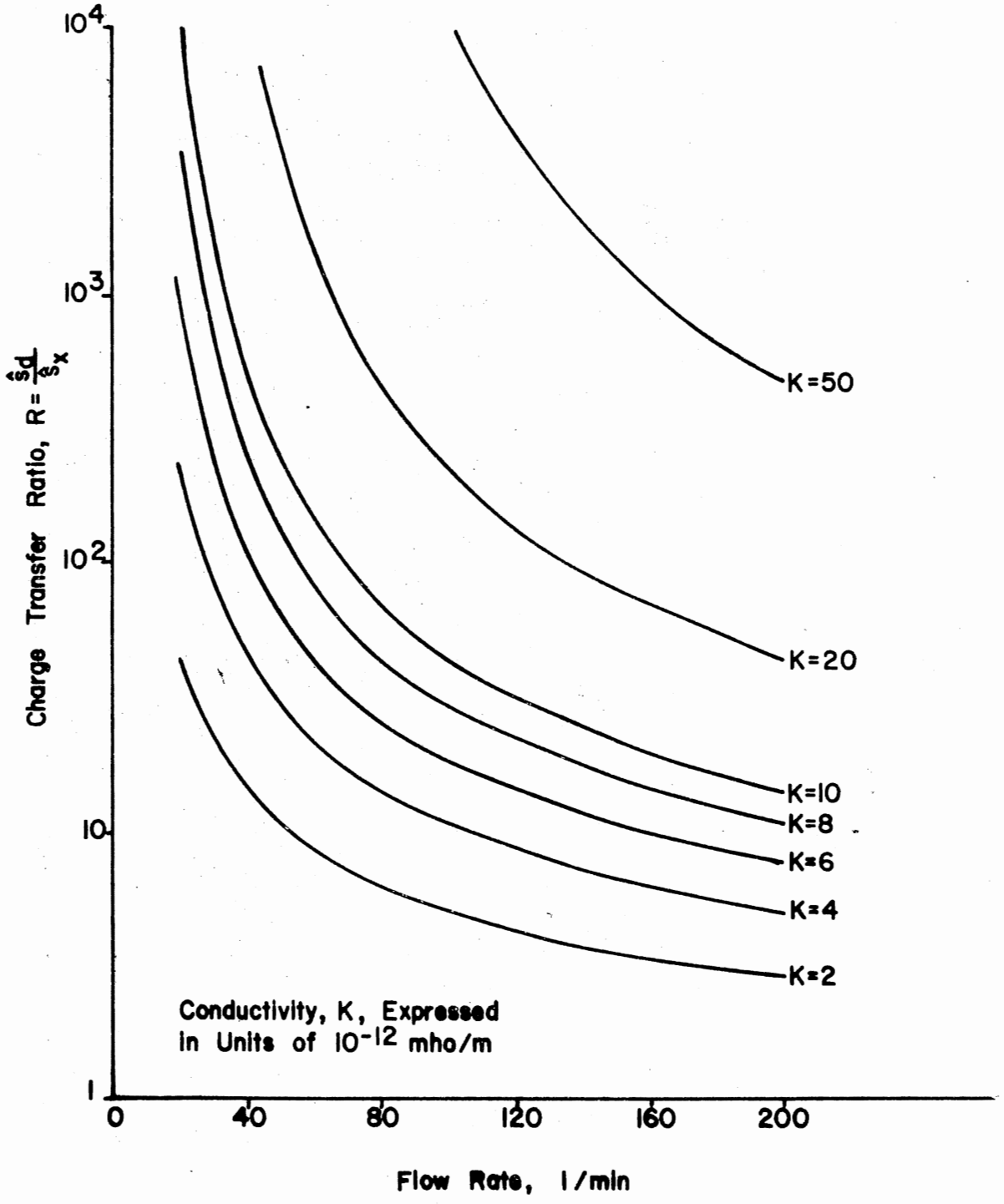

Figure 17. Exponential Charge Accumulation Model

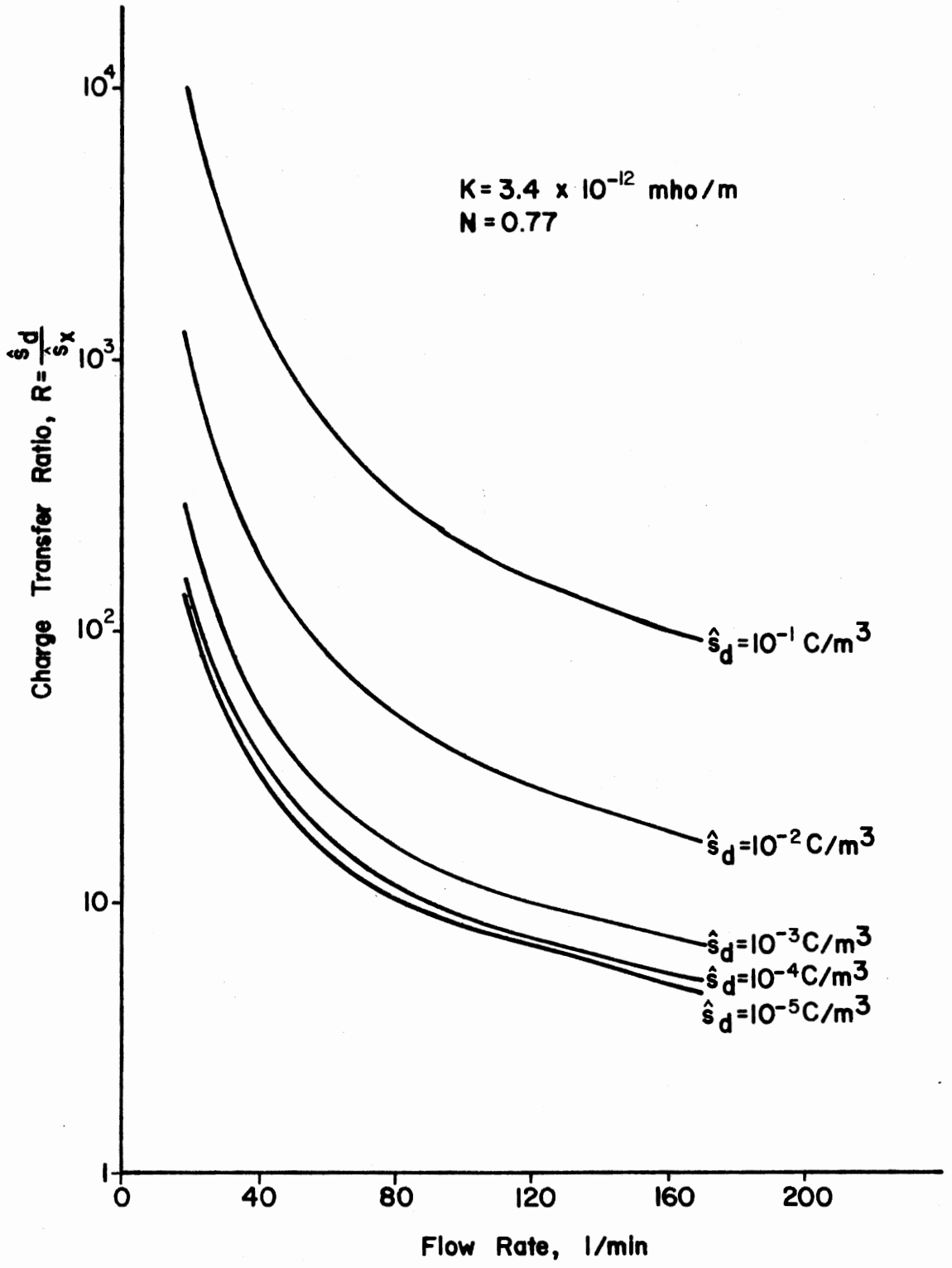

Figure 18. Generalized Charge Accumulation Model

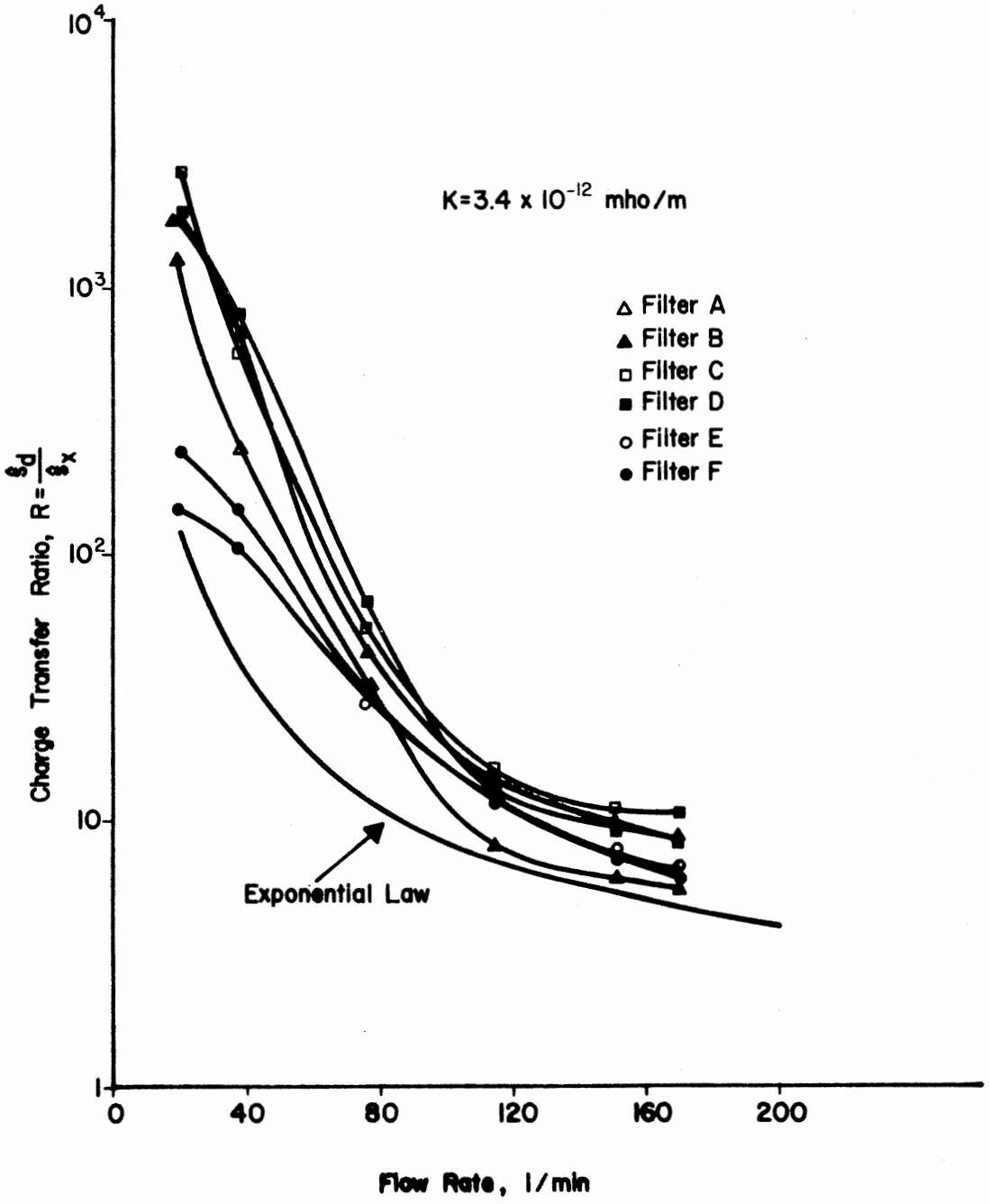

Figure 19. Charge Transfer and the Exponential Law

to be much closer to the actual data at 19 l/min, for instance, for filters E and F which both had much lower values of downstream charge density than the other filters. This would imply that the charge transfer ratio is indeed a function of the initial charge density as given by the generalized model.

In order to verify the generalized charge accumulation model as presented in Chapter III it was first necessary to determine the value for the exponent, n, in the conductivity versus charge equation:

$$K = K_e + K_o s^n$$

A computer program was written to calculate estimated values of $\hat{s}_x$ and R for the test conditions presented previously under various conditions of downstream charge densities, $\hat{s}_d$, and values for the exponent, n. A multiple correlation coefficient, r, was then calculated for the actual values of $\hat{s}_x$ versus the estimates using the technique from reference (35). The coefficient of determination was then calculated as r^2. An iterative searching computer routine was written based upon the golden section method given by Mischke (36) to maximize r^2 for various values of n. All 102 data points were considered and the computer produced a value for n = 0.77 and r^2 = 0.90.

Figure 20 illustrates the effect of flow and initial charge upon the charge transfer ratio under the generalized model for a value of K = 3.4 pmho/m and n = 0.77. Actual data points are superimposed about the theoretical curves. It can be seen that the actual data, although there appears to be some scatter, basically follows the theoretical curves. A possible explanation for the data scatter is the variations in the system fluid volume during the testing. Prior to conducting the

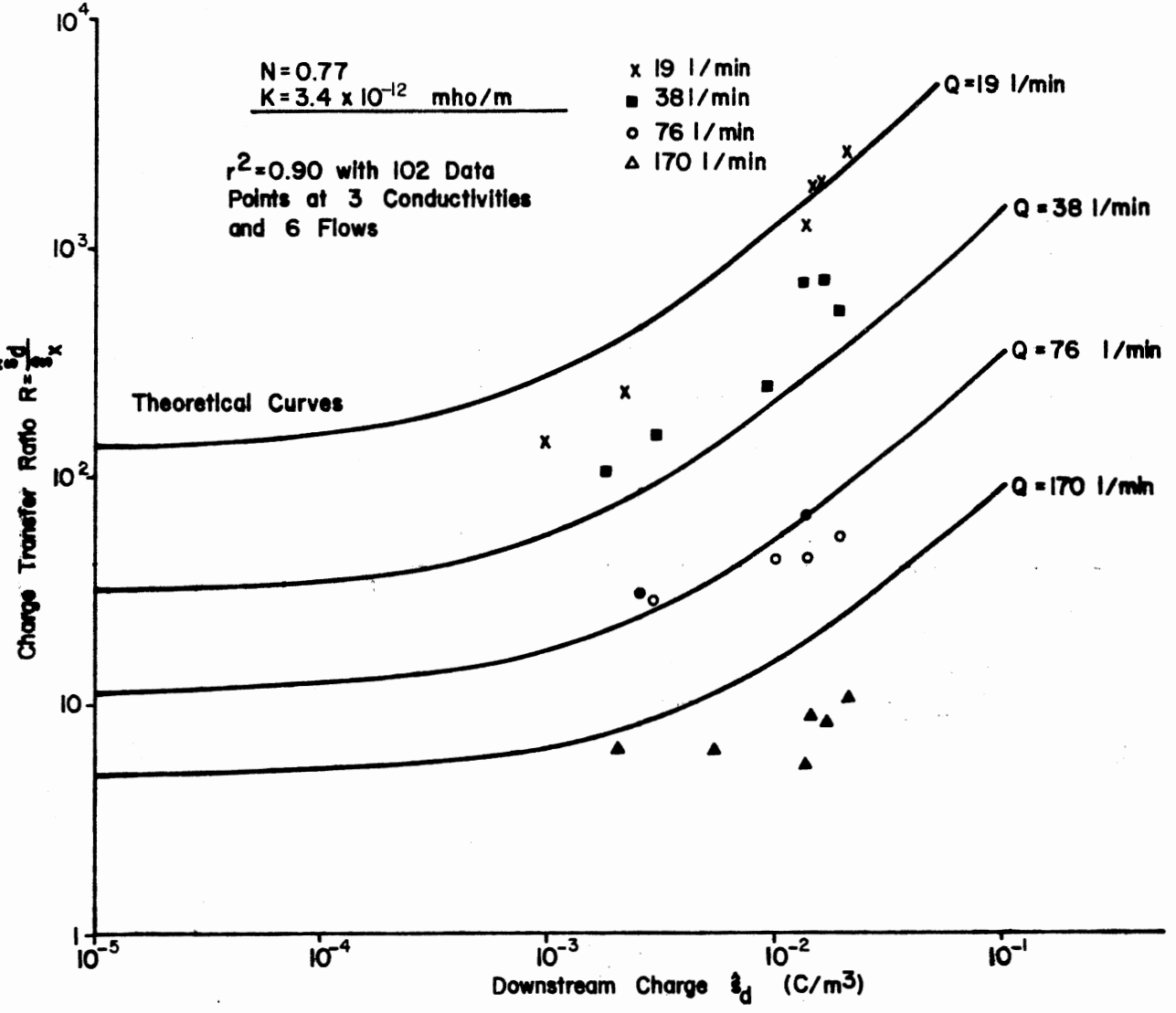

Figure 20. Effect of Flow and Charge Level Under the Generalized Model

experiments, the importance of the system volume in the charge accumulation relationships was not known. An attempt was made to maintain the system volume at approximately 40 litres; however, the volume did vary somewhat due to fluid sampling during the charge measurements.

In addition to the volume changes, another explanation for the difference between the actual and theoretical charge transfer ratios, especially at the higher flow rates, is the generation of charge by the fluid lines. The theoretical model for charge accumulation under the generalized law given in Chapter III is based upon the assumption that no charge is generated except that produced by the filter. In reality, at high flow velocities and low conductivities there will be some charge developed in the piping as shown by Klinkenbert (1) and others. For a more precise accumulation relationship, this additional charge generation should be considered; however, the flow velocity (7.4 m/sec) at which the larger variations from the theory were noted in these experiments were at least 2 to 3 times the values encountered in actual hydraulic systems. Thus, for most applications, the generalized charge accumulation model presented in Chapter III should apply.

Figure 21 illustrates the effect of conductivity and initial charge density upon the charge transfer ratio under the generalized model with $N = 0.77$ and $Q = 76$ l/min. Again, the actual data points are plotted by the theoretical curves. It can be seen that the actual data generally follows the theoretical model at the various conductivities. The coefficient of determination value, $r^2 = 0.90$, obtained when considering all 102 data points certainly indicates that the quality of the fit between the actual and estimated points is good.

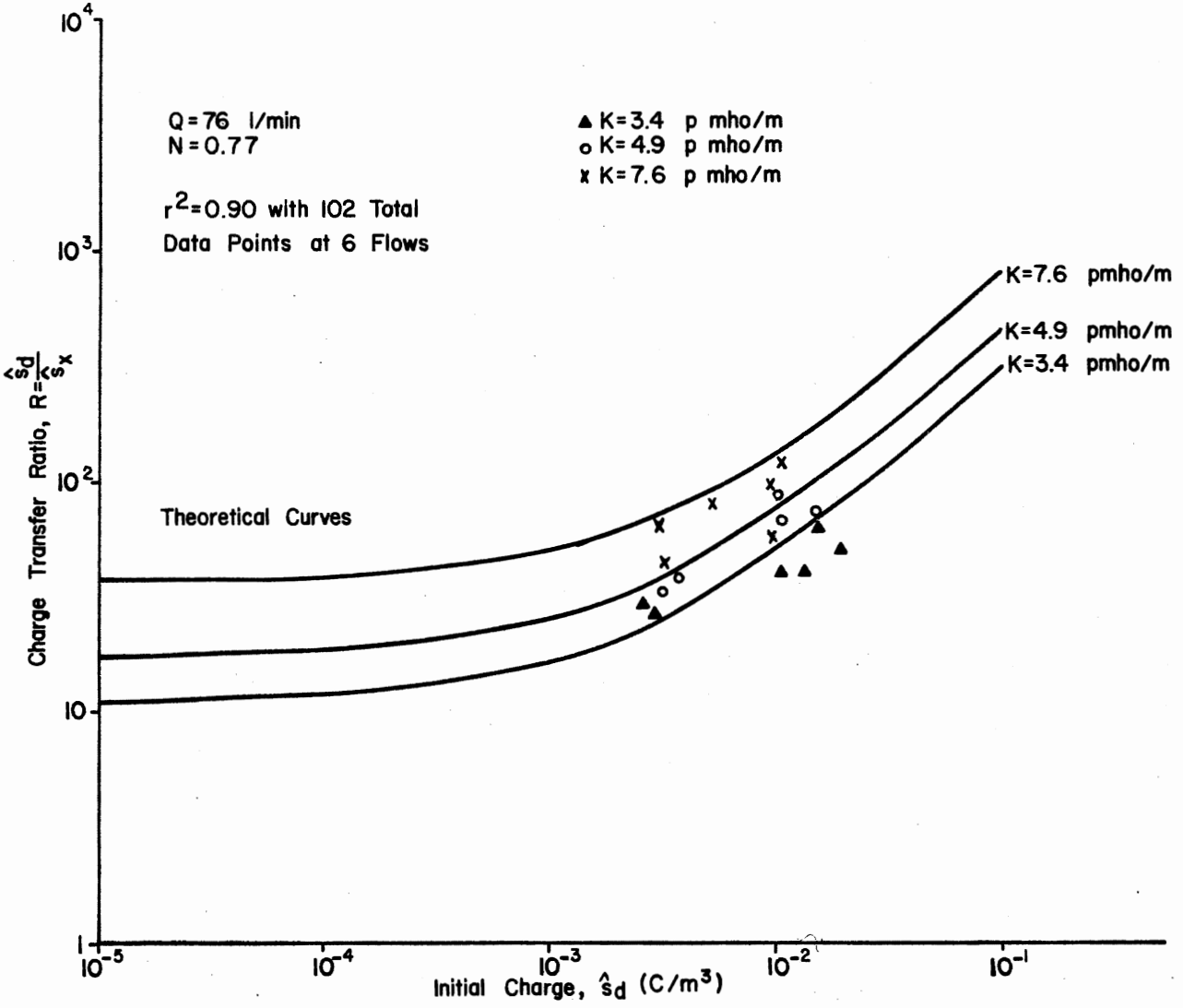

Figure 21. Effect of Equilibrium Conductivity and Charge Under the Generalized Model

CHAPTER V

EXPERIMENTAL EVALUATION OF CHARGE INFLUENCES

A large number of experimental tests were performed as a part of this research investigation to establish the influence of electrostatic charge upon filter performance. A total of six different filter models were donated for the tests by the filter manufacturers noted in the Preface. These filters were selected to cover a broad range of filtration characteristics or "effective pore size distributions." They are all representative of filters currently being specified and used in the Fluid Power Industry. The experimental program was primarily designed to evaluate the changes in separation performance and contaminant capacity which occurs when electrostatic charges are present.

Filter Test Method and Typical Results

The multi-pass filter test method (27) which was originally developed at Oklahoma State University (24, 25) is recognized throughout the world as a standard method for evaluating the performance characteristics of hydraulic filters. It has received adoption by both national and international standards bodies. The test method, due to its recirculatory nature, provides a realistic representation of actual operating environments for field systems. Because of the applicability of the test results and the wide acceptance of the method, the multi-pass method was used for all evaluations in this study. Electrostatic

charge density measurements were taken upstream and downstream of the test filter before and during each test.

The multi-pass test method requires the continuous introduction of AC Fine Test Dust into the reservoir of the recirculating filter test system. Appendixes A and B describe the test facility and test method in detail. The rate of contaminant injection is controlled to result in a theoretical base upstream gravimetric level of 10 mg/l calculated by the following relationship:

$$\text{Injection Rate (mg/min)} = (10 \text{ mg/l}) \times (\text{filter flow rate l/min})$$

Fluid samples are taken from the upstream and downstream lines for particulate analyses and determination of filtration ratios or separation efficiency. The test time required for the filter to plug to a designated pressure differential is recorded and the apparent contaminant capacity (ACFTD capacity) is calculated by multiplying this time by the injection rate.

Table V represents a typical summary of data resulting from a multi-pass test. The large magnitude of information resulting from such a test (as well as the effort required to conduct the procedure) can be appreciated from Table V. Particle counts were performed during this investigation at particle sizes of 2, 3, 5, 7, 10, 15, 20, 25, 30, 35, 40, and 50 micrometres on a cumulative basis. An average of three separate counts is reported. The values for beta listed in Table V are simply the ratio of the upstream count at some particle size to the respective downstream count. The efficiency values are calculated as $100\ (1-\overline{N}_d/\overline{N}_u)$. The average values reported at the bottom of Table V are divided into two groups — the average of all samples taken during the

TABLE V

SUMMARY OF RESULTS FOR FILTER F-7

FILTER ID: F 7 FPRC NO: 545H CHARGE: 2.67E-03 C/M**3 NO. OF SAMPLES 4

FLOW RATE = 76 L/MIN PPM = 0 RH = 37% BP = 18.8 CM. H2O

PRESSURE DIFF. (BAR): TERMINAL = 2.67 HOUSING = 0.44 CLEAN ASSEMBLY = 0.46

	2.5%	5%	10%	20%	40%	80%	100%
ASSEMBLY PRESSURES (BAR)	0.54	0.60	0.73	0.99	1.53	2.59	3.13
TEST TIMES(MIN.)	3.90	4.80	5.85	6.80	7.55	8.20	8.40

INITIAL INJECTION: .268 L/MIN. 2604 MG/L FINAL GRAVIMETRIC: 22.0 MG/L

FINAL INJECTION: .268 L/MIN. 2672 MG/L ACFTD CAPACITY: 5.9 GRAMS

TIME		>2	>3	>5	>7	>10	>15	>20	>25	>30	>35	>40	>50
5.85	UP AVG	15747.0	9674.0	5705.00	2985.10	1453.10	500.90	228.70	124.90	73.90	46.15	29.98	15.64
	DOWN AVG	3900.0	1030.0	238.60	46.80	11.80	3.14	0.77	0.46	0.38	0.31	0.15	0.00
	BETA	4.04	9.39	23.91	63.78	123.14	159.52	297.01	271.52	194.47	148.87	199.87	*****
	EFFIC.	75.23	89.35	95.82	98.43	99.19	99.37	99.66	99.63	99.49	99.33	99.50	100.00
6.80	UP AVG	16093.0	9716.0	5649.00	2939.70	1427.60	488.60	224.70	114.70	69.60	42.40	27.45	13.34
	DOWN AVG	4093.0	1065.0	254.30	53.90	17.20	5.21	1.92	0.92	0.69	0.69	0.54	0.23
	BETA	3.93	9.12	22.21	54.54	83.00	93.78	117.03	124.67	100.87	61.45	50.83	58.00
	EFFIC.	74.57	89.04	95.50	98.17	98.80	98.93	99.15	99.20	99.01	98.37	98.03	98.28
7.55	UP AVG	16600.0	10150.0	5951.00	3086.30	1517.00	523.80	236.00	120.90	69.80	40.71	25.53	12.50
	DOWN AVG	3897.0	1074.0	282.00	70.80	23.50	7.13	2.68	1.15	0.61	0.38	0.23	0.08
	BETA	4.26	9.45	21.10	43.59	64.55	73.46	88.06	105.13	114.43	107.13	111.00	156.25
	EFFIC.	76.52	89.42	95.26	97.71	98.45	98.64	98.86	99.05	99.13	99.07	99.10	99.36
8.20	UP AVG	16479.0	10251.0	6079.00	3195.60	1565.70	551.20	252.90	130.40	77.50	46.92	30.28	15.87
	DOWN AVG	3496.0	1026.0	298.90	80.80	27.50	7.36	1.99	0.61	0.31	0.23	0.15	0.00
	BETA	4.71	9.99	20.34	39.55	56.93	74.89	127.09	213.77	250.00	204.00	201.87	*****
	EFFIC.	78.79	89.99	95.08	97.47	98.24	98.66	99.21	99.53	99.60	99.51	99.50	100.00
AVERAGE BETA		4.22	9.48	21.81	48.64	75.15	91.12	128.46	154.47	143.91	107.44	103.52	169.19
AVG EFFICIENCY		76.28	89.45	95.42	97.94	98.67	98.90	99.22	99.35	99.31	99.07	99.03	99.41
10/80 AVG BETA		4.22	9.48	21.81	48.64	75.15	91.12	128.46	154.47	143.91	107.44	103.52	169.19
10/80 AVG EFF		76.28	89.45	95.42	97.94	98.67	98.90	99.22	99.35	99.31	99.07	99.03	99.41

test, and the average of only the samples corresponding to 10, 20, 40, and 80% pressure drop increases in accordance with the standard method. Additional samples were sometimes collected during the tests to provide further information about the filtration characteristics. The averages for separation efficiencies are strictly arithmetic averages, however, the average betas, because of the non-linear characteristic of the filtration ratio were calculated by $\beta_{avg} = 100/(100 - \eta_{avg})$ per the discussions in reference (37).

The upstream and downstream particle counts for the filter F-7 from Table V are plotted on log-log[2] coordinates in Figure 22. The "spread" between the two curves is representative of the filtration ratio or efficiency and it can be seen that the distance between the lines generally increases with increasing particle sizes. For large particle sizes there is usually more random error associated with the particle counts from a statistical basis (38) because of the low particle population. Thus, the filtration ratios at large sizes (especially with high efficiencies producing a very small particle population) shows a greater degree of scatter. In addition, if any fluid leakage occurs across the element seals (from upstream to downstream), the filtration ratios show a tendency to become constant for all larger particle sizes at a value which can be calculated from the percentage leakage (39). In this case, only filtration ratios below the "leakage ratio" can be used to represent the true characteristics of the filter element alone.

Figure 23 illustrates the particle separation spectrum for the 80% samples collected during the test on Element E-2. This filter has much less efficiency than element F-7 as can be visualized from Figure 23 by the closeness of the upstream and downstream particle size distributions.

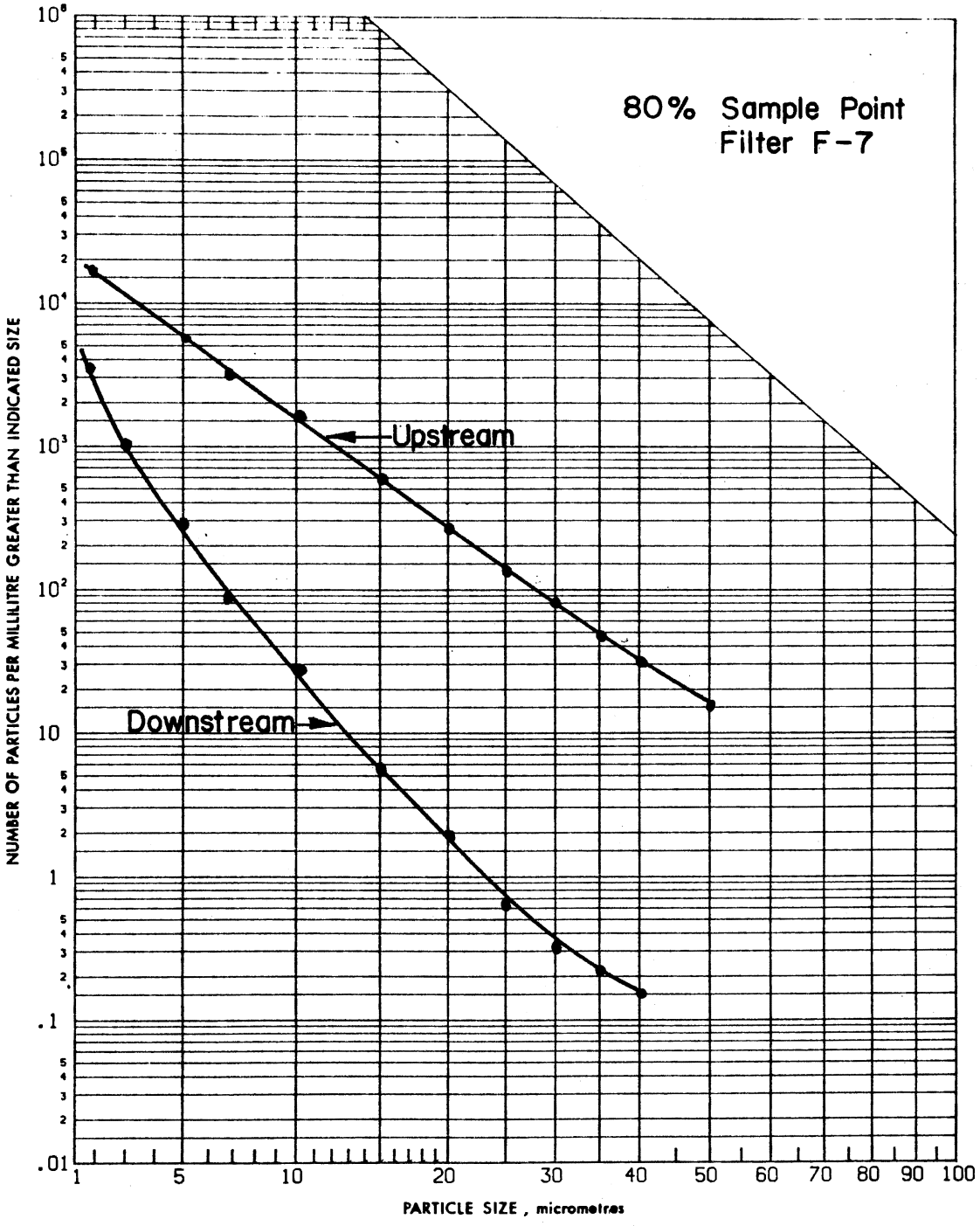

Figure 22. Particle Separation Spectrum for Filter F-7

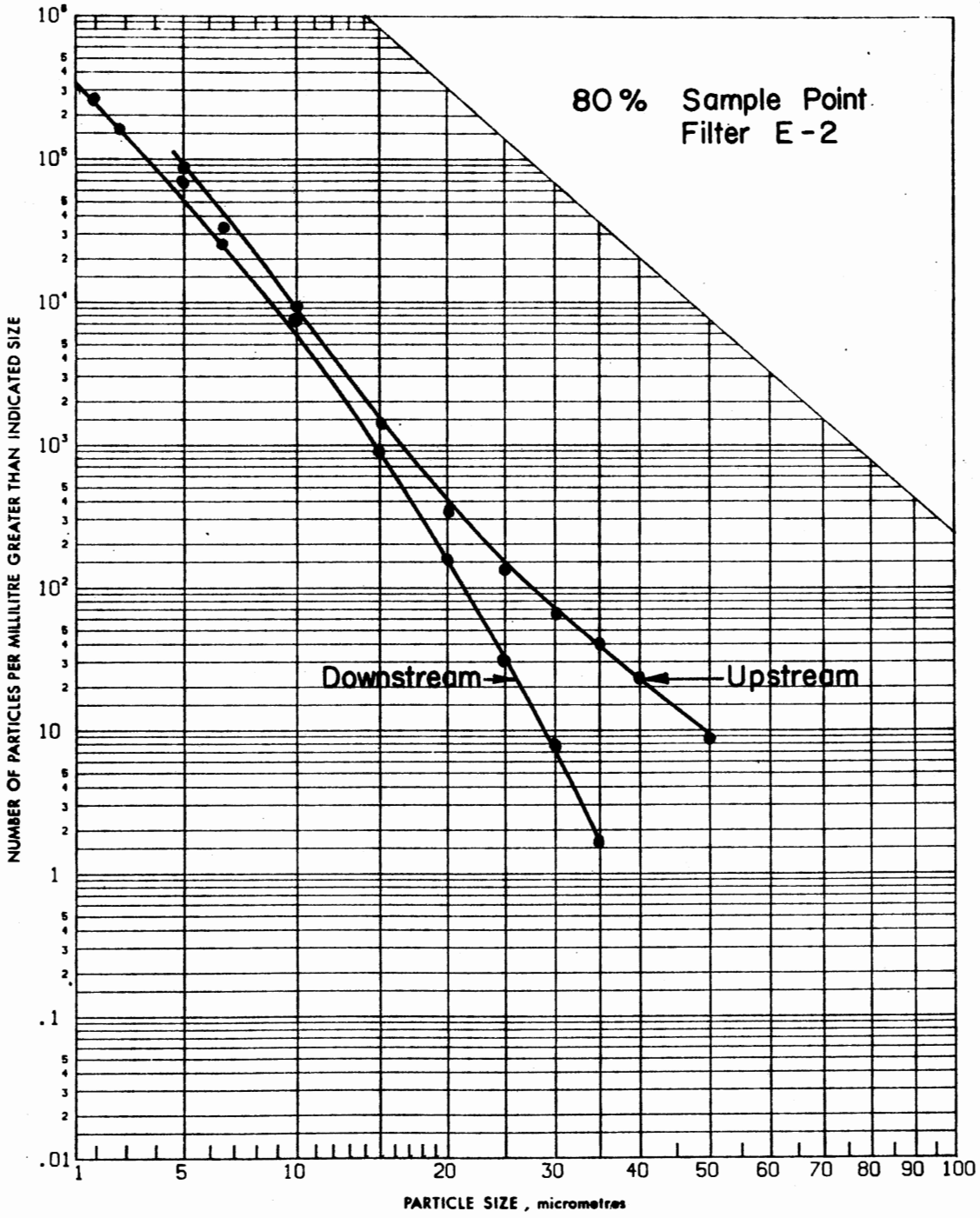

Figure 23. Particle Separation Spectrum for Filter E-2

The particle separation characteristics for a given filter must be considered as the most important of the various performance parameters. If a filter is not capable of controlling the contamination level of a hydraulic system below some critical level, it would be meaningless to consider such parameters as pressure drop and contaminant capacity. However, if a filter possesses at least the desired retention characteristics, the capacity becomes a quite important performance parameter. Figure 24 illustrates pressure drop/contaminant loading characteristics for elements F-7 and E-2. Considering that both filters were subjected to approximately the same contaminant injection rate, it is easily seen from Figure 24 that element E-2 had a much higher ACFTD capacity than element F-7.

A complete summary of the average filtration performance capabilities of the thirty-nine filters evaluated during this investigation is included in Appendix D. The filtration ratios, as well as efficiencies, are averages of the samples extracted at the 10, 20, 40, and 80% pressure increase points. These points were selected for the summary because the standard multi-pass procedure calls for sampling at these respective points and because these samples were available for all the filters evaluated. Each set of average filtration ratios or efficiencies thus represents a compilation of eight samples and a total of thirty-six particle counts per sample (12 particle sizes x 3 counts for each size) or a total of 288 numbers. Because of the magnitude of numbers and calculations required, all the data was entered into a computer bank for summarizing and data reduction purposes.

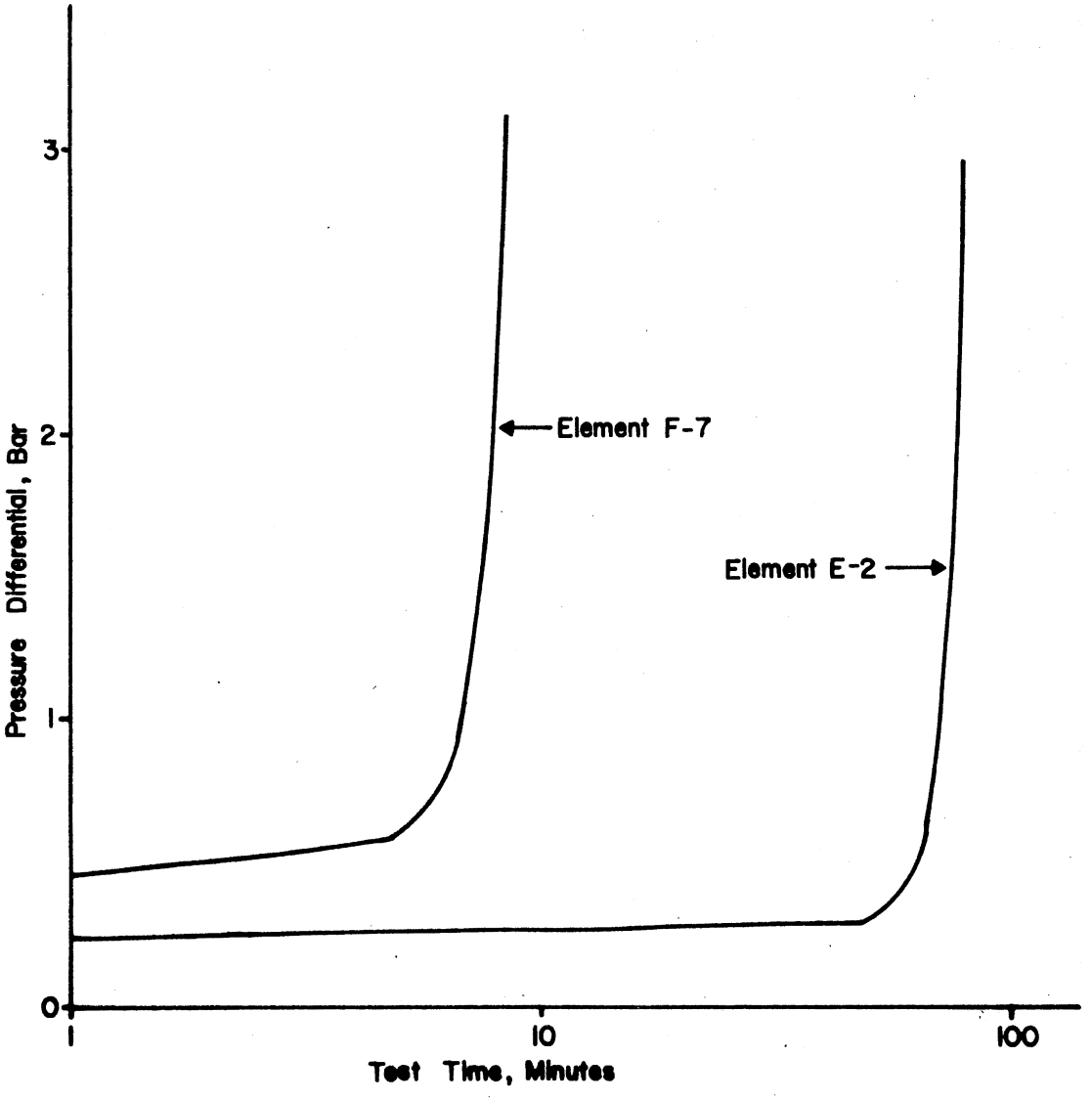

Figure 24. Contaminant Loading Characteristics of Typical Filters

Experimental Results of Charge Influence Tests

As mentioned before, a total of thirty-nine complete multi-pass tests were conducted under various charging levels. A complete summary including the measured charge density values is contained in Appendix D. There was no convenient method for controlling the electrostatic charge density at a desired value for any given test as the charge level is a function of filter properties, fluid properties, and flow rate. Tests were therefore conducted with various amounts of conductivity additive (ASA-3) in the test fluid (MIL-H-5606) in order to establish various charging levels.

During the tests, the charge densities in the fluid upstream of the test filter were measured but were always at least an order of magnitude less than the downstream fluid. Generally, the difference corresponded to several orders of magnitude as predicted by the generalized relaxation law developed in Chapter III. The downstream charge density is therefore the only value reported in the summary of Appendix D.

It was suggested to the author that perhaps the addition of the ASA-3 anti-static additive to the test fluid could increase the particle dispersancy characteristics of the fluid thus changing the apparent performance of the test filter. Past experience has shown that with the turbulent mixing (flow passing through the pump, tubing, elbows, difusers, etc.) that exists in a multi-pass test facility, AC Fine Test Dust becomes fully dispersed. A test was conducted however to determine the effects, if any, of ASA-3 upon the particle size distribution of ACFTD in MIL-H-5606 hydraulic fluid. A quantity of dust was mixed in a small recirculating test stand with new MIL-H-5606 fluid. Samples were

then extracted for particle count analysis. A quantity of ASA-3 additive (40 PPM by volume) was then added to fluid and the circulation was allowed to continue for 30 minutes. Samples were again extracted for analysis. Table VI presents the average results of particle counts conducted on two samples taken before and after the addition of the ASA-3. It can be seen that the particle size distribution with the ASA-3 is essentially equal to the distribution with no additives.

TABLE VI

DISPERSANCY CHARACTERISTICS OF SHELL ASA-3 ADDITIVE

Particle Size (μm)	Cumulative Particle Count/ml	
	No Additive	40 PPM ASA-3
2	6398	6384
3	4319	4421
5	2636	2602
7	1373	1401
10	646	670
15	206	208
20	85.0	91
25	40.3	41.5
30	21.5	20.3
35	11.3	12.7
40	6.8	6.9
45	1.7	2.5

It can be noted from the data summary in Appendix D that several filters of each model were evaluated with extremely low downstream charge densities. For instance, with filter A, the maximum charge density obtained was with no conductivity additive and was equal to 11.7×10^{-3} C/m^3. The minimum level was 1.87×10^{-7} C/m^3 or almost five orders of magnitude lower. The extremely low charge measurements were difficult to measure accurately and variations of up to 100% were not uncommon. However, when the charge level was approximately 10^{-4} C/m^3 or greater the charge measurements were highly repeatable and successive reading would usually fall within 5% of the average value. The primary reason for the large number of data points at the low charge values was the fact that the effect of the conductivity additive on a particular filter was unknown prior to the addition of the ASA-3; thus, it was difficult to determine the required concentration of additive in advance. Various levels of additive from 2 PPM up to 40 PPM were used during the investigation and the filters were evaluated at each additive level. There was a large time delay from the time a test was conducted until particle counts were completed which also increased the difficulty in determining which levels of charge resulted in an effect on the filter performance.

In order to establish the effect of electrostatic charge upon the filter's particle separation capabilities for various particle sizes, it is more convenient to examine particle counts and efficiencies on an incremental size basis rather than cumulative. This allows the isolation of any influences on a given particle size or size range. Appendix D also includes a summary table of filter separation characteristics based upon size interval calculations. The values presented are similar to

filtration ratios except on a size interval basis and are called "retention ratios" to prevent confusion with the cumulative parameter. The retention ratios are calculated by the following relationship:

$$\Phi_{D_1-D_2} = \frac{\overline{N}_{u_1} - \overline{N}_{u_2}}{\overline{N}_{d_1} - \overline{N}_{d_2}}$$

where

Φ = retention ratio for particle size interval $D_1 - D_2$

D_i = particle size

$\overline{N}_{u_i}$ = particles greater than size D_i in upstream fluid

$\overline{N}_{d_i}$ = particles greater than size D_i in downstream fluid.

Figures 25 through 30 illustrate the relationship between average retention ratio and downstream charge density for the six filter models evaluated. To prevent the larger number of data points at extremely low charge levels from biasing regressions, an average value of the retention ratios for these charges were plotted at zero charge on Figures 25-30. Charge values below 10^{-4} C/m^3 were considered alike and the retention rations were averaged to produce a best estimate of the zero charge point. Typical coefficients of variation (100% x ratio of sample standard deviation to sample mean) for this averaging fell between 2% and 10% for retention ratios with a value under two. The variation increased in most instances for higher retention ratios and at higher particle sizes.

The lines drawn through the data points in Figures 25-30 represent a least squares curve fit to an equation of the form:

$$\Phi = \Phi_o e^{\alpha_1 \hat{s}_d} \qquad (5\text{-}1)$$

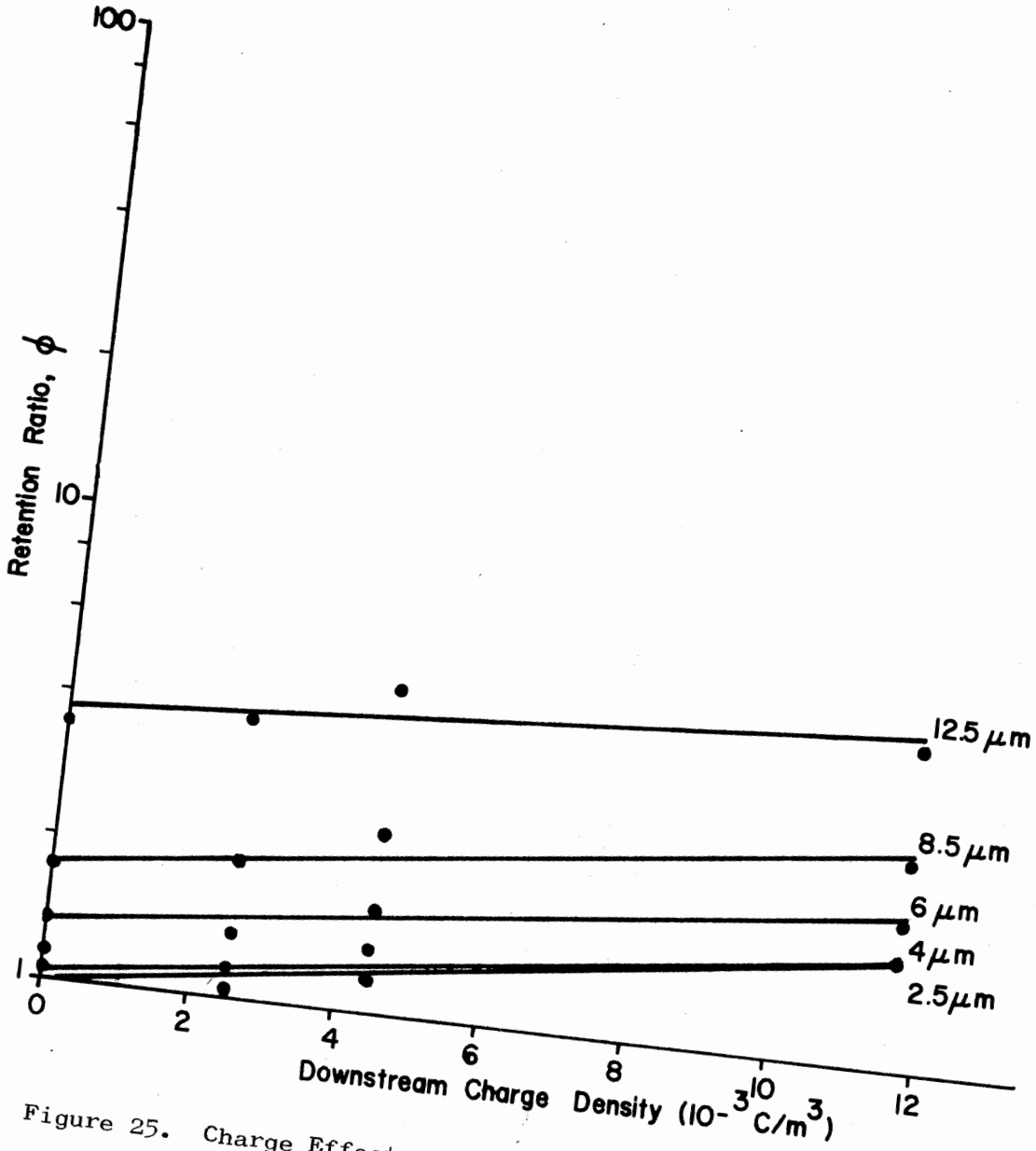

Figure 25. Charge Effects on the Retention Characteristics of Element A

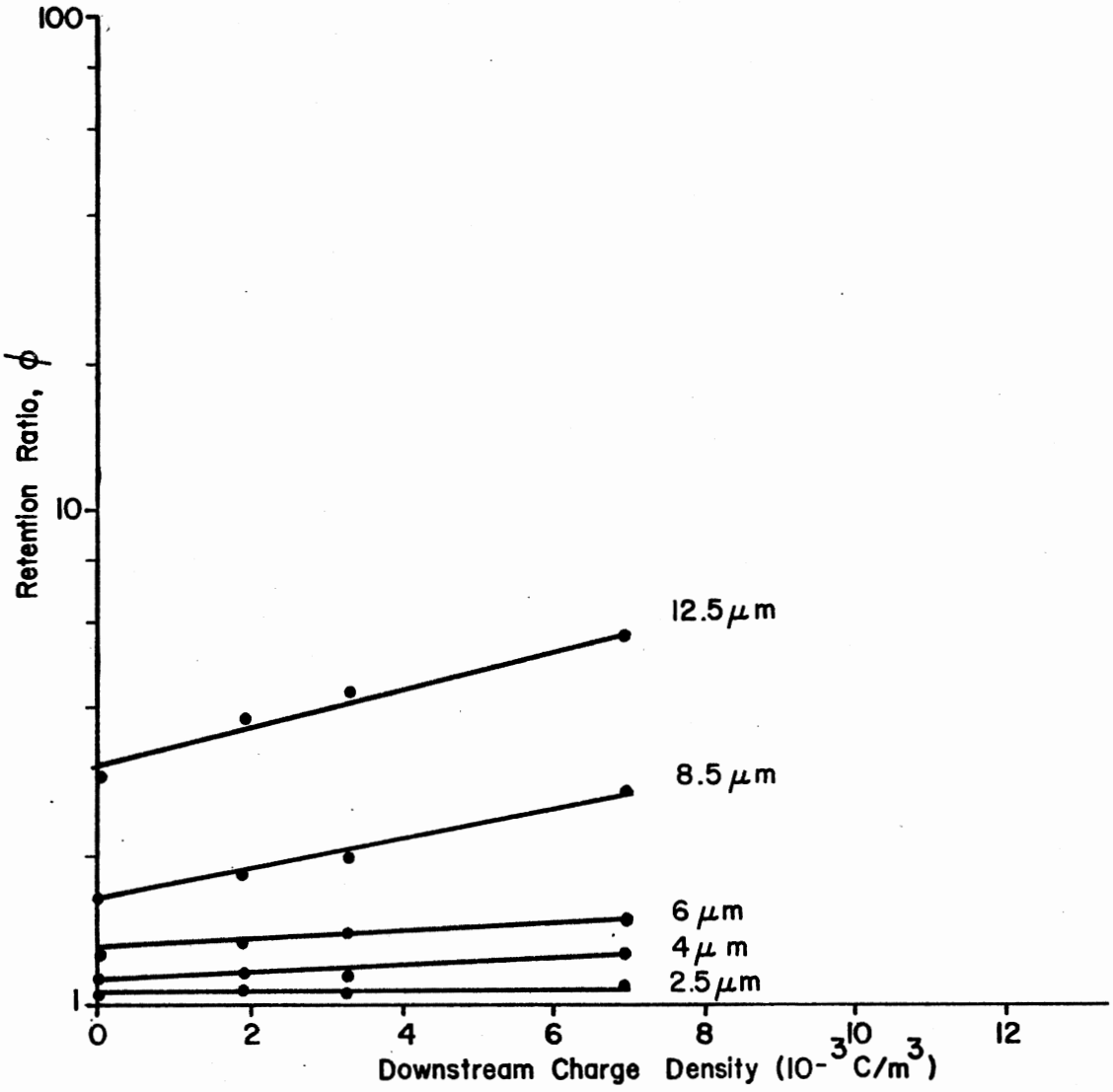

Figure 26. Charge Effect on the Retention Characteristics of Element B

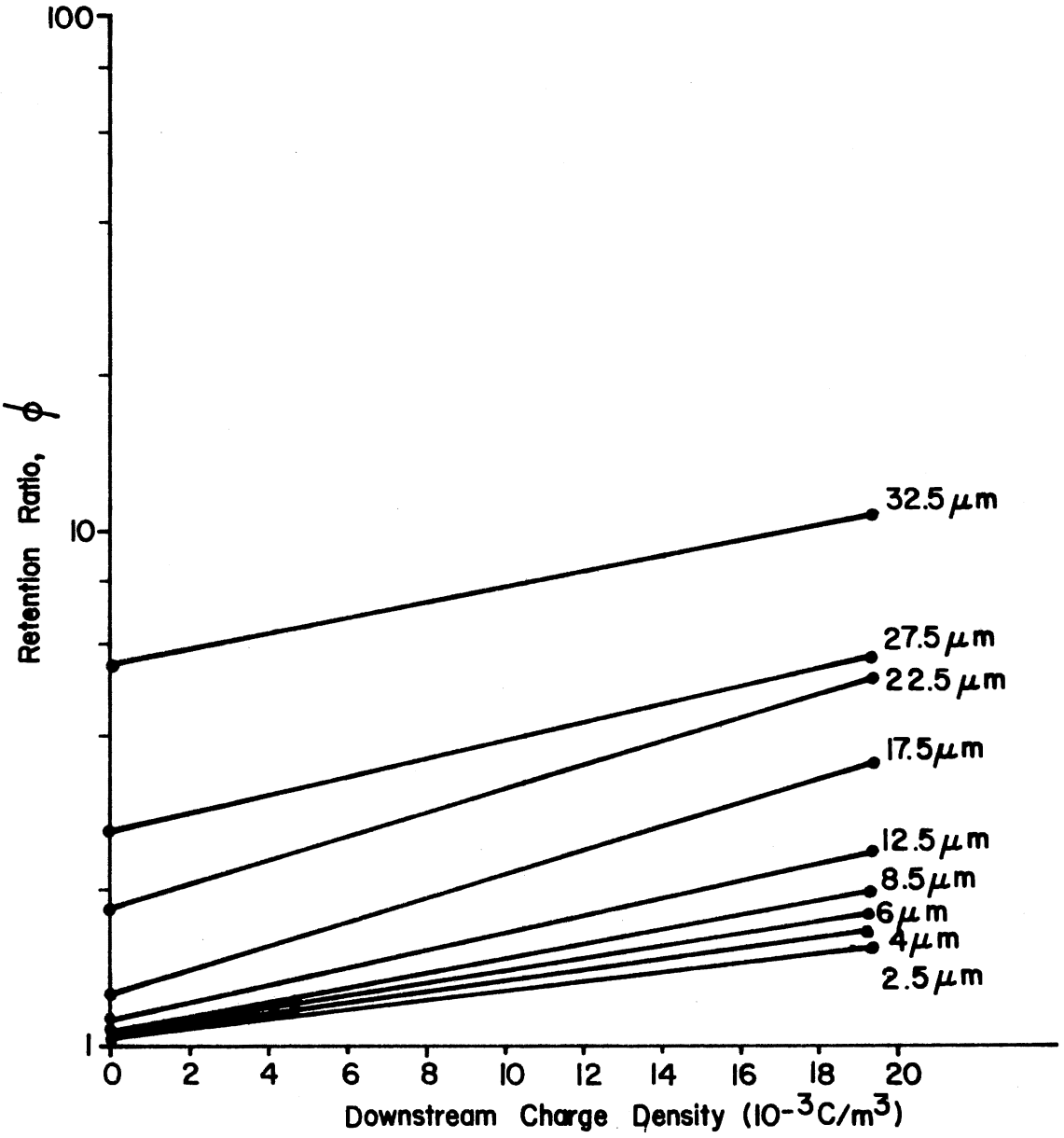

Figure 27. Charge Effect on the Retention Characteristics of Element C

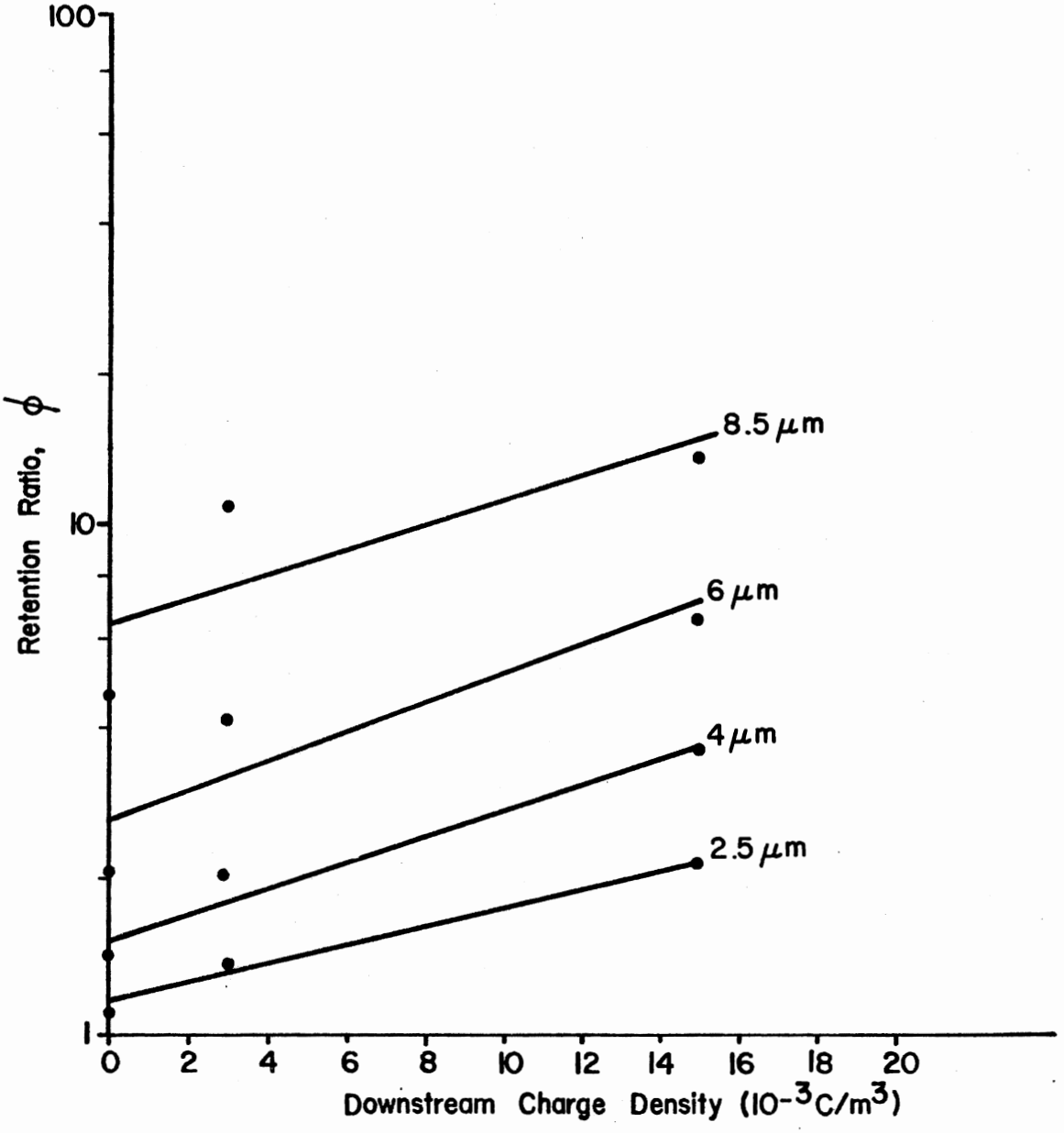

Figure 28. Charge Effect on the Retention Characteristics of Element D

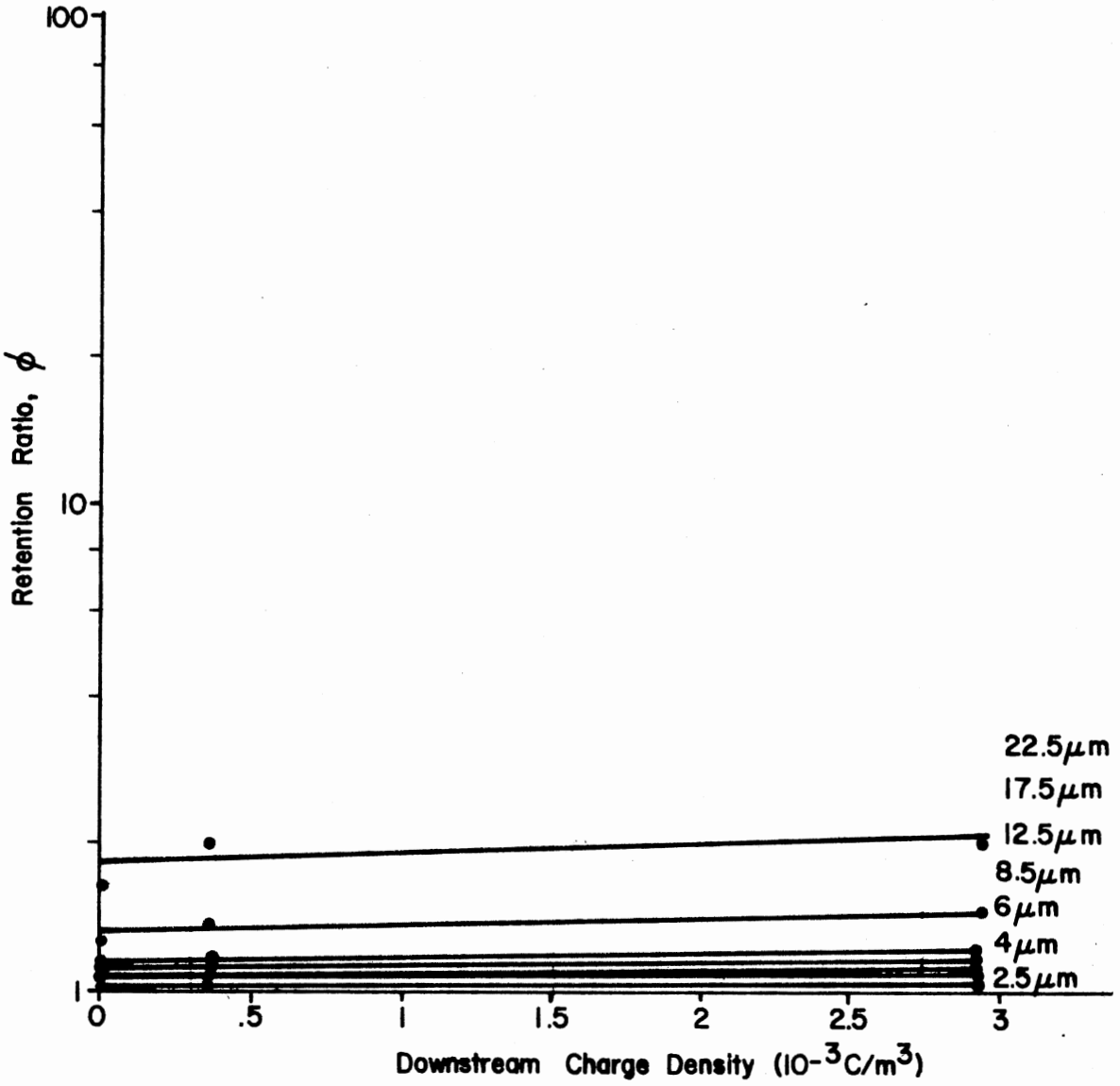

Figure 29. Charge Effect on the Retention Characteristics of Element E

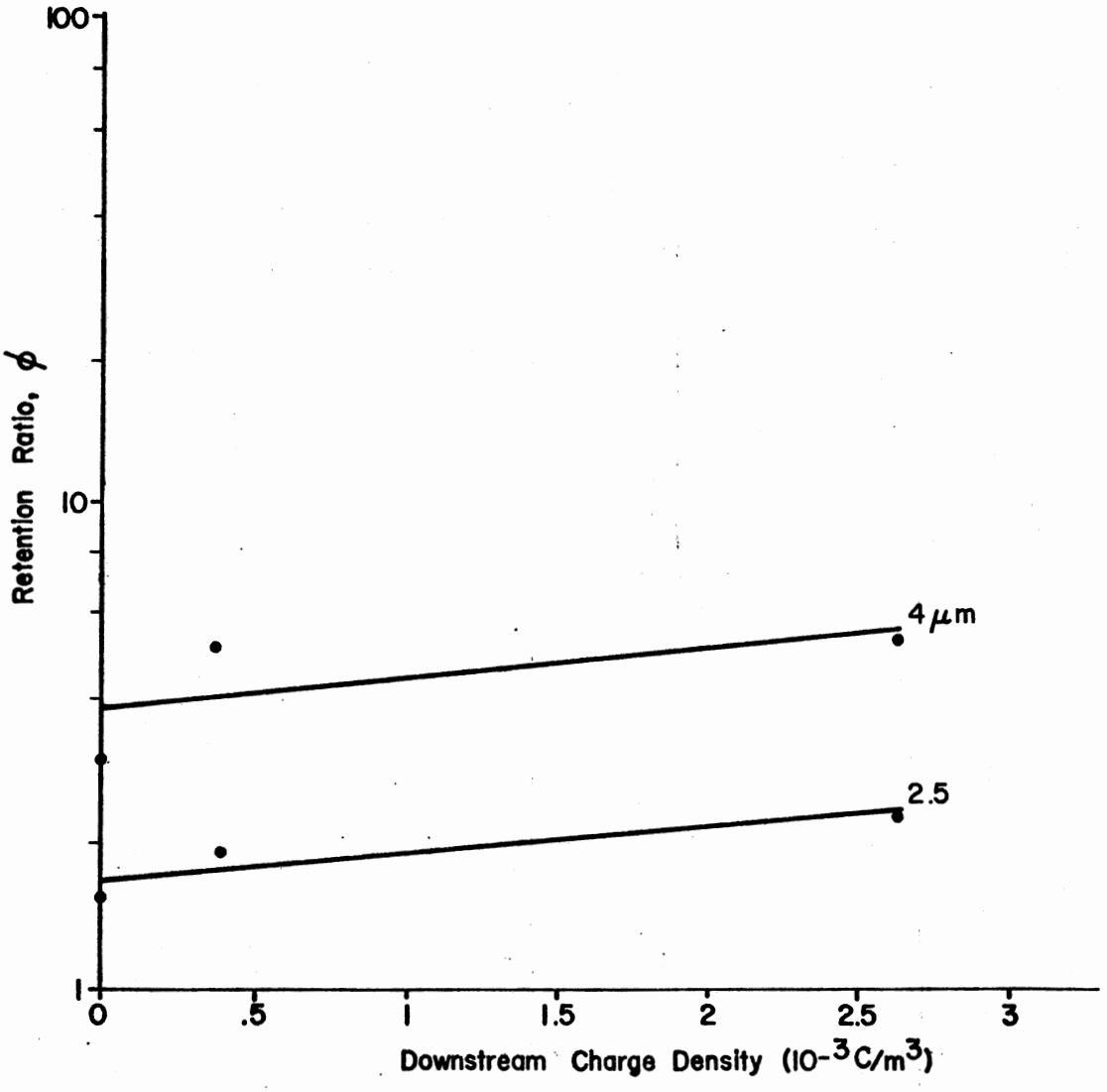

Figure 30. Charge Effect on the Retention Characteristics of Element F

where

Φ_o = retention ratio at zero charge level

α_1 = constant, m^3/C

$\hat{s}_d$ = downstream steady state charge density, C/m^3

The intercept of the lines at the zero charge ordinate represent the value Φ_o in Equation 5-1 while the slope of the lines are reflected by α_1. Typical coefficients of determination (r^2) for these curves fell between 0.5 and 1.0; however, most r^2 values were above 0.85 for particle sizes below 15 μm. Experience has shown (38) that for high separation efficiencies and large particle sizes, the downstream particle population is extremely small and random measurement errors may alter the data significantly. Therefore the curves for retention ratios in excess of ten are not shown in Figures 25-30. In such instances, the coefficients of determination were generally below 0.5.

An additional result from the charge influence tests was ACFTD capacities for the various filters and charge levels. Figure 31 illustrates the data collected from the experimental program. Again, the capacity values for filters with approximately zero charge were averaged and plotted as one point at zero. The coefficients of variation for this averaging process were all less than ten percent with the exception of element F which had a 14.8% C.O.V. Regression analyses for the data plotted (semi-log coordinates) generally produced low values for r^2 and "flat" slopes which indicates little effect of charge on capacity.

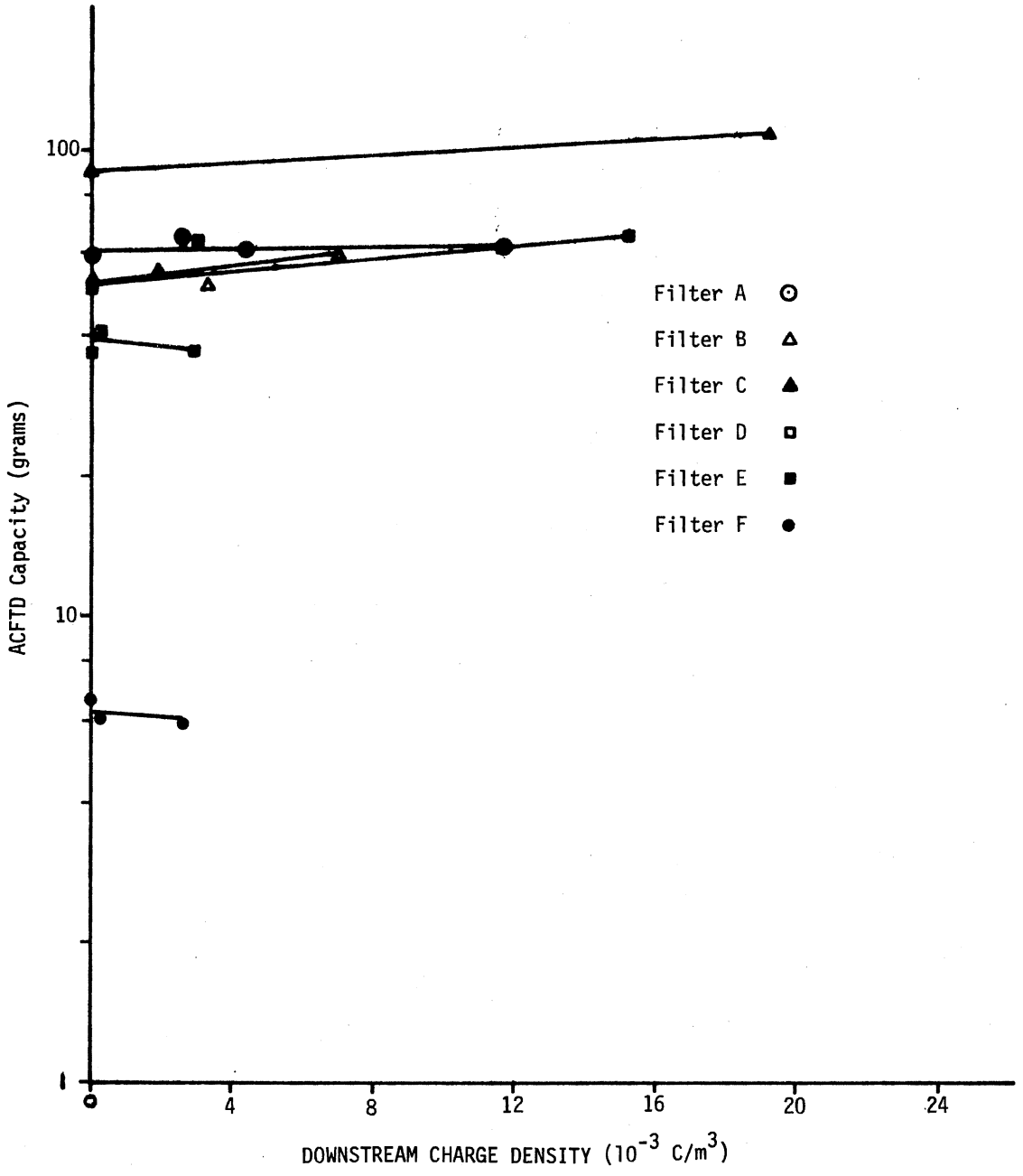

Figure 31. Effect of Charge Density on ACFTD Capacity

Empirical Models for Charge Influence

The equation which best describes the relationship between retention ratio and electrostatic charge density from Figures 25-30 is of the form of Equation (5-1). Reference (40) summarizes an investigation by Chen in which he considered the overall collection efficiency of a fibrous aerosol filter as a function of the single fiber efficiency. He developed an equation of which can be written as:

$$\Phi = e^{\frac{4\,\eta_s\,B_1 h}{\pi\,D_f(1-B_1)}} \qquad (5\text{-}2)$$

where

B_1 = filter fiber packing density

h = filter thickness

D_f = filter fiber diameter

If Equation (5-2) is rewritten with one term representing retention with no charge and one term representing charge effects, the following is obtained:

$$\Phi = \Phi_o\, e^{F_P\,\eta_{s/q}} \qquad (5\text{-}3)$$

where

F_P = filter parameter constant = $\dfrac{4\,B_1\,h}{\pi\,D_f(1-B_1)}$

$\eta_{s/q}$ = single fiber efficiency due to charge only.

Equation (5-3) is of the same form as Equation (5-1) which describes the data from this investigation.

In order to determine the single fiber efficiency equation most applicable for use in Equation (5-3), the earlier review of Kraemer and Johnstone's work (16) should be considered. Equation (2-14) for the

condition of charged fiber and charged particle predicted a decreasing effect of efficiency with increasing particle size; whereas, Equation (2-15) for charged fiber and uncharged particle predicted the opposite. The effect of various particle sizes can most easily be recognized by observing the slope (α_1) of the Φ versus $\hat{s}_d$ curves plotted in Figures 25-30. From these figures it can be seen that the slope of the curves generally increase with increasing particle sizes.

To obtain a more precise indication, the slopes, α_1, from the least squares curve fits in Figures 25-30 were plotted in Figure 32 as a function of particle size for the various filters. Because of the poor correlation between retention ratio and charge for the larger particles and higher retention ratios, an arbitrary decision was made not to consider curves from Figures 25-30 if their respective r^2 values were less than 0.7. In fact, because of the low coefficient of determination, filter F could not be represented in Figure 32.

It can be recognized from Figure 32 that all of the curves except for element A show increasing slope, α_1, with increasing particle size. Element A in fact, exhibited almost no change. This increasing slope certainly indicates that an equation for single fiber efficiency such as Equation (2-15) is more applicable than Equation (2-14). From Kraemer and Johnstone's investigation (16), this implies that the filters which were tested have the characteristics of charged fibers and uncharged particles. Because of the extremely low upstream fluid charge densities measured in this investigation, it is certainly reasonable to assume that this could be the general case, and that the particle, if they were previously charged could be discharged by the time they reach a point directly upstream of the filter.

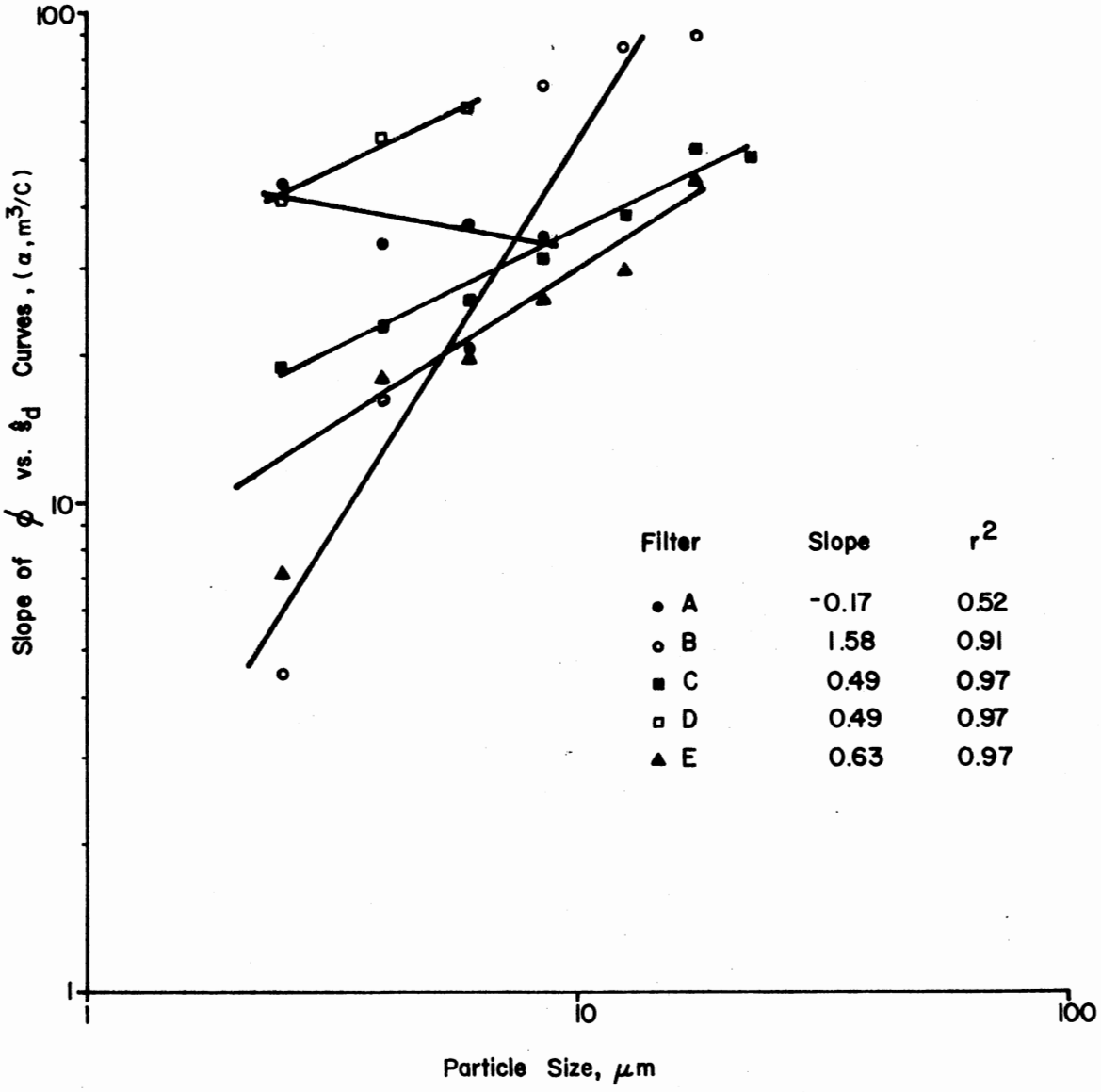

Figure 32. Retention/Charge Relationship as a Function of Particle Size

The only filter which did not show an increasing α_1 with increasing particle size was element A. This element was evaluated at a flow rate 50% higher than all the other filters. It is certainly conceivable that the higher flow rate (114 ℓ/min) contributed to some charge transfer from the fluid to the particle. From the charge accumulation theory previously developed, it is known that the charge relaxation from downstream to upstream of the filter is less at higher flow rates. It is thus possible that in this one instance, the filter acted in a somewhat different mode that reflects the particles being somewhat charged.

If it is assumed that in most multi-pass filter test situations the ACFTD particles are uncharged then Equation (5-3) can be rewritten in terms of Equation (2-15) to produce:

$$\Phi = \Phi_o \, e^{F_P \theta \, q_c^{.66} \, D_P^{.66}} \tag{5-4}$$

As stated earlier, the fiber charge is not readily measurable for hydraulic fibrous filters but from the curves in Figures 25-30 it is known that the retention ratio varies exponentially with a linear function of downstream charge density. Therefore, a more generalized form of Equation (5-4) that agrees with the current experiments can be written as:

$$\Phi = \Phi_o \, e^{\alpha \hat{s}_d \, D_P^n} \tag{5-5}$$

where

α = a characteristic constant made up of filter, particle, and fluid parameters

n = constant in exponent.

The value for n for the various filters evaluated appears to be a function of the filter; however, n is positive for all filters except

filter A. The values for n for filters B, C, D, and E were 1.58, 0.49, 0.49, and 0.63, respectively. These are of the same sign and have a general order of magnitude the same as the theoretical equation for aerosol filtration, Equation (5-4), which has an exponent of 0.66.

Influence of Charge on Filtration Models

Because of the complexity of the log-normal filter performance model presented in Chapter III, one can not solve explicitly for any of the parameters for determination of charge influences. It is more convenient to use a graphical approach with log-probability coordinates. Figure 33 illustrates the base (no charge) models for the filters evaluated in this investigation. The data points were calculated from the average retention ratios ($\eta = 1 - 1/\Phi_o$) at the zero charge levels. It can be seen from Figure 33 that the separation efficiency characteristics of each filter follow the log-normal model almost exactly with the exception of filters C and E at values below ten to fifteen percent efficiency. It is believed that the curved lines below 10% efficiency are a result of high particle build-up during a multi-pass test in the low particle sizes (because the filter is removing essentially no particles) thus affecting both the apparent filter characteristics and the particle counting accuracy.

Table VII is a summary of the geometric mean and geometric standard deviation determined from the filter models of Figure 33 in accordance with the method described in Chapter III. It should be noted that the geometric standard deviations for filters A, B, D, and F were almost identical. Filters C and E which had much lower separation efficiencies deviated somewhat from this constant slope.

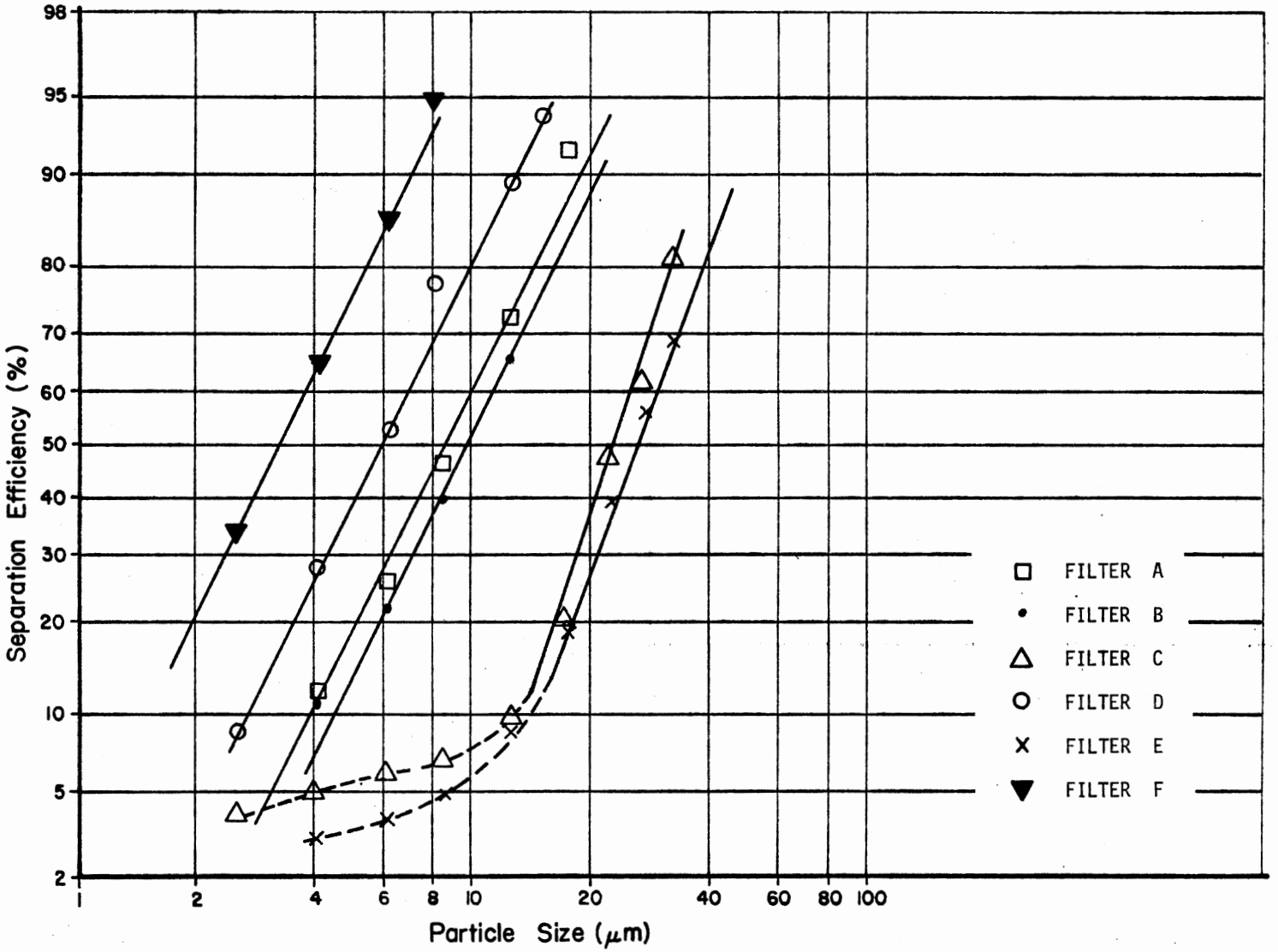

Figure 33. Basic Filter Performance Models for Test Elements

TABLE VII

FILTER PERFORMANCE MODEL PARAMETERS

Filter	Geometric Mean Particle Size ($\overline{D}_g$), μm	Geometric Standard Deviation, σ_g
A	8.5	1.85
B	9.6	1.82
C	22.5	1.51
D	5.8	1.83
E	26.0	1.57
F	3.2	1.81

In order to determine the effects of charge density upon the filter performance model parameters, $\overline{D}_g$ and σ_g, log-normal curves were constructed for the various charge levels as illustrated in Figure 34 for element D. It can be seen from Figure 34 that the geometric mean diameter, $\overline{D}_g$, decreased with increasing charge. The geometric standard deviation, σ_g, increased for increasing charge values. Similar curves to those in Figure 34 were also constructed for the other six filters. Each of the other filters generally showed similar trends to filter D.

To demonstrate the generalized effect of charge upon the filter model variables, each value of $\overline{D}_g$ and σ_g for each filter was normalized by dividing by their respective values at "zero" charge. Figures 35 and 36 contain a summary of all data points from the six filters for the normalized parameters. A least squares curve fit (semi-log) to the data

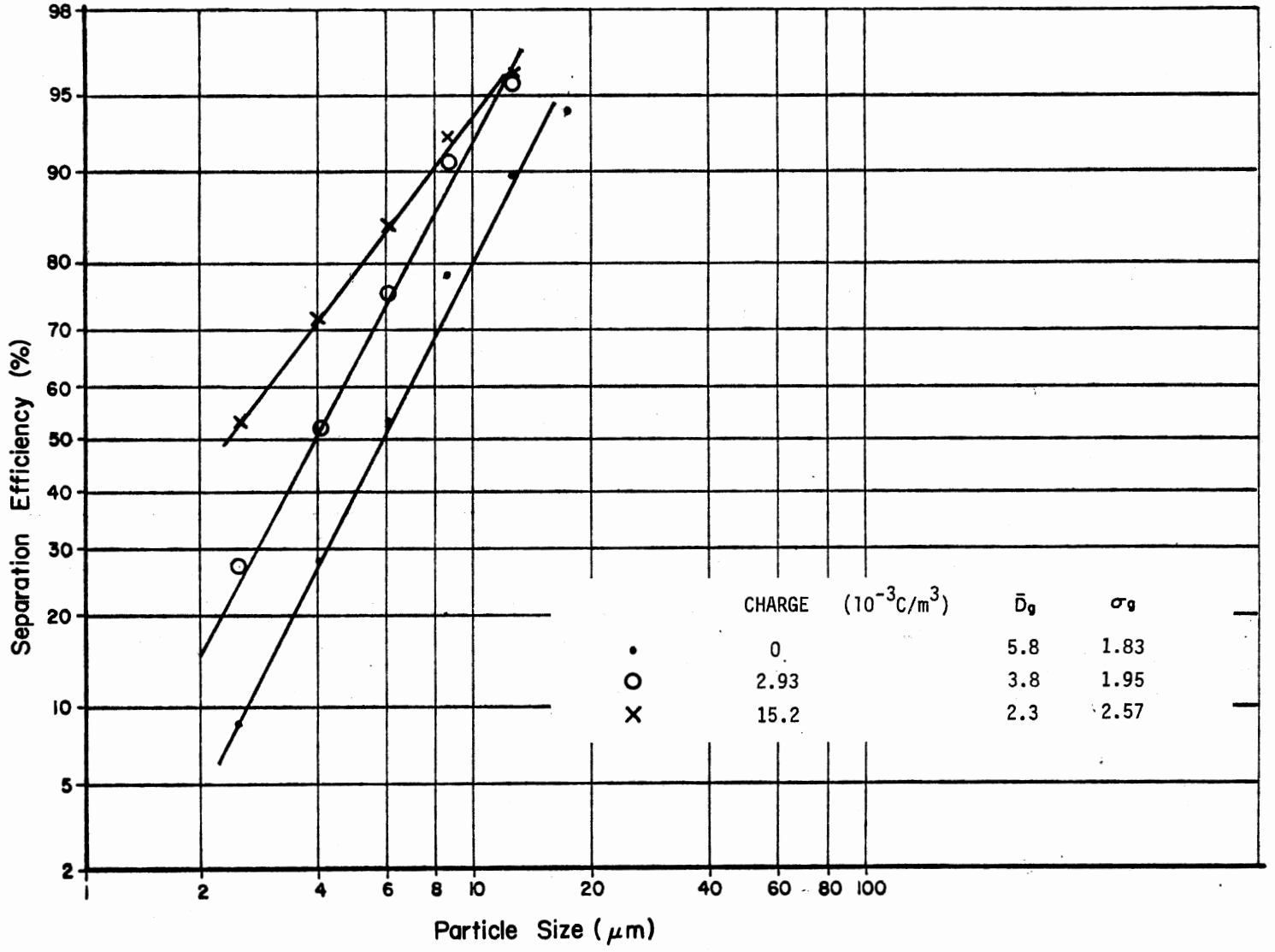

Figure 34. Filter D Performance Curves for Various Charge Levels

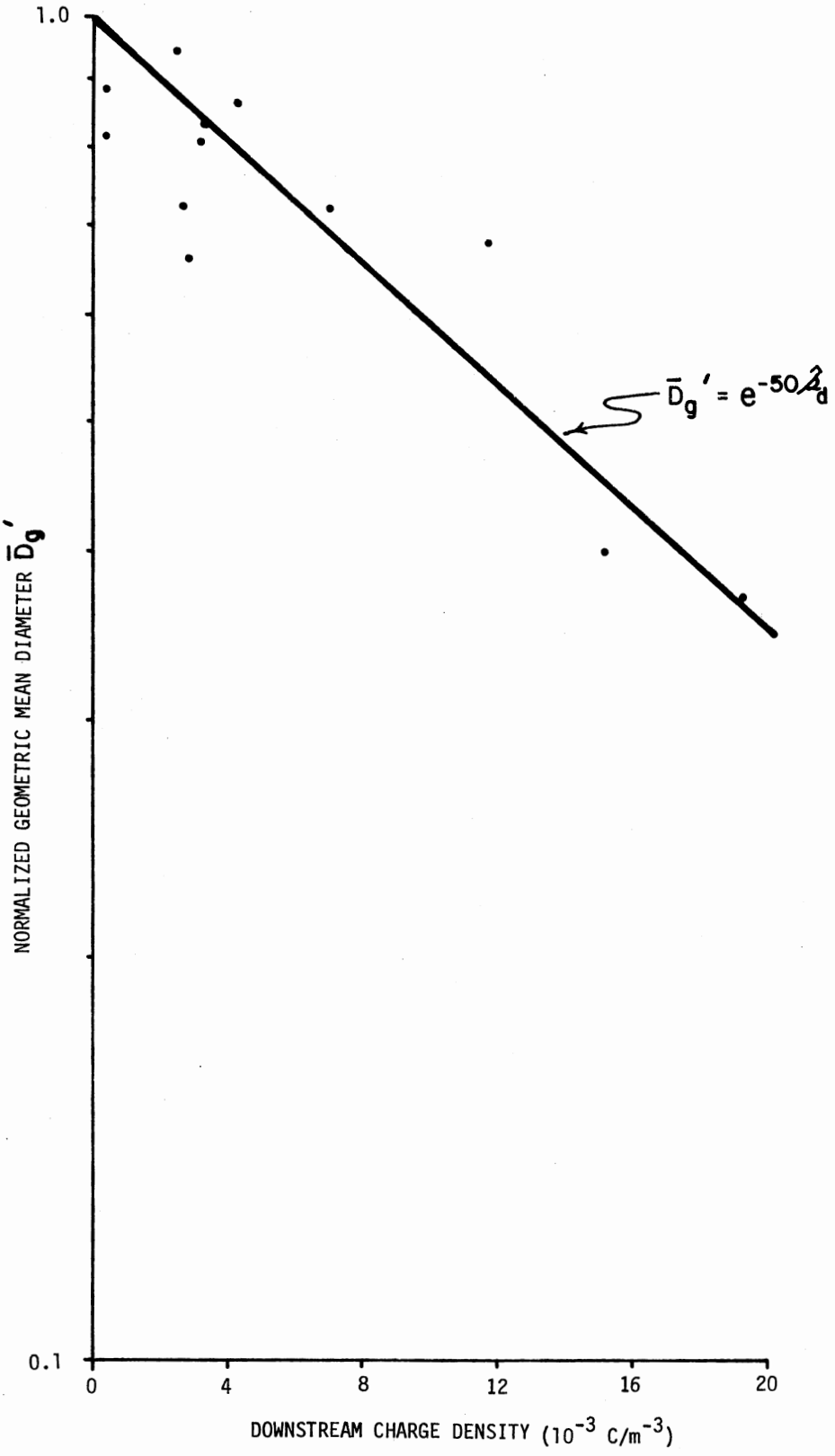

Figure 35. Effect of Charge on Geometric Mean Diameter

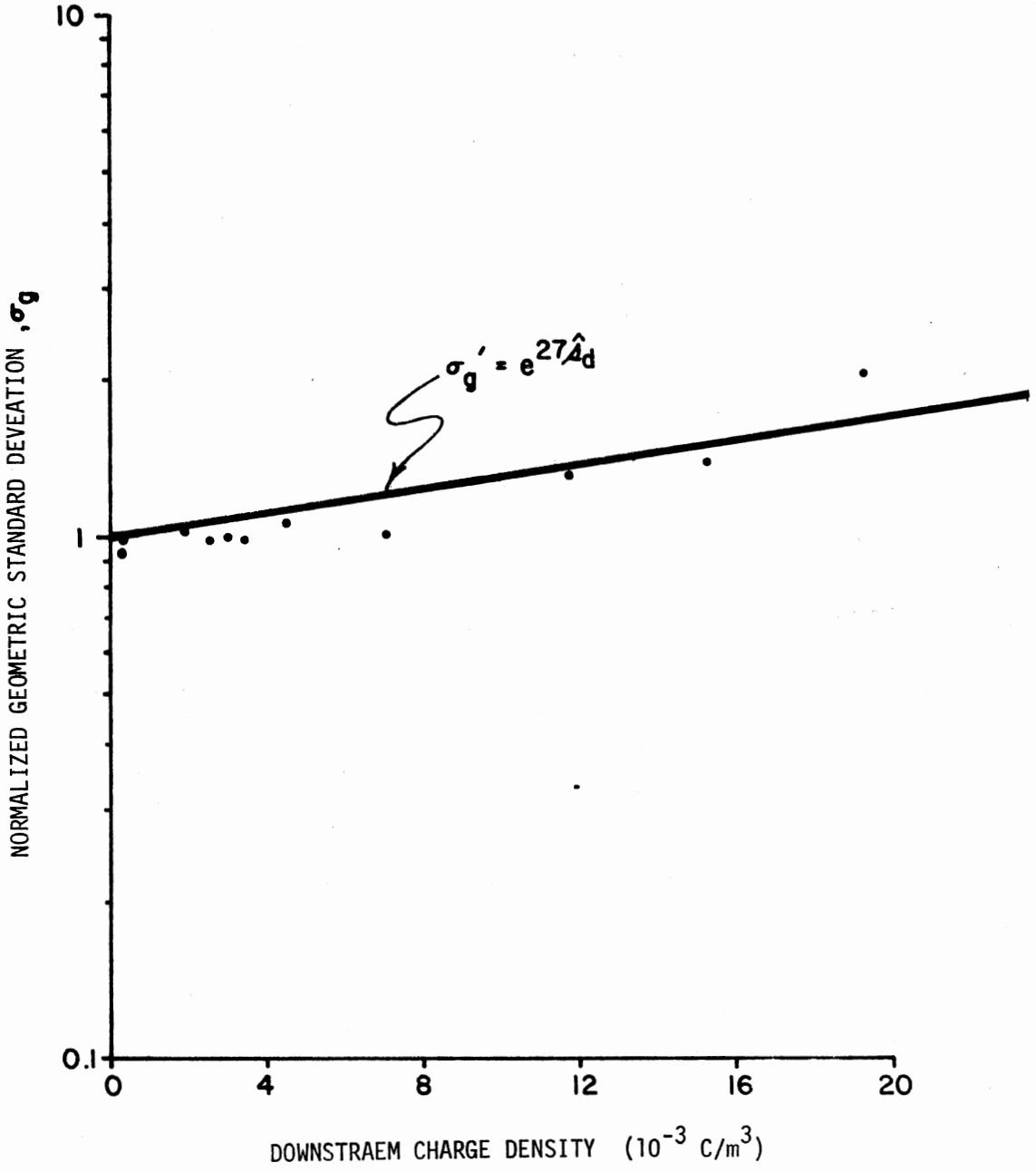

Figure 36. Effect of Charge on Geometric Standard Deviation

in Figure 35 resulted in an expression for the normalized geometric mean diameter, $\overline{D}_g$, of the following form:

$$\overline{D}'_g = e^{-50\,\hat{s}_d} \tag{5-6}$$

where the value, 50, has units of m^3/C. In an un-normalized form Equation (5-6) can be written as follows:

$$\overline{D}_g = \overline{D}_{go}\, e^{-50\,\hat{s}_d} \tag{5-7}$$

where $\overline{D}_{go}$ is the geometric mean diameter at zero charge density. A similar analysis can be performed on the data in Figure 36 to produce an equation for σ_g as:

$$\sigma_g = \sigma_{go}\, e^{27\,\hat{s}_d} \tag{5-8}$$

where σ_{go} is the geometric standard deviation at zero charge density.

If the geometric mean diameter is thought of as representative of the mean "effective" pore size of the filter and the value σ_g as indicative of the pore size standard deviation, a meaningful interpretation of Equations (5-7) and (5-8) can be obtained. Equation (5-7) shows that the "effective" mean pore size is reduced significantly under the presence of electrostatic charge. The standard deviation of the "effective" pore size distribution is increased with increasing charge as shown by Equation (5-8).

CHAPTER VI

APPLICATIONS AND EXTENSIONS OF THE RESEARCH

Multi-Pass Test Influence

It has been suspected that the results of a "standard" multi-pass filtration performance test (27) on a hydraulic filter can be influenced by electrostatic charge effects. The results of this investigation certainly confirm these suspicions by illustrating the improvement in particle separation characteristics which can be obtained with electrostatic charge influences. Because of these effects, the multi-pass method as it is now written can not always be relied upon to give accurate and unbiased filtration performance data. Any user of the procedure could unknowing or "intentionally" influence the results by conducting tests under conditions conducive to electrostatic charge generation. Such conditions would be the use of new test fluid and operation in a low humidity environment.

The results of this study revealed that the filtration performance of hydraulic filters is significantly improved under the presence of electrostatic charge especially when charge density levels exceed 10^{-4} C/m^3 immediately downstream of the filter. In terms of the filtration ratio, which is based upon cumulative particle counts, and is most familiar to the Fluid Power Industry, the improvement can be summarized by Figure 37. The values plotted are the average five micrometre filtration ratios for the various conductivities utilized in the

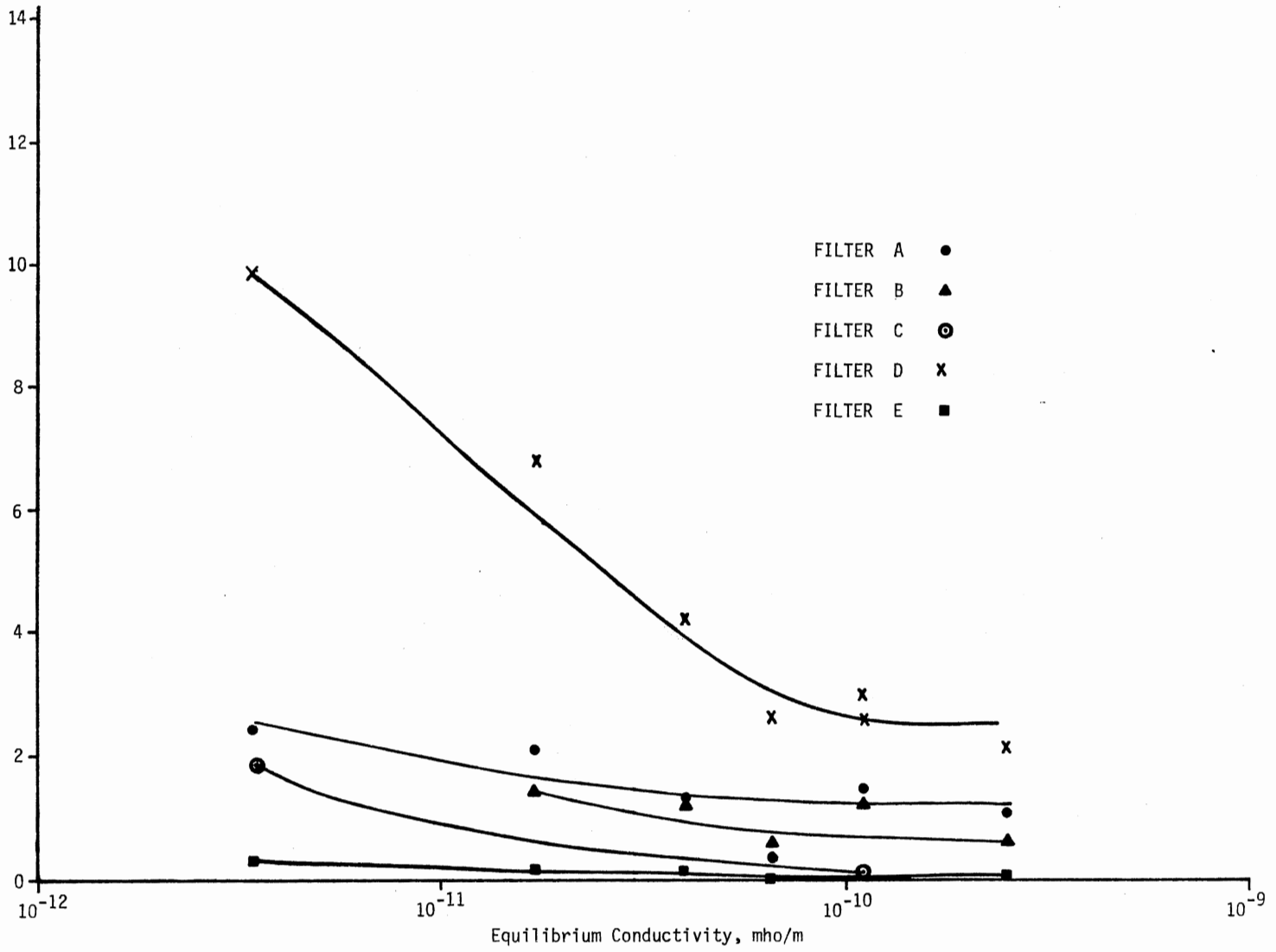

Figure 37. Conductivity Influence on Filtration Ratio

experiments. It can be seen from Figure 37 that as the conductivity is decreased, the filtration ratios increase. This is due to increased charge densities as shown in Figure 38.

It can be concluded from the data in Figure 38 that the charge levels for all filters was extremely low (less than 10^{-5} C/m^3) when the equilibrium conductivity was 10^{-10} mho/m or greater. Figure 37 illustrates for conductivities above approximately 10^{-10} C/m^3 that the filtration ratios are essentially constant at some minimum value. The fluid equilibrium conductivity can easily be controlled by the addition of a conductivity improver additive such as the ASA-3 or DCA-48 used in this investigation. With the ASA-3 additive, the conductivity can be increased above 10^{-10} C/m^3 for amounts in excess of approximately twenty PPM by volume.

It would be recommended from the results of this investigation that the multi-pass test method of Reference (27) be modified to include the addition of ASA-3 additive to the test fluid by an amount in excess of 20 PPM. The stability of the additive to perform over long periods of time is unknown; therefore, it would also be recommended that the minimum amount of additive be added to the test system before each filter evaluation. The experiments conducted with various relative humidities in the surrounding environment showed that the higher humidities have a tendency to reduce charge influences; however, humidity changes alone can not eliminate the electrostatic charge below a signifilevel. Only in the presence of conductivity additives was this accomplished.

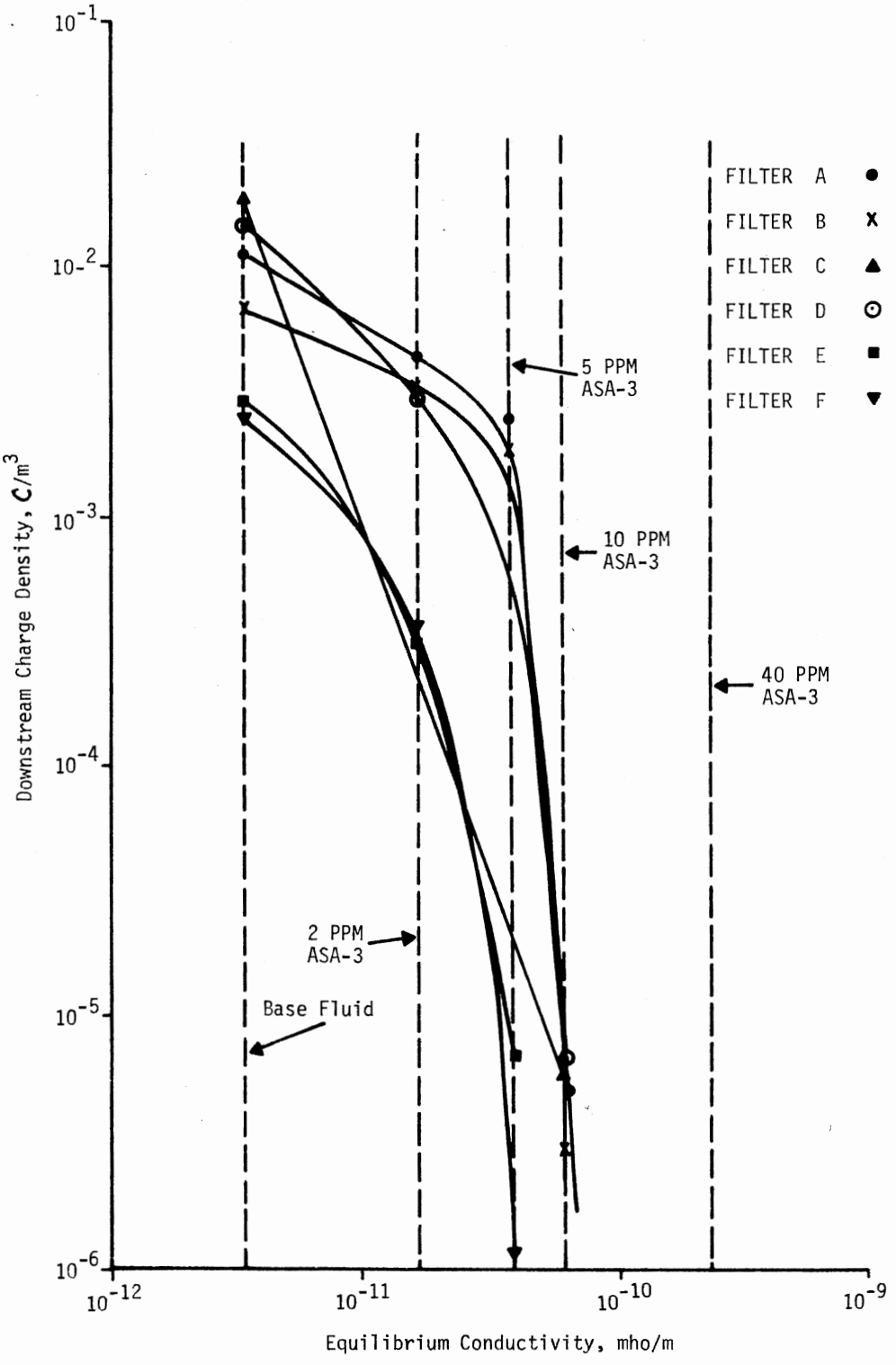

Figure 38. Conductivity Influence on Charge Density

Filter Performance Improvements

The knowledge gained as a result of this investigation should be of help to filter designers in the improvement of their products. A study of the microscopic filter design parameters was beyond the scope of this study; however, the experimental results generally followed trends predicted by equations based upon theory which included filter design parameters. In general, if a filter element can be designed to produce high electrostatic charge generation, a significant improvement in the particle separation characteristics could be expected.

During actual operation of a hydraulic system, large electrostatic charge accumulations would be undesirable. There have been reported instances of hydraulic valve erosion due to internal static discharges. According to the theory for charge dissipation developed in Chapter III, large charge accumulations are unnecessary if flow rates are maintained relatively low and the reservoir volume is large.

A typical situation which would increase hydraulic filter performance in an operating system would be to locate the filter in the return line upstream of the system reservoir. Operating with a low conductivity fluid would then create localized charging within the filter which should be dissipated within the reservoir, if it is well grounded, before the fluid reaches any critical components in the system. The high charge level encountered at the filter should increase the separation performance, yet the charge would cause no damage to the remainder of the system.

Recommendations for Further Study

This investigation has resulted in a great deal of valuable information relative to the performance of hydraulic fibrous filters with electrostatic charge influences. In order to continue the advancement of this field, the following related investigations are recommended for future study:

1) Further experimentation should be conducted to determine the degree of influence of even higher charge generations than were used in this study. The degree of improvement of filtration characteristics appears to be unlimited if charge levels are of sufficient magnitude.

2) A continued thrust should be made into the determination of filter performance in terms compatible with filter media design specifications. The influence of various media parameters such as fiber size, material, and thickness should be evaluated in terms of their contribution to electrostatic charge generation and filtration.

3) An investigation of the dynamic retention characteristics for filters utilizing the electrostatic charge capture mechanism is an important extension of the current study. It is known that when subjected to cyclic or unsteady flow, many hydraulic filters have a tendency to retain less particulate contamination than under steady flow conditions. The ability for a filter to retain particles captured by electrostatic forces is a necessary area of investigation.

4) Finally, in order to maintain the wide acceptance and

confidence that industry is gaining in the multi-pass test method, it is suggested that the recommendations made in this study be implemented as soon as possible. Furthermore, additional experiments should be conducted to determine the stability of the ASA-3 additive, the applicability of other additives such as DCA-48, and the influence of other hydraulic fluids.

CHAPTER VII

SUMMARY AND CONCLUSIONS

Summary

Electrostatic charge forces have long been recognized as a major factor in aerosol filtration. It was generally thought however that such forces were not of significance in hydraulic filtration due to the much higher viscosity and drag forces created by the surrounding fluid. It was recently discovered through continued use of the standard multi-pass hydraulic filter evaluation method (27) that, under specific conditions, electrostatic charge generation was high and filter performance was changed.

The original objectives of this investigation were to examine, both theoretically and experimentally, the charge generation and accumulation characteristics of a recirculating filtered hydraulic system. In addition, the influence of this electrostatic charge upon filter performance was to be studied.

A thorough literature survey revealed a large magnitude of published information relative to the generation of electrostatic charge by fueling systems. None of these studies were directly applicable to recirculating type systems as encountered in the hydraulics field. A generalized charge relaxation and accumulation law was derived and experimentally verified for a multi-pass filter test facility. Experiments were conducted to determine the various effects of fluid conductivity, fluid

additives, particulate impurities, relative humidity, and flow rate.

In order to determine the influence of electrostatic charge on filter performance parameters, a log-normal was proposed for describing filter efficiency. The efficiency distribution function can be thought of as an "effective pore size" distribution. A total of thirty-nine filter tests were conducted to determine the effects of electrostatic charge on these filter performance parameters. The results indicated that the separation efficiency was almost always increased with increasing charge. Empirical equations based upon theoretical developments and test results were proposed for predicting the influence of electrostatic charge on the geometric mean particle size and geometric standard deviation which appear in the log-normal filter model.

Conclusions

From the research investigation described in the preceding chapters, a number of conclusions can be made. The following list summarizes the major accomplishments and conclusions:

1) A generalized model for the accumulation and relaxation of electrostatic charge in a recirculating system was developed to include concepts from both the exponential and hyperbolic relaxation laws.

2) Experimental results confirmed the accuracy of the charge accumulation model and demonstrated that neither the exponential nor hyperbolic relaxation laws proposed by other investigators are applicable to hydraulic recirculating systems.

3) Log-Normal filter efficiency models were proposed for representing the particle separation characteristics of a hydraulic

filter. Graphical techniques for determining the parameters of the model were presented. It can be concluded that in general the filter element separation performance can be modeled according to a log-normal distribution function, especially for separation efficiencies above ten percent.

4) Experiments were conducted to determine the various interactions between electrostatic charge generation, fluid conductivity, surrounding environment relative humidity, particulate contaminants, and the addition of fluid conductivity improver additives. The results show that although each parameter has some influence on charge generation, the conductivity additives have a much broader and predictable effect.

5) Experimental evaluations were performed to determine the influence of electrostatic charge upon the apparent contaminant capacity of hydraulic filter elements. Although slight trends towards increasing capacity with increasing charge were noted, no significant conclusions can be drawn.

6) The influence of electrostatic charge upon the filter particle separation characteristics was determined experimentally. It can definitely be concluded that electrostatic charge forces can become a dominant factor in hydraulic fluid filtration by fibrous filters. The particle separation characteristics are improved as electrostatic charge densities are increased.

7) Based upon theoretical concepts and the experimental results, empirical equations were developed to model the particle retention characteristics as a function of charge density and particle size. It can generally be concluded that in multi-pass

type hydraulic systems, the contaminant particles act as if they were uncharged. The empirical equations developed show that particle retention (due to electrostatics alone) increases with increasing charge and increasing particle size.

8) Utilizing the log-normal model proposed for the filter efficiency or "effective pore size distribution," empirical equations were developed to show the effect of electrostatic charges. Although the precise characteristics appeared to be somewhat a function of the undetermined filter design parameters it can be concluded that generally the geometric mean diameter is reduced and the geometric standard deviation is increased with increasing charge levels.

9) Recommendations were made for modifying the "standard" multi-pass filter test method by including the addition of a minimum of twenty parts per million conductivity additive to the test system fluid before performing a test. This will increase the conductivity and thus reduce the charge generation below significant levels.

10) The general methods developed herein should prove to be useful tools for extended research in filtration mechanics and fluid power system contamination control.

A SELECTED BIBLIOGRAPHY

(1) Klinkenberg, A., and J. L. Van Der minne. Electrostatics in the Petroleum Industry. Amsterdam: Elservier, 1958.

(2) Strauss, K. H., W. G. Dukek, and R. E. Langston. "The Electrostatic Charging Tendencies of Jet Fuel Filtration Equipment." Paper No. 720866 (October, 1972). New York: Society of Automotive Engineers.

(3) Rice, C. L., and R. Whitehead. "Electrokinetic Flow in Narrow Cylindrical Capillary." Journal of Physical Chemistry, Vol. 69 (1965), 4017-4023.

(4) Burgreen, D., and F. R. Nakache. "Electrokinetic Flow in Ultrafine Capillary Slits." Journal of Physical Chemistry, Vol. 68 (1964), 1084-1091.

(5) Gavis, J., and J. P. Wagner. "Electric Charge Generation During Flow of Hydrocarbons Through Microporous Media." Chemical Engineering Science, Vol. 23 (1968), 381-391.

(6) Leonard, J. T., and H. W. Carhart. "Effect of Conductivity on Charge Generation in Hydrocarbon Fuels Flowing Through Fiber Glass Filters." Journal of Colloid and Interface Science, Vol. 32 (1970), 383-394.

(7) Lauer, J. L., and P. G. Antal. "Electrostatic Charge Generation During Nonuniform Flow of Hydrocarbons Through Porous Insulators." Journal of Colloid and Interface Science, Vol. 32 (1970), 407-423.

(8) Huber, P. W., and A. A. Sonin. "Theory for Electric Charging in Liquid Hydrocarbon Filtration," submitted to Journal of Colloid and Interface Science (1976).

(9) Huber, P. W., and A. A. Sonin. "Comments on Gavis and Wagner's Correlation for the Charging Current Generated During Liquid Hydrocarbon Filtration," submitted to Chemical Engineering Science (1976).

(10) Huber, P. W., and A. A. Sonin. "Electric Charging in Liquid Hydrocarbon Filtration: A Comparison of Theory and Experiments," submitted to Journal of Colloid and Interface Science (1976).

(11) Winter, E. F. "The Electrostatic Problem in Aircraft Fueling." Journal of the Royal Aeronautical Society, Vol. 66 (July, 1962), 429-446.

(12) Agnew, J. B. "Static Electricity Generation by Flowing Hydrocarbon Liquids." National Chemical Engineering Conference 1974, Surfers Paradise, Queensland, Australia, July 10-12, 1974.

(13) Vallenga, S. J., and A. Klinkenberg. "On the Rate of Discharge of Electrically Charged Hydrocarbon Liquids." Chemical Engineering Science, Vol. 20 (1965), pp. 923-930.

(14) Carruthers, J. A., and K. J. Marsh. "Charge Relaxation in Hydrocarbon Liquids Flowing Through Conducting and Non-Conducting Pipes." Journal of the Institute of Petroleum, Vol. 48 (1962), 169-179.

(15) Gavis, J. "Transport of Electric Charge in Low Dielectric Constant Fluids." Chemical Engineering Science, Vol. 19 (1964), 237-252.

(16) Kraemer, H. R., and H. F. Johnstone. "Collection of Aerosol Particles in Presence of Electrostatic Fields." Industrial and Engineering Chemistry, Vol. 47 (1955), 2426-2434.

(17) Gillespie, T. "The Role of Electric Forces in the Filtration of Aerosols by Fiber Filters." Journal of Colloid Science, Vol. 10 (1955), 299-314.

(18) Lundgren, D. A., and K. T. Whitby. "Effect of Particle Electrostatic Charge on Filtration by Fibrous Filters." I & EC Process Design and Development, Vol. 4 (1965), 345-349.

(19) Stenhouse, J. I. T. "The Influence of Electrostatic Forces in Fibrous Filtration." Filtration and Separation, Vol. 11 (1974), 25-26.

(20) Zebel, G. "Deposition of Aerosol Flowing Past A Cylindrical Fiber in a Uniform Electric Field." Journal of Colloid Science, Vol. 20 (1965), 522-543.

(21) Loffler, F., and W. Muhr. "A Study of the Deposition of Particles in the 1-10 Microns Range in Model Filters." Filtration and Separation, Vol. 11 (1974), 172-178.

(22) Loffler, F. "Investigation Adhesive Forces Between Solid Particles and Fiber Surfaces." STAUB, Reinhault den Lauf (Engl. Trans.), Vol. 26 (1966), 10-17.

(23) Tucker, R. H. "The Development and Verification of Theoretical Models for the Performance of Wire Cloth Filter Media." (Ph.D. Dissertation, Oklahoma State University, 1966.)

(24) Tessmann, R. K. "Filtration Performance Testing." Basic Fluid Power Research Program Supplement 7-1, Oklahoma State University, 1970.

(25) Bensch, L. E. "Multi-Pass Filtration Performance Test." Basic Fluid Power Research Program Section 71-2, Oklahoma State University, 1971.

(26) Fitch, E. C., and R. K. Tessmann. "Practical and Fundamental Descriptions of Fluid Power Filters," Paper No. 730796. New York: Society of Automotive Engineers (September, 1973).

(27) "American National Standard Multi-Pass Method for Evaluating the Filtration Performance of a Fine Hydraulic Fluid Power Filter Element." ANSI B93.31-1973. New York: American National Standards Institute (1973).

(28) Herdan, G. Small Particle Statistics. London: Butterworth and Company, 1960.

(29) Allen, T. Particle Size Measurement. New York: John Wiley & Sons, 1975.

(30) Smith, J. E., and M. L. Jordan. "Mathematical and Graphical Interpretation of the Log-Normal Law for Particle Size Distribution Analysis." Journal of Colloid Science, Vol. 19 (1964), 549-559.

(31) Cole, F. W. "Particle Count Rationalization." Bendix Corporation, Filter Division Technical Report (1966).

(32) Corte, H. "Pore Size Distribution of Paper." Filtration and Separation, Vol. 3 (1966), pp. 396-403.

(33) Miller, I., and J. E. Freund. Probability and Statistics for Engineers. Englewobd Cliffs, New Jersey, 1965.

(34) Fitch, E. C., and R. K. Tessmann. "Controlling Contaminant Wear Through Filtration," Paper P75-9, Ninth Annual Fluid Power Research Conference, Oklahoma State University, Stillwater, Oklahoma (1975).

(35) Moroney, M. J. Facts From Figures. Baltimore, Maryland: Penguin Books, Inc., 1974.

(36) Mischke, C. R. An Introduction to Computer-Aided Design Englewood Cliffs, New Jersey: Prentice-Hall, Inc., 1968.

(37) Surjaatmadja, J. B., E. C. Fitch, and L. E. Bensch. "Trends in Hydraulic Filtration as Revealed by the Multi-Pass Test," Paper 76-13 Tenth Annual Fluid Power Research Conference, Oklahoma State University, Stillwater, Oklahoma, 1976.

(38) Bensch, L. E., and R. K. Tessmann. "Particle Counting Statistics," Paper 75-11, Ninth Annual Fluid Power Research Conference, Oklahoma State University, Stillwater, Oklahoma (1975).

(39) Grade, L. V. "The Problem of Filter Element By-Pass Leakage," Paper 74-35, Eighth Annual Fluid Power Research Conference, Oklahoma State University, Stillwater, Oklahoma (1974).

(40) Removal of Particulate Matter From Gaseous Wastes (Filtration). New York, N. Y.: American Petroleum Institute, 1961.

(41) "Hydraulic Fluid Power--Calibration of Liquid Automatic Particle-Count Instruments-Method Using Air Cleaner Fine Test Dust Contaminant," ISO 4402-1977 (E), International Organization for Standardization, Geneva, Switzerland (1977).

(42) "Standard Method of Test for Specific Resistance of Electrical Insulating Liquids," ASTM D 1169-74, American Society for Testing and Materials, Philadelphia, Pa. (1974).

(43) "Standard Method of Test for Power Factor and Dielectric Constant of Electrical Insulating Liquids," ASTM D 924-65, American Society for Testing and Materials, Philadelphia, Pa. (1965).

(44) "Standard Method of Test for Electrostatic Charge," ASTM D 2679-73, American Society for Testing and Materials, Philadelphia, Pa. (1973).

APPENDIX A

MULTI-PASS HYDRAULIC FILTER TEST FACILITY

All filter tests which were performed as a part of this research investigation were conducted utilizing the multi-pass test facility shown in the photograph in Figure 39. The hydraulic system can be illustrated in a simplified manner as shown in Figure 40. A detailed circuit schematic showing all components is presented in Figure 41.

The main filter test system was essentially composed of a reservoir hydraulic gear pump and circulating system with controls for temperature and flow rate. The facility was constructed of nearly all metallic components including lines and fittings. The tubing in the test circuit had a nominal size of 2.54 cm (1 inch) with an inside diameter of 2.21 cm. Thus the cross sectional or flow area of the tubing was 3.84×10^{-4} m^2. The approximate lengths of lines for the test circuit are shown in Figure 40.

The contaminant injection system consisted of a reservoir, pump, and appropriate controls. During testing the injection contamination level may be extremely high (several thousand mg/l concentration); therefore, the injection pump was a centrifugal type which has been found to be relatively insensitive to contaminant. The primary purpose of the injection circuit was to maintain a uniform contaminant suspension with a constant particle size distribution. This contaminant slurry is injected into the main filter test system during a complete multi-pass test.

In addition to the test and injection systems, the multi-pass facility also consisted of a contaminant clean-up system. The function of the clean-up system was to clean the system fluid to the required contamination level prior to conducting a test. The clean up filters utilized had an average filtration ratio of 10 micrometres in excess of

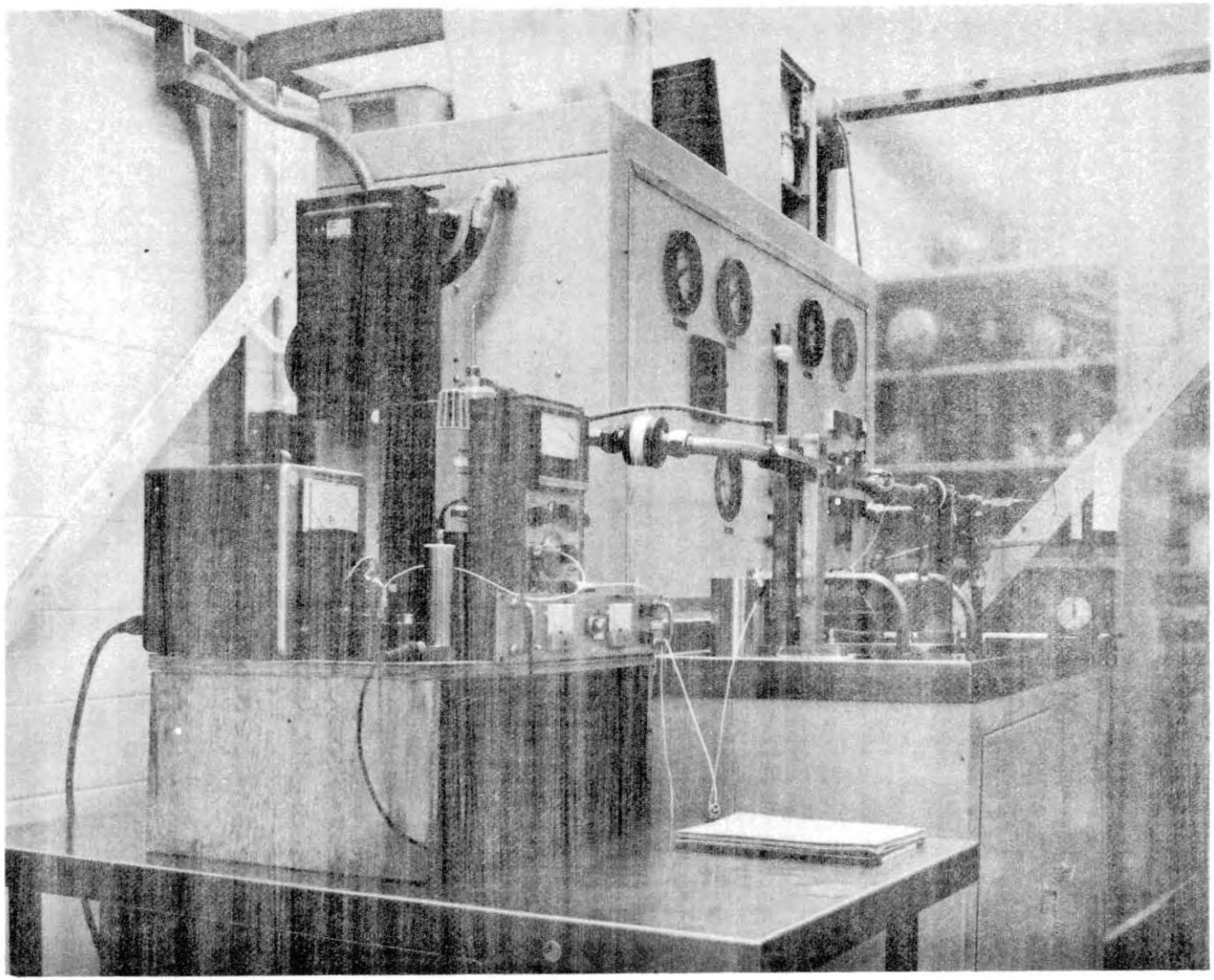

Figure 39. Experimental Set-Up for Electrostatic Charge Tests

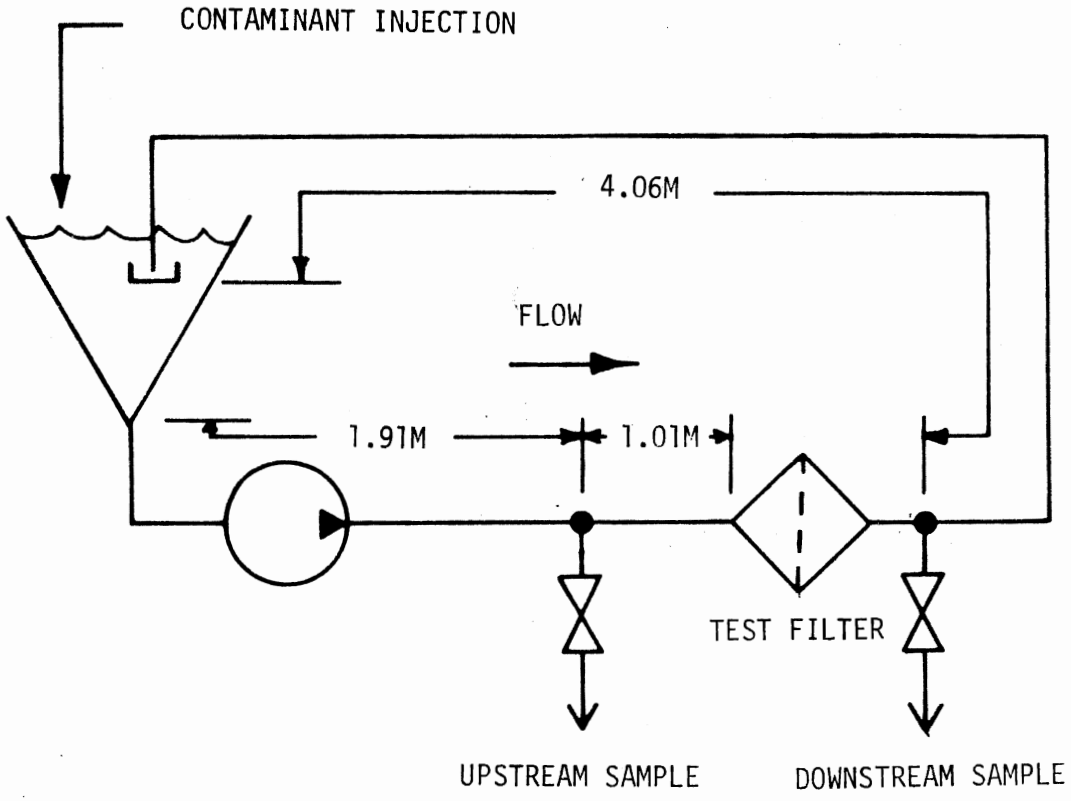

Figure 40. Simplified Multi-Pass Circuit Schematic

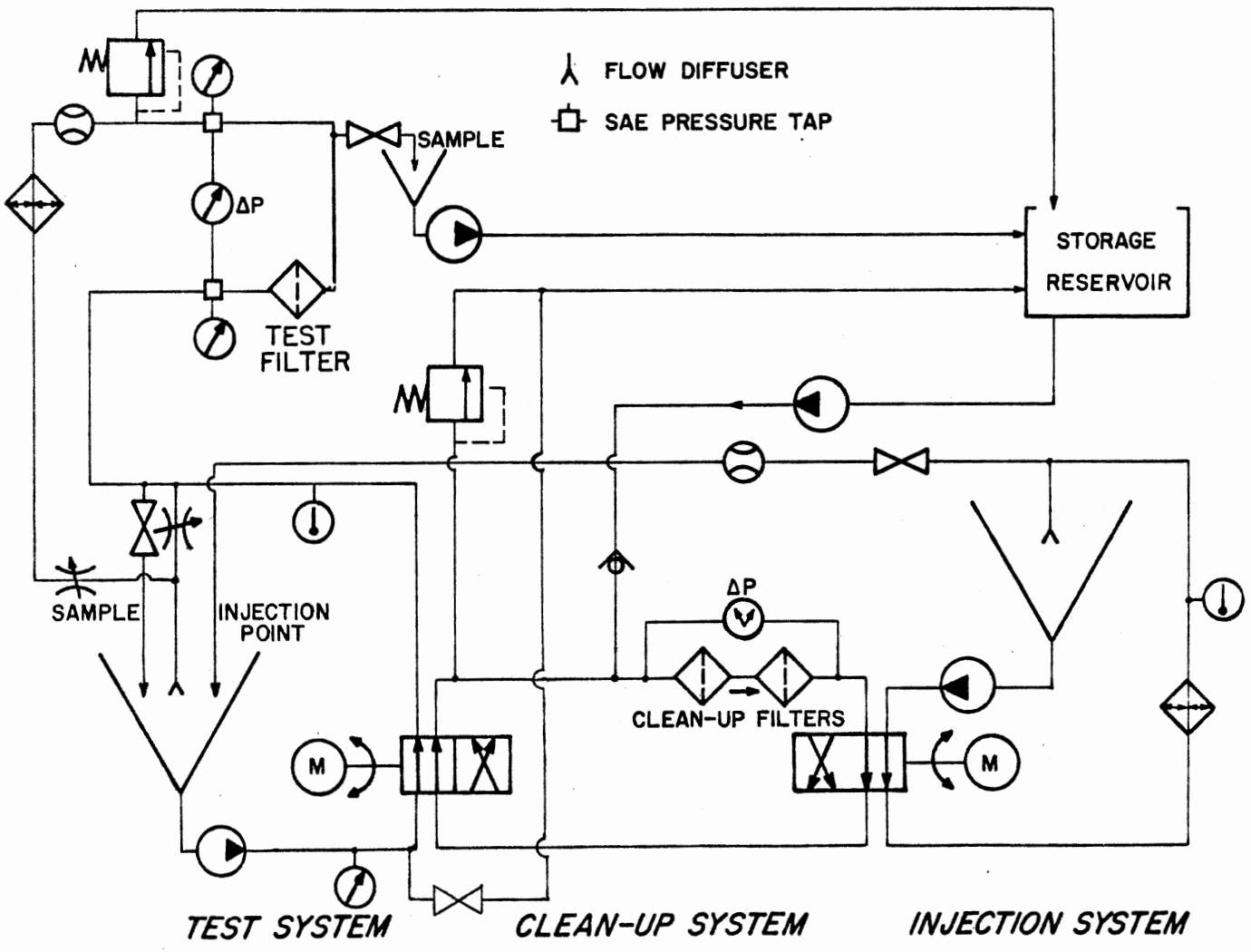

Figure 41. Detailed Multi-Pass Test Circuit Schematic

500 which corresponds to a cumulative efficiency of 99.8%. This high filtration ratio resulted in shorter clean up times between tests.

A transparent plastic enclosure was constructed to completely house the multi-pass test facility as well as the electrostatic measurement apparatus. This enclosure allowed the environmental conditions surrounding the test facility to be accurately controlled. Relative humidity was controlled by an automatic humidifier and de-humidifier and temperature was controlled by an air conditioner and heater as required. Relative humidity measurements were made with a Beckman "Humi-Chek" solid state relative humidity indicator as well as with a sling psychrometer. The variation between the two measurement devices was generally less than 10%; however, the calibrated Beckman instrument readings were reported in the data.

APPENDIX B

MULTI-PASS HYDRAULIC FILTER TEST PROCEDURE

The standard multi-pass test method (27) utilizes the test facility described in Appendix A for evaluating the filtration performance characteristics of a hydraulic filter. The name "multi-pass" was derived from the most characteristic feature of the test — the recirculation of the contaminant which permeates through the filter. In addition to the "multi-passed" contaminant, a fresh amount of contaminant is continually introduced into the reservoir from the injection system. The contaminant injection is continued until the filter pressure differential has increased above a predetermined level called the terminal pressure drop.

The multi-pass test was developed in order to simulate an actual operating environment as closely as possible while still maintaining repeatability and reproducibility characteristics. AC Fine Test dust (commercially available from the AC Spark Plug Division of General Motors Corporation) is utilized as the test contaminant. This test dust was chosen to simulate actual contaminants found in operating systems and because of the consistency of the dust from batch to batch.

The contaminant injection is made in a slurry form at a flow rate generally in the range of 0.25 - 0.50 ml/min. The injection rate expressed in milli-grams/minute is determined such that the theoretical contamination level upstream of the filter is 10 mg/l. The 10 mg/l level is an arbitrary number selected to improve test repeatability. The injection rate can be calculated as follows:

$$\text{Injection Rate (mg/min)} = (10 \text{ mg/1}) \times (\text{Filter flow rate, 1/min})$$

The volume of fluid (Mil-H-5606 hydraulic fluid) in the test system is set equal to one-fourth the filter flow rate (per minute) value.

Thus, a 40 l/min filter would be tested with a total circulating system volume of 10 litres. A continuous sample is removed from the system at a point downstream of the test filter. This downstream sample flow rate is set equal to the injection flow rate, thus the volume of fluid in the test circuit is maintained constant. Numerous tests as well as mathematical analyses have shown that the contaminant removed by the downstream sample is insignificant for all practical test conditions and does not alter the test results.

During a multi-pass test, fluid samples are extracted from a turbulent region both upstream and downstream of the test filter. The sample times are determined by the pressure loading characteristics of the filter such that they occur at designated predetermined pressure drop values. This helps to insure test repeatability. During the research effort reported in this dissertation additional samples were also occasionally taken at predetermined intervals in order to allow a more complete description of the filter performance throughout the life of the filter.

The fluid samples from a multi-pass test are analyzed for particle size distribution with an automatic particle counter calibrated with AC Fine Test Dust per Reference (41). The particle counter utilized during this research investigation was a HIAC model PC-320 with twelve particle size ranges. All particle counts were determined on a cumulative basis at 2, 3, 5, 7, 10, 15, 20, 25, 30, 35, 40, and 50 micrometres.

The primary figure of merit for a hydraulic filter is the indicator of its ability to capture and retain particles of contaminant. In a standard multi-pass test, this parameter is the filtration ratio defined as the number of particles greater than a given particle size in the

influent fluid divided by the number of particles greater than the same size in the effluent fluid. A filtration or "beta" ratio of unity signifies no particle separation while a high beta ratio means that the filter is removing a significant amount of contaminant. A beta value of two indicates a 50% cumulative efficiency as the downstream contamination level would be one-half of the upstream value.

In addition to the filtration ratio, another important figure of merit resulting from the multi-pass test is the ACFTD capacity. This is the apparent contaminant capacity of the filter when exposed to AC Fine Test Dust on a multi-pass basis. The ACFTD capacity is calculated by multiplying the injection rate (mg/min) times the test termination time (minutes) and is usually expressed in grams. The ACFTD capacity is referred to as an apparent capacity because it represents the amount of contaminant added to the filter system before plugging and not the amount retained by the filter. An extremely poor filter will generally exhibit a high ACFTD capacity because it is removing very little contaminant. Thus, the ACFTD capacity cannot alone be a useful merit parameter but should be reported with the filtration ratios.

Some modifications to the standard multi-pass filter test method were made during this investigation as reported previously. However, the basic concepts and standardized test conditions were followed. The test results obtained as a result of this program should thus have a greater applicability to existing data from other laboratories and can be directly compared to other multi-pass test results.

APPENDIX C

ELECTRICAL MEASUREMENT TECHNIQUES

During the course of this investigation, it was desired to conduct measurements of several electrically associated parameters — fluid conductivity, dilectric constant, electrostatic charge density, and streaming current. Whenever possible, standard techniques were utilized; however, most measurements required modifications for the particular application. The following is a detailed summary of the measurement apparatus and techniques utilized in the study.

Fluid Electrical Conductivity

The electrical conductivity of a fluid is a measure of the discharge time of a capacitor which uses the fluid as a dielectric. The units of conductivity are $\frac{1}{\Omega m}$ or mho/m. Because of the magnitude of the conductivity for many hydrocarbons, it is sometimes expressed in units of picomho/m. The D. C. method was utilized in this investigation for measurement of conductivity. The procedure followed was generally in accordance with ASTM D 1169-74 (42) which is actually a method for determining the specific resistance or resistivity (inverse of conductivity) of electrical insulating liquids.

The conductivity cell utilized was a standard commercially available device manufactured by Balsbaugh Laboratories, Model No. LRC-1. The cell has a nominal air capacitance of 50 pf, a 1.27 mm electrode spacing, and requires approximately 25 ml of fluid for measurements. The actual capacitance of the cell was measured with a Tektronix type 130 L-C meter to be 55.5 pf. Figure 42 is a photo of the cell in an assembled and disassembled configuration.

The test procedure for measuring the conductivity of the test fluids was the following:

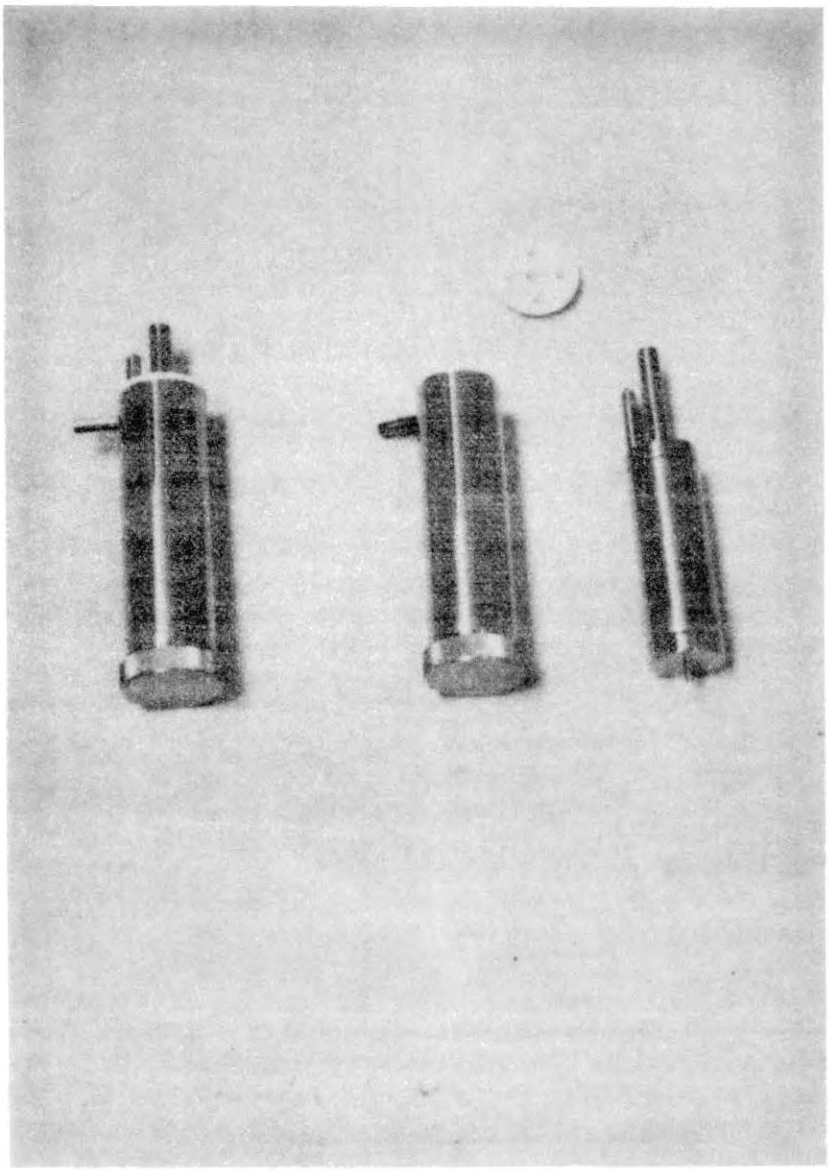

Figure 42. Model LRC-1 Liquid Reference Cell

1) Clean the test cell with petroleum ether then allow to dry.
2) Check the resistivity of the cell with air as the dielectric to insure adequate cleaning and drying.
3) Add 25 ml of liquid to be tested.
4) Apply a constant DC voltage equal to 100 V across the cell electrodes.
5) Measure and record the current after two minutes have elapsed.
6) Calculate the resistivity by dividing the measured amperage into 100 V and multiplying by the cell constant.
7) Calculate the conductivity by taking the inverse of the resistivity.

The cell constant expressed in metres was calculated in accordance with ASTM 1169 by multiplying the cell capacitance with air as the dielectric times 0.113. Thus the cell constant for the model LRC-1 cell utilized was 0.113 x 55.5 = 6.27 m. The voltage and current measurement were performed with a Keithley model 610C solid state electrometer. The electrometer has an input resistance of greater than 10^{14} ohms and an offset current of less than $5X10^{-15}$ amperes. A large number of tests were conducted on fluid samples with various conductivities in order to refine the test method for obtaining highest repeatability.

Fluid Dielectric Constant

The dielectric constant of the MIL-H-5606 hydraulic fluid was measured with the Balsbaugh reference cell utilized for the conductivity measurements. The ASTM D 924 procedure (43) was generally followed when making the dielectric measurements. The dielectric constant of a liquid is determined by dividing the capacitance of the test cell with the

liquid as the dielectric by the capacitance with air as the dielectric. The capacitances were measured with the Tektronix L-C meter. The dielectric constant for MIL-H-5606 hydraulic fluid was measured to be 1.79 and did not vary significantly under the presence of anti-static additives.

Electrostatic Charge Density

A most important measurement taken during this study was the electrostatic charge density in the liquids. The ASTM D 2679 procedure (44) for measuring electrostatic charge was generally followed during the testing. A Faraday cage was constructed as illustrated in Figure 43 with two concentric stainless steel containers. The volume of the inner container utilized was 425 ml. The measured capacitance of the Faraday cage was 205 pf with the line and electrometer adding an additional 120 pf. For high charge measurements, two additional shunt capacitors were utilized with values of 0.018 and 0.10 pf.

The test procedure for measuring electrostatic charge density in the fluid consisted of the following:

1) Clean Faraday cage and dry thoroughly.
2) Select appropriate shunt capacitor if required and connect into circuit.
3) Zero, then open the electrometer in the voltage mode.
4) Insert the fluid sample to the designated level in the inner container (425 ml). (This was accomplished by opening a sample valve on the test stand and allowing fluid to flow into the container at a rate of approximately 5 l/min.)
5) Measure and record the voltage on the electrometer as soon as

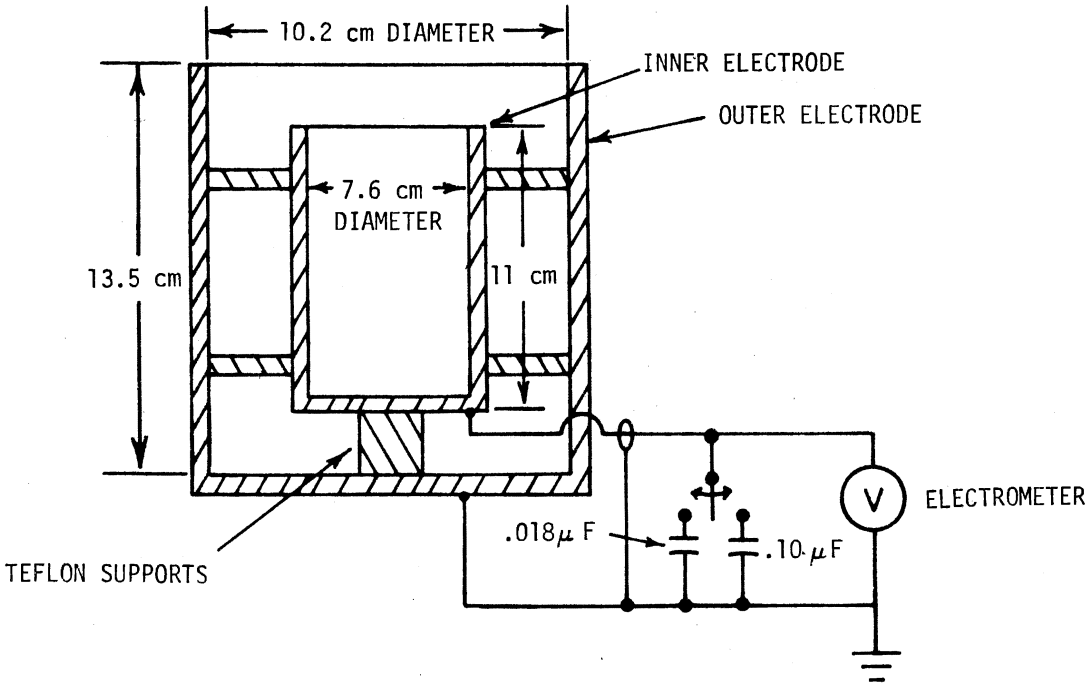

Figure 43. Faraday Cage for Electrostatic Charge Measurements

the sample is inside the container.

6) Calculate the electrostatic charge density by the following relationship:

$$\text{Charge Density } \frac{C}{m^3} = \frac{(\text{total capacitance, farads}) \times (\text{voltage, volts})}{\text{Fluid Volume } (m^3)}$$

When the relative humidity of the surrounding atmosphere was less than approximately 50%, the voltage reading was extremely stable for a period of several seconds and was independent of the fluid sample flow rate. However, with high relative humidities in the order of 80%, the charge decay was much more rapid and accurate readings become more difficult to measure. To maintain maximum repeatability, the voltage reading was recorded as quickly as possible after the sample flow was stopped. A high sample flow rate (approximately 5 litres (minute) was also utilized to minimize charge relaxation during the sample period.

Streaming Current

In order to measure the streaming current generated across the test filter during the flow of fluid through it, electrodes were inserted in the test line upstream and downstream of the filter. The current flowing between the two electrodes was measured with the Keithley electrometer. The test set-up was as illustrated in Figure 44. The electrodes were constructed of 10 mesh stainless steel screen approximately 5 cm in diameter. The electrodes were supported and electrically isolated from the remainder of the test system by Teflon supports as illustrated in Figure 44.

With this test set-up, high accuracy in the streaming current measurement was not possible. Because the lines connecting the inlet

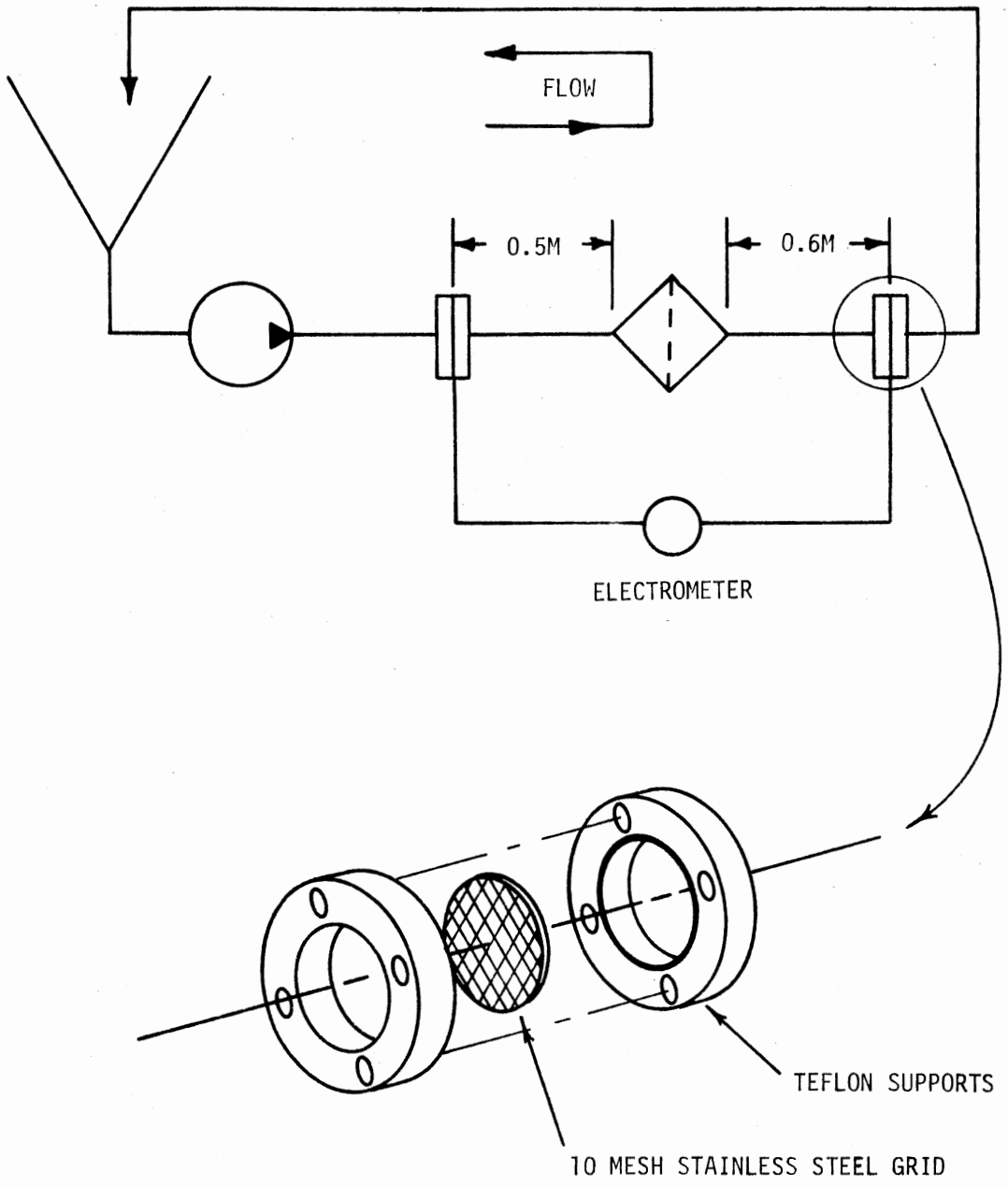

Figure 44. Set-Up for Measuring Streaming Current

and outlet of the filter and also the filter housing were electrically conductive, a portion of the current generated was probably shorted back to the upstream side of the filter assembly. Readings were taken, however, in order to find a relative determination of the current magnitude, its sign, and changes in current with respect to other operating variables. Figure 45 gives a relative indication of the streaming currents measured during this investigation. The data shown in Figure 45 were taken with a fluid conductivity of 3.4×10^{-12} mho/m.

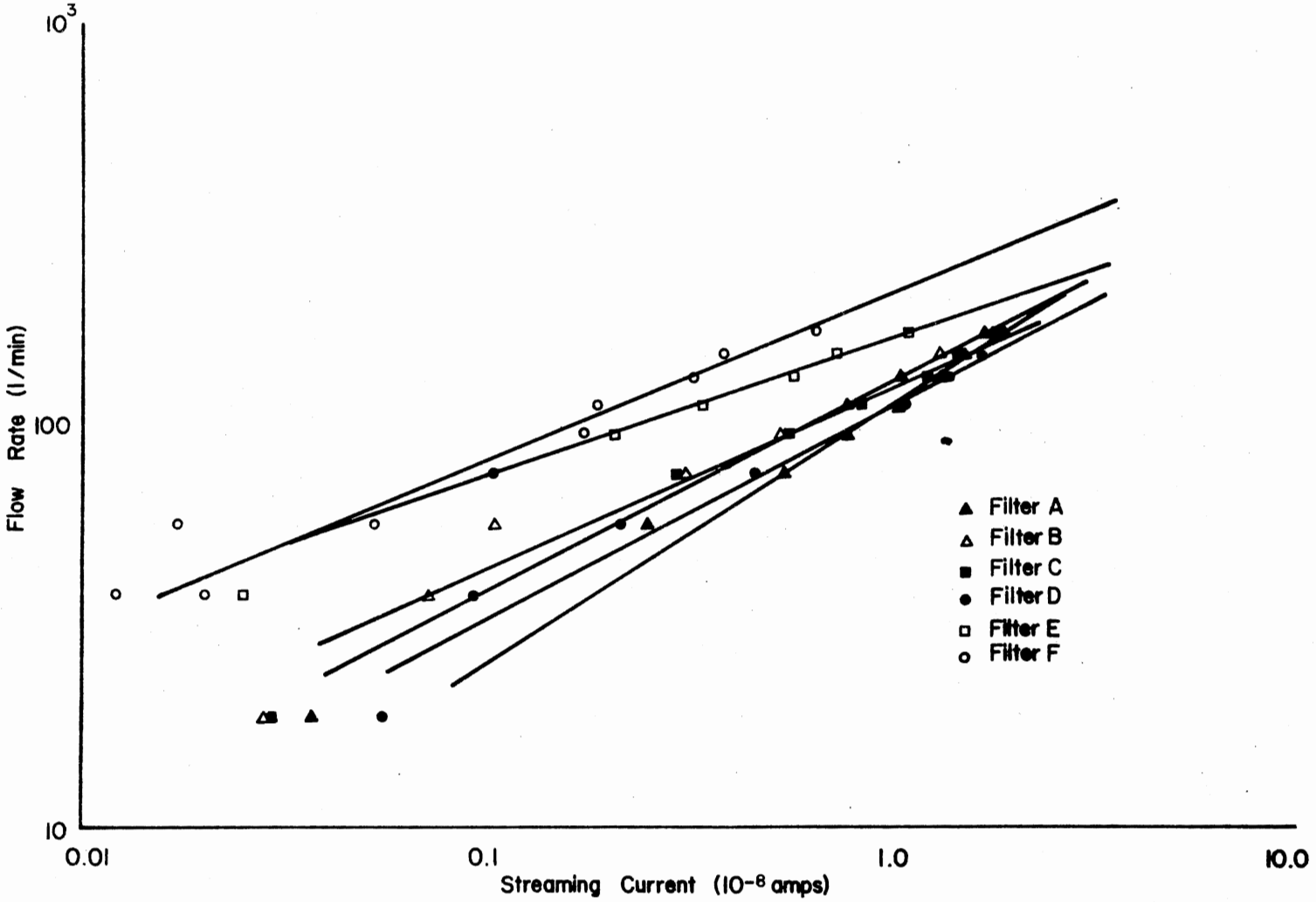

Figure 45. Typical Streaming Current Measurements With Varying Flow Rate

APPENDIX D

SUMMARY OF REPRESENTATIVE TEST DATA

CHARGE ACCUMULATION DATA SUMMARY

FILTER		FLOW RATE(L/MIN.)					
		19.0	38.0	76.0	114.0	151.0	170.0
A	SD	1.37E-02	9.24E-03	1.09E-02	1.17E-02	1.28E-02	1.34E-02
	SX	1.10E-05	3.58E-05	2.51E-04	1.50E-03	2.01E-03	2.37E-03
	R	1.25E+03	2.58E+02	4.34E+01	7.80E+00	6.37E+00	5.65E+00
B	SD	1.48E-02	1.34E-02	1.36E-02	1.39E-02	1.43E-02	1.43E-02
	SX	8.20E-06	1.85E-05	3.05E-04	9.58E-04	1.42E-03	1.64E-03
	R	1.80E+03	7.24E+02	4.46E+01	1.45E+01	1.01E+01	8.72E+00
C	SD	2.02E-02	1.92E-02	1.92E-02	1.97E-02	2.04E-02	2.09E-02
	SX	7.50E-06	3.36E-05	3.42E-04	1.26E-03	1.79E-03	1.96E-03
	R	2.69E+03	5.71E+02	5.61E+01	1.56E+01	1.14E+01	1.07E+01
D	SD	1.59E-02	1.61E-02	1.52E-02	1.63E-02	1.66E-02	1.65E-02
	SX	8.30E-06	2.16E-05	2.22E-04	1.27E-03	1.83E-03	1.92E-03
	R	1.92E+03	7.45E+02	6.85E+01	1.28E+01	9.07E+00	8.59E+00
E	SD	9.90E-04	1.80E-03	2.92E-03	4.13E-03	5.06E-03	5.45E-03
	SX	6.90E-06	1.68E-05	9.92E-05	3.24E-04	6.90E-04	8.37E-04
	R	1.43E+02	1.07E+02	2.94E+01	1.27E+01	7.33E+00	6.51E+00
F	SD	2.29E-03	3.01E-03	2.67E-03	2.24E-03	2.14E-03	2.04E-03
	SX	9.40E-06	1.95E-05	8.41E-05	1.90E-04	2.85E-04	3.15E-04
	R	2.44E+02	1.54E+02	3.17E+01	1.18E+01	7.51E+00	6.48E+00

CONDUCTIVITY = 3.4, MIL-H-5606, RH = 35.%
SD = C/M**3, SX = C/M**3, R = SD/SX

CHARGE ACCUMULATION DATA SUMMARY

FILTER		FLOW RATE(L/MIN.)					
		19.0	38.0	76.0	114.0	151.0	170.0
A	SD	1.24E-02	8.99E-03	1.06E-02	1.22E-02	1.24E-02	1.31E-02
	SX	9.90E-06	2.48E-05	1.12E-04	1.47E-03	2.09E-03	2.22E-03
	R	1.25E+03	3.63E+02	9.46E+01	8.30E+00	5.93E+00	5.90E+00
B	SD	1.12E-02	1.01E-02	1.08E-02	1.16E-02	1.22E-02	1.24E-02
	SX	8.30E-06	1.98E-05	2.56E-04	9.83E-04	1.55E-03	1.73E-03
	R	1.35E+03	5.10E+02	4.22E+01	1.18E+01	7.87E+00	7.17E+00
C	SD	1.65E-02	1.53E-02	1.53E-02	1.65E-02	1.68E-02	1.82E-02
	SX	7.50E-06	2.01E-05	1.92E-04	1.27E-03	1.81E-03	1.98E-03
	R	2.20E+03	7.61E+02	7.97E+01	1.30E+01	9.28E+00	9.19E+00
D	SD	8.75E-03	9.97E-03	1.09E-02	1.16E-02	1.24E-02	1.29E-02
	SX	8.20E-06	1.85E-05	1.48E-04	9.49E-04	1.42E-03	1.64E-03
	R	1.07E+03	5.39E+02	7.36E+01	1.22E+01	8.73E+00	7.85E+00
E	SD	4.01E-03	2.67E-03	3.74E-03	4.76E-03	5.47E-03	5.59E-03
	SX	7.90E-06	1.81E-05	9.10E-05	4.40E-04	8.07E-04	9.06E-04
	R	5.08E+02	1.48E+02	4.11E+01	1.08E+01	6.78E+00	6.17E+00
F	SD	2.41E-03	3.45E-03	3.21E-03	2.80E-03	2.41E-03	2.36E-03
	SX	8.50E-06	1.70E-05	9.06E-05	2.11E-04	3.19E-04	3.62E-04
	R	2.84E+02	2.03E+02	3.54E+01	1.33E+01	7.55E+00	6.52E+00

CONDUCTIVITY = 4.9, MIL-H-5606, RH = 55.%
SD = C/M**3, SX = C/M**3, R = SD/SX

CHARGE ACCUMULATION DATA SUMMARY

FILTER		FLOW RATE(L/MIN.)				
		19.0	38.0	76.0	114.0	151.0
A	SD	1.02E-02	8.27E-03	1.05E-02	1.14E-02	1.26E-02
	SX	8.50E-06	1.81E-05	8.10E-05	9.27E-04	1.42E-03
	R	1.20E+03	4.57E+02	1.30E+02	1.23E+01	8.87E+00
B	SD	8.50E-04	2.92E-03	5.25E-03	5.93E-03	6.20E-03
	SX	7.80E-06	1.51E-05	6.04E-05	2.46E-04	4.92E-04
	R	1.09E+02	1.93E+02	8.69E+01	2.41E+01	1.26E+01
C	SD	6.32E-03	7.29E-03	9.72E-03	1.12E-02	1.24E-02
	SX	6.70E-06	1.60E-05	1.60E-04	5.18E-04	8.63E-04
	R	9.43E+02	4.56E+02	6.07E+01	2.16E+01	1.44E+01
D	SD	2.29E-03	6.61E-03	9.48E-03	1.02E-02	1.02E-02
	SX	6.90E-06	1.64E-05	1.68E-04	5.31E-04	9.40E-04
	R	3.32E+02	4.03E+02	5.64E+01	1.92E+01	1.09E+01
E	SD	1.36E-03	2.21E-03	3.21E-03	4.25E-03	5.01E-03
	SX	6.90E-06	1.51E-05	6.69E-05	2.46E-04	4.92E-04
	R	1.97E+02	1.46E+02	4.80E+01	1.73E+01	1.02E+01
F	SD	2.10E-03	3.28E-03	3.06E-03	2.67E-03	2.11E-03
	SX	8.40E-06	1.68E-05	4.46E-05	1.64E-04	2.50E-04
	R	2.50E+02	1.95E+02	6.86E+01	1.63E+01	8.44E+00

CONDUCTIVITY = 7.6, MIL-H-5606, RH = 80.%
SD = C/M**3, SX = C/M**3, R = SD/SX

SUMMARY OF FILTRATION RATIOS

FILTER ID.	DOWNSTREAM CHARGE (.001C/M**3)	(PARTICLE SIZES INDICATED IN MICROMETERS) >2	>3	>5	>7	>10	>15	>20	>25	>30	>35	>40	>50
A 1	1.87E-04	1.21	1.40	1.75	2.68	5.22	18.07	40.99	49.34	46.97	38.88	41.73	34.37
A 2	6.58E-04	1.15	1.27	1.51	2.23	4.28	16.59	48.96	79.56	81.83	73.26	50.84	36.54
A 3	8.72E-04	1.24	1.40	1.75	2.62	5.17	22.27	59.89	78.79	64.87	76.20	67.13	70.87
A 4	5.74E-03	1.09	1.17	1.36	1.86	3.24	11.16	21.36	26.03	20.18	15.86	15.83	14.26
A 5	2.55E+00	1.17	1.31	1.64	2.50	4.86	13.05	17.61	17.14	17.63	15.62	12.76	16.21
A 6	4.38E+00	1.39	1.64	2.08	3.19	6.37	23.46	48.02	47.13	43.65	40.90	37.73	36.75
A 7	1.17E+01	1.85	1.96	2.43	3.42	5.41	8.47	10.10	13.62	14.34	16.06	12.62	14.85
A 8	1.09E+01	2.67	3.38	4.63	7.62	13.22	19.39	20.15	24.11	42.72	51.76	58.57	50.75
B 1	1.45E-05	1.09	1.15	1.31	1.74	3.01	9.12	15.40	15.87	15.25	11.83	8.34	10.42
B 2	1.76E-04	1.19	1.31	1.58	2.30	4.39	14.31	24.58	28.21	27.19	25.01	23.34	20.71
B 3	2.14E-04	1.21	1.34	1.59	2.28	4.25	15.85	35.34	45.72	43.81	34.07	30.87	28.75
B 4	2.45E-03	1.08	1.15	1.31	1.77	3.19	8.43	12.83	14.39	13.84	12.56	12.48	16.01
B 5	1.87E+00	1.19	1.32	1.60	2.38	4.84	19.02	46.82	51.65	47.52	46.62	44.92	30.17
B 6	3.31E+00	1.21	1.37	1.72	2.72	5.98	31.03	99.83	117.49	143.95	104.93	89.34	40.30
B 7	7.05E+00	1.30	1.52	1.91	3.57	7.20	26.95	37.94	40.73	55.64	60.87	59.89	71.38
C 1	5.74E-04	1.04	1.05	1.06	1.09	1.15	1.44	2.22	3.93	8.58	18.81	37.91	*****
C 2	5.96E-03	1.06	1.07	1.07	1.10	1.15	1.44	2.53	4.67	11.00	29.31	27.09	33.23
C 3	1.92E+01	1.67	1.80	1.94	2.21	2.69	4.16	5.92	7.56	10.38	10.31	10.44	8.22
D 1	2.83E-04	1.19	1.43	2.15	4.34	8.36	13.33	14.28	14.72	14.78	13.87	11.99	12.61
D 2	4.21E-04	1.29	1.67	2.62	4.94	7.48	8.33	8.52	7.87	7.09	6.63	5.37	5.64
D 3	6.66E-03	1.29	1.63	2.56	5.79	16.33	40.13	45.68	48.15	43.51	44.48	42.04	32.94
D 4	7.65E-03	1.66	2.54	4.27	8.40	12.50	13.98	14.71	16.10	17.26	14.97	14.55	12.11
D 5	1.19E-02	1.33	1.73	2.98	7.52	11.56	13.67	15.06	12.70	10.37	11.34	11.14	9.76
D 6	2.93E+00	1.93	3.14	6.39	15.26	26.61	33.99	37.15	37.68	33.11	33.46	35.50	27.89
D 7	1.52E+01	3.36	5.55	9.82	18.20	27.24	29.94	32.51	32.17	33.04	32.20	33.83	29.37
E 1	1.21E-04	1.01	1.01	1.02	1.02	1.06	1.23	1.88	3.45	5.74	10.59	9.62	7.19
E 2	1.45E-04	1.03	1.03	1.04	1.07	1.13	1.36	1.96	3.46	5.67	10.43	12.96	18.17
E 3	1.11E-03	1.03	1.05	1.06	1.08	1.14	1.36	1.78	2.83	4.16	6.99	7.56	5.93
E 4	1.26E-03	1.04	1.05	1.06	1.09	1.14	1.36	1.84	2.60	3.93	5.06	5.64	5.59
E 5	7.04E-03	1.04	1.06	1.08	1.10	1.17	1.46	2.27	2.56	3.67	4.11	3.94	3.18
E 6	3.35E-01	1.06	1.07	1.10	1.14	1.23	1.59	2.68	5.04	11.84	23.20	57.36	115.46
E 7	2.92E+00	1.09	1.11	1.14	1.19	1.28	1.68	2.72	5.41	10.82	21.67	28.34	51.04
F 1	9.18E-05	2.63	5.03	11.42	23.38	27.80	29.20	52.27	68.46	88.97	93.28	112.75	186.93
F 2	7.76E-04	2.09	3.72	8.53	25.28	63.67	106.16	119.12	142.09	137.33	162.96	114.52	123.04
F 3	1.09E-03	3.08	6.16	14.37	34.61	57.68	76.23	90.80	127.16	139.83	166.60	198.79	337.08
F 4	1.15E-03	2.10	4.03	9.88	23.14	34.56	40.74	49.62	73.89	84.80	107.70	102.82	152.40
F 5	1.19E-03	2.87	5.91	13.70	45.19	147.07	348.61	379.58	394.65	536.87	461.32	395.67	329.29
F 6	3.82E-01	3.97	10.31	32.26	95.45	179.54	183.37	238.03	307.82	368.50	369.59	425.08	******
F 7	2.67E+00	4.22	9.48	21.81	48.64	75.15	91.12	128.46	154.47	143.91	107.44	103.52	169.19

FLOW RATE FOR A1 - A7 WAS 114 L/MIN.
FLOW RATE FOR OTHERS WAS 76 L/MIN.
TEST FLUID: MIL - H - 5606, 38C

SUMMARY OF AVERAGE RETENTION RATIOS

FILTER ID.	DOWNSTREAM CHARGE (.001C/M**3)	(PARTICLE SIZE INTERVALS INDICATED IN MICROMETERS) 2-3	3-5	5-7	7-10	10-15	15-20	20-25	25-30	30-35	35-40	40-50	>50
A 1	1.87E-04	1.06	1.20	1.44	2.04	3.98	12.27	34.33	53.71	68.25	32.34	52.55	34.37
A 2	6.58E-04	1.06	1.14	1.30	1.78	3.32	10.96	33.33	76.68	96.37	238.29	78.66	36.54
A 3	8.72E-04	1.09	1.21	1.45	2.00	3.89	14.39	47.36	121.29	53.23	101.26	67.12	70.87
A 4	5.74E-03	1.03	1.08	1.21	1.54	2.60	8.21	18.20	39.91	30.86	14.95	16.26	14.26
A 5	2.55E+00	1.04	1.15	1.38	1.94	3.84	10.82	18.03	16.61	22.04	26.51	10.46	16.21
A 6	4.38E+00	1.18	1.36	1.67	2.37	4.77	16.30	48.73	53.84	49.36	49.56	36.99	36.75
A 7	1.17E+01	1.72	1.67	2.03	2.74	4.71	7.27	7.95	12.84	11.49	28.38	10.46	14.85
A 8	1.09E+01	2.02	2.49	3.26	5.46	10.78	18.36	17.32	15.47	47.64	43.83	64.85	50.75
B 1	1.45E-05	1.04	1.08	1.18	1.46	2.44	6.94	14.96	17.04	27.23	33.57	7.03	10.42
B 2	1.76E-04	1.06	1.15	1.34	1.81	3.41	10.66	21.37	29.72	31.30	29.52	26.16	20.71
B 3	2.14E-04	1.08	1.18	1.36	1.82	3.29	10.86	28.31	47.00	60.65	42.56	36.59	28.75
B 4	2.45E-03	1.03	1.07	1.18	1.47	2.61	6.53	11.36	15.18	16.37	12.50	10.56	16.01
B 5	1.87E+00	1.07	1.17	1.36	1.85	3.69	12.52	42.18	56.34	51.48	51.36	80.43	30.17
B 6	3.31E+00	1.06	1.16	1.42	2.04	4.38	19.32	85.82	90.23	299.48	123.51	449.98	40.30
B 7	7.05E+00	1.09	1.27	1.47	2.71	5.45	21.58	35.21	29.40	48.97	61.65	53.14	71.38
C 1	5.74E-04	1.03	1.04	1.05	1.06	1.11	1.27	1.82	2.27	5.09	9.77	18.41	*****
C 2	5.96E-03	1.05	1.06	1.06	1.08	1.10	1.23	1.93	2.90	5.85	33.85	22.31	33.23
C 3	1.92E+01	1.50	1.64	1.75	1.96	2.34	3.52	5.01	5.69	10.40	11.02	12.32	8.22
D 1	2.83E-04	1.06	1.21	1.67	3.18	7.01	12.54	13.67	14.55	15.62	19.82	11.41	12.61
D 2	4.21E-04	1.08	1.34	1.99	3.86	7.06	8.16	9.43	9.21	7.73	10.16	5.14	5.64
D 3	6.66E-03	1.04	1.25	1.83	3.86	12.50	36.43	43.36	56.10	42.85	48.26	55.78	32.94
D 4	7.65E-03	1.20	1.83	2.99	6.44	11.79	13.38	13.31	14.70	22.33	15.47	17.35	12.11
D 5	1.19E-02	1.07	1.29	2.13	5.82	10.66	11.85	17.51	15.00	5.81	11.72	12.63	9.76
D 6	2.93E+00	1.36	2.06	4.14	10.88	23.71	31.64	36.69	48.33	31.32	30.39	45.10	27.89
D 7	1.52E+01	2.13	3.52	6.63	13.81	25.93	27.99	32.88	30.84	34.63	29.39	36.62	29.37
E 1	1.21E-04	1.00	1.01	1.01	1.01	1.03	1.11	1.50	2.52	3.69	11.55	9.47	7.19
E 2	1.45E-04	1.01	1.02	1.03	1.04	1.10	1.23	1.55	2.37	3.31	6.64	9.59	18.17
E 3	1.11E-03	1.00	1.04	1.04	1.06	1.11	1.25	1.45	2.16	2.60	6.01	9.55	5.93
E 4	1.26E-03	1.02	1.04	1.04	1.06	1.10	1.25	1.59	2.00	3.11	4.59	5.63	5.59
E 5	7.04E-03	1.03	1.04	1.06	1.08	1.12	1.29	2.09	1.89	2.73	3.81	5.38	3.18
E 6	3.35E-01	1.03	1.05	1.07	1.10	1.17	1.36	2.04	3.10	6.57	12.90	41.80	115.46
E 7	2.92E+00	1.04	1.09	1.11	1.15	1.22	1.46	2.01	3.45	6.44	16.06	20.90	51.04
F 1	9.18E-05	1.54	2.92	7.42	20.27	27.10	21.51	42.08	53.08	81.12	75.84	83.06	186.93
F 2	7.76E-04	1.28	2.21	5.13	16.14	52.28	97.25	101.34	148.65	113.40	566.86	108.42	123.04
F 3	1.09E-03	1.73	3.53	8.85	24.87	50.60	66.72	68.07	108.96	110.72	128.57	141.27	337.08
F 4	1.15E-03	1.27	2.35	6.20	17.57	31.92	35.34	36.13	62.31	62.29	119.76	82.26	152.40
F 5	1.19E-03	1.45	3.48	7.90	27.06	110.21	324.62	364.14	274.13	742.78	403.44	1028.46	329.29
F 6	3.82E-01	1.96	5.19	18.53	65.45	177.66	154.11	191.48	249.11	373.23	300.31	225.77	******
F 7	2.67E+00	2.25	5.25	13.61	36.38	68.73	73.21	109.18	174.61	306.60	115.55	73.59	169.19

FLOW RATE FOR A1 - A7 WAS 114 L/MIN.
FLOW RATE FOR OTHERS WAS 76 L/MIN.
TEST FLUID: MIL - H - 5606, 38C

VITA[3]

Leonard Ernest Bensch

Candidate for the Degree of

Doctor of Philosophy

Thesis: THE INFLUENCE OF ELECTROSTATIC CHARGE ON THE FILTRATION OF HYDRAULIC FLUIDS BY FIBROUS FILTERS

Major Field: Mechanical Engineering

Biographical:

Personal Data: Born in Chester, Oklahoma, July 7, 1946, the son of Mr. and Mrs. Lloyd Bensch. Married in Seiling, Oklahoma, March 25, 1967, to Diana Lee Hunnell. Beget Cristy Lynn Bensch, September 23, 1967, and Alicia Diane Bensch, December 4, 1974.

Education: Graduated from Seiling High School, Seiling, Oklahoma, in May, 1964; received the Bachelor of Science degree from Oklahoma State University in 1970, with a major in Mechanical Engineering; received the Master of Science degree from Oklahoma State University in 1970, with a major in Mechanical Engineering; completed requirements for the Doctor of Philosophy degree at Oklahoma State University in July, 1977.

Professional Experience: Engineering Assistant, Oklahoma City Air Material Area, Summer, 1966; Project Engineer, Fluid Power Research Center, 1967-1969; Research Associate, Fluid Power Research Center 1969-1971; Research Engineer and Program Manager, Fluid Power Research Center, 1971 - Present; Industrial Consultant, 1969 - Present.

Professional Affiliations: Society of Automotive Engineers, National Fluid Power Association, Pi Tau Sigma.

Publications: More than fifty papers and published research reports in the areas of Filtration Performance, Contamination Analysis, Contamination Control, and Fluid Logic.